Dynamics and Control of Global Instabilities in Open-Flows: A Linearized Approach

Article *in* Applied Mechanics Reviews · May 2010

DOI: 10.1115/1.4001478

CITATIONS
141

READS
259

4 authors, including:

Denis Sipp
The French Aeropace Lab ONERA, Meudon, France
125 PUBLICATIONS **2,385** CITATIONS
SEE PROFILE

Olivier Marquet
The French Aerospace Lab ONERA
40 PUBLICATIONS **662** CITATIONS
SEE PROFILE

Alexandre Barbagallo
13 PUBLICATIONS **371** CITATIONS
SEE PROFILE

Dynamics and Control of Global Instabilities in Open-Flows: A Linearized Approach

Denis Sipp
e-mail: denis.sipp@onera.fr

Olivier Marquet
e-mail: olivierket@yahoo.fr

Philippe Meliga[1]
e-mail: philippe.meliga@epfl.ch

ONERA-DAFE,
8 rue des Vertugadins,
F-92190 Meudon, France

Alexandre Barbagallo
ONERA-DAFE,
8 rue des Vertugadins,
F-92190 Meudon, France;
Ladhyx-Ecole Polytechnique,
CNRS,
F-91128 Palaiseau, France
e-mail: alexandre.barbagallo@googlemail.com

This review article addresses the dynamics and control of low-frequency unsteadiness, as observed in some aerodynamic applications. It presents a coherent and rigorous linearized approach, which enables both to describe the dynamics of commonly encountered open-flows and to design open-loop and closed-loop control strategies, in view of suppressing or delaying instabilities. The approach is global in the sense that both cross-stream and streamwise directions are discretized in the evolution operator. New light will therefore be shed on the streamwise properties of open-flows. In the case of oscillator flows, the unsteadiness is due to the existence of unstable global modes, i.e., unstable eigenfunctions of the linearized Navier–Stokes operator. The influence of nonlinearities on the dynamics is studied by deriving nonlinear amplitude equations, which accurately describe the dynamics of the flow in the vicinity of the bifurcation threshold. These equations also enable us to analyze the mean flow induced by the nonlinearities as well as the stability properties of this flow. The open-loop control of unsteadiness is then studied by a sensitivity analysis of the eigenvalues with respect to base-flow modifications. With this approach, we manage to a priori identify regions of the flow where a small control cylinder suppresses unsteadiness. Then, a closed-loop control approach was implemented for the case of an unstable open-cavity flow. We have combined model reduction techniques and optimal control theory to stabilize the unstable eigenvalues. Various reduced-order-models based on global modes, proper orthogonal decomposition modes, and balanced modes were tested and evaluated according to their ability to reproduce the input-output behavior between the actuator and the sensor. Finally, we consider the case of noise-amplifiers, such as boundary-layer flows and jets, which are stable when viewed in a global framework. The importance of the singular value decomposition of the global resolvent will be highlighted in order to understand the frequency selection process in such flows. [DOI: 10.1115/1.4001478]

1 Introduction

In aeronautical applications, unsteady flows, whose characteristic spatial scales are on the order of those of the studied object and whose temporal frequencies are low, are commonly encountered. Within the range of the Kolmogorov turbulent energy cascade, these phenomena are located at the left edge of a wavenumber or frequency spectrum, at scales where energy is injected. Within the framework of steady configurations, these fluctuations are intrinsic to the fluid, and stability theory can explain at least some of these phenomena, such as how structures of a specific frequency and scale are selected and emerge in a flow. The occurrences of these unsteadiness are usually detrimental to a satisfactory operation, which can be illustrated by a number of examples. On a wing profile, the boundary-layer at the upstream stagnation point is usually laminar. Tollmien–Schlichting waves, however, destabilize the flow, and the boundary-layer subsequently becomes turbulent [1]. This induces an increase in skin friction at the wall and thus a loss of performance of the vehicle linked to the increase in its drag. Inside the booster of a space launcher, the flow generated by solid combustion is characterized by a rather small Reynolds number, on the order of a few thousands [2]. However, very strong unsteadiness is generated by the flow, inducing thrust oscillations and vibrations of the vehicle. A transport aircraft produces a swirling flow in its wake. These structures are dangerous for following airplanes, which may be subjected to violent rolling moments [3]. These structures ought to be quickly destroyed by triggering the natural instabilities of the swirling system, such as the Crow instability. The flight envelope of a transport airplane is currently limited in the Mach-angle of attack (AoA) plane by the shock-induced buffeting phenomenon on the airfoil. For Mach numbers on the order of 0.8 and high AoAs, the shock located on the suction side of the wing suddenly starts to oscillate [4], which in turn causes vibrations that are detrimental to the airplane. When passing to the transonic regime, a space launcher such as Ariane V is subjected to strong vibrations, which originate from instabilities developing in the wake of the vehicle and are particularly harmful for the payload [5]. Fighter aircraft are vulnerable due to the strong infrared signature of the hot jet exiting the engine. In this application, the triggering of unstable modes in the hot jet by actuators placed at the nozzle exit constitutes a possible mechanism to promote turbulent mixing with the atmosphere, which in turn reduces the extent of the jet's hot zones as quickly as possible [6]. Cavity flows, such as those observed over bomb bays, are the site of violent unsteadiness related to powerful sound pressure waves that can cause severe structural vibrations [7]. Fatigue problems are the result, which significantly increase the cost of vehicle maintenance or decrease vehicle lifetime. The sound waves, arising from a hydrodynamic instability, propagate over long distances and can be the cause of extensive noise pollution. Furthermore, on transport aircraft, the slat on a multi-element wing configuration acts as a cavity and generates intense noise during landing when these high-lift devices are deployed [8]. The noise-related environmental problems have been an issue of increasing concern for many years. Many other examples, where occurrences of low-frequency unsteadiness cause noise, are worth mentioning: among them, the noise known as blade-wake interac-

[1]Present address: EPFL-LFMI, CH-1015 Lausanne, Switzerland.

Published online April 27, 2010. Transmitted by Assoc. Editor: Mohamed Gad-el-Hak.

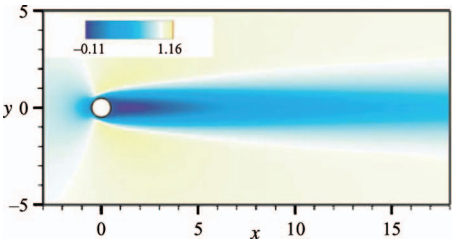

Fig. 1 Flow around a cylinder for Re=47. Base-flow $\mathbf{u}^B$ visualized by isocontours of streamwise velocity. Adapted from Ref. [38].

tion (BWI) caused by helicopter rotors [9] and the "tonal noise" related to laminar flow over an airfoil profile [10].

1.1 Models, Base-Flow, and Perturbation Dynamics. The main hypothesis underlying this review is that all phenomena presented in Sec. 1 can be properly described within a linearized framework, despite the fact that the Navier–Stokes equations, which govern them, are strongly-non-linear due to the convective term. At first sight then, a linearized description of the dynamics seems rather limiting. Moreover, the following question needs to be asked: Around which field must the equations be linearized? For flow configurations that deal with the destabilization of a steady flow-field, the answer is straightforward: the steady solutions of the Navier–Stokes equations; that is to say, the equilibrium points of these equations. These flow-fields usually exist at sufficiently low-Reynolds numbers, even if they are not observed in reality owing to instabilities. From a physical point of view, this means that we will focus on a low-amplitude perturbation that is superposed on a desirable base-flow. We then wish to stabilize the flow by various means in the vicinity of this equilibrium point.

Why come back to linear dynamics? The tools available within this framework, such as eigenvalue decomposition, singular value decomposition, the adjoint matrix, reduced-order-models based on controllability and observability concepts, $\mathcal{H}_2$ and $\mathcal{H}_\infty$ control techniques, etc., are well-established and powerful and provide a rigorous mathematical foundation for the study of the dynamics and control of a fluid system. It should also be noted that it has been the studies of transition in Poiseuille and Couette flows that in the 1990s gave rise to a renewed interest in linear theory and linear processes based on non-normal operators. Moreover, linear algebra (including its numerical algorithms) has continued to evolve significantly over the past 50 years, and many complex phenomena that were initially attributed to nonlinearity have found an explanation by using these tools.

Throughout this review, the equations governing the dynamics of the flow are the incompressible homogeneous Navier–Stokes equations. They will be written in the form

$$\frac{d\mathbf{u}}{dt} = \mathbf{R}(\mathbf{u}) \tag{1}$$

where $\mathbf{u}$ denotes the divergence-free velocity field and $\mathbf{R}(\mathbf{u})$ the residual. A *base-flow* $\mathbf{u}^B$, or an equilibrium point of Eq. (1), is defined by

$$\mathbf{R}(\mathbf{u}^B) = \mathbf{0} \tag{2}$$

An example of base-flow is shown in Fig. 1 in the case of the cylinder flow at Re=47: Isocontours of streamwise velocity show a recirculation zone with negative velocities of up to 11% of the upstream velocity.

The dynamics of the small perturbations $\mathbf{u}'$ superimposed on this field are governed by

$$\frac{d\mathbf{u}'}{dt} = \mathcal{A}\mathbf{u}' \tag{3}$$

The operator $\mathcal{A}$ corresponds to the Navier–Stokes equations linearized about the base-flow $\mathbf{u}^B$. Formally, the operator $\mathcal{A}$ may be written as $\mathcal{A}=\partial\mathbf{R}/\partial\mathbf{u}|_{\mathbf{u}^B}$. This operator involves spatial streamwise and cross-stream derivatives, which may be discretized with finite differences or finite elements to lead to a large-scale matrix. In the following, and throughout the whole article, $\mathcal{A}$ will stand for this large-scale matrix rather than the operator.

1.2 Asymptotic and Short-Term Instabilities. The dynamics of a low-level amplitude perturbation $\mathbf{u}'$ is governed by linearized Navier–Stokes equation (3). According to Schmid [11], a base-flow or a matrix $\mathcal{A}$ is said to be *asymptotically stable* if the modulus of any initial perturbation tends to zero for large times; otherwise it is *asymptotically unstable*. Based on this definition, the stability of a base-flow is determined by scrutinizing the spectrum of the matrix $\mathcal{A}$. To this end, particular solutions of Eq. (3) are sought in the form

$$\mathbf{u}' = e^{\lambda t}\hat{\mathbf{u}} \tag{4}$$

The corresponding dynamical structures are the *global modes* of the base-flow $\mathbf{u}^B$: Their spatial structure is characterized by the complex vector field $\hat{\mathbf{u}}$ and their temporal behavior by the complex scalar λ, whose real part (σ) designates the amplification rate and its imaginary part (ω) the frequency. The global modes $(\lambda,\hat{\mathbf{u}})$ correspond to eigenvalues/eigenvectors of the matrix $\mathcal{A}$ as follows:

$$\mathcal{A}\hat{\mathbf{u}} = \lambda\hat{\mathbf{u}} \tag{5}$$

Note that the global modes defined here are eigenvectors of the discrete matrix $\mathcal{A}$ and do therefore depend a priori on the chosen discretization, which led to $\mathcal{A}$. Among all eigenvectors of $\mathcal{A}$, only a few of them are somehow independent of the chosen discretization and have an intrinsic existence. These eigenvectors are only moderately sensitive to external perturbations of the matrix $\mathcal{A}$. For example, they exhibit good spatial convergence properties; i.e., as the mesh is refined or the computational domain is varied these eigenvalues/eigenvectors may be tracked and converge toward fixed quantities. These eigenvectors are the *physical global modes*. We note that, if at least one of the eigenvalues has a positive real part ($\sigma>0$), then the base-flow is asymptotically unstable. This instability is also called a *modal instability*, or even an *exponential instability*. On the other hand, if all of the eigenvalues have negative real parts ($\sigma<0$), the global modes will eventually all decay at large times, and the base-flow is asymptotically stable.

In the case of an asymptotically stable flow, the ability of this flow to amplify perturbations transiently is given by analyzing the instantaneous energetic growth of perturbations in the flow. The energy of a perturbation $\mathbf{u}'$ reads $\langle\mathbf{u}',\mathbf{u}'\rangle$, where $\langle\cdot,\cdot\rangle$ designates the scalar product associated with the energy in the whole domain. The equation governing the perturbation energy is then given by (see Ref. [12])

$$\frac{d}{dt}\langle\mathbf{u}',\mathbf{u}'\rangle = \langle\mathbf{u}',(\mathcal{A}+\mathcal{A}^*)\mathbf{u}'\rangle \tag{6}$$

Here $\mathcal{A}^*$ is the adjoint matrix and is defined such that

$$\langle\mathbf{u}_A,\mathcal{A}\mathbf{u}_B\rangle = \langle\mathcal{A}^*\mathbf{u}_A,\mathbf{u}_B\rangle \tag{7}$$

for any vector pair $\mathbf{u}_A$ and $\mathbf{u}_B$. Equation (6) shows that a necessary and sufficient condition for instantaneous energetic growth in a flow is that the largest eigenvalue of the matrix $\mathcal{A}+\mathcal{A}^*$ is positive. A matrix is said to be *normal* if $\mathcal{A}\mathcal{A}^*=\mathcal{A}^*\mathcal{A}$; i.e., the Jacobian matrix commutes with its adjoint. In this case, all global modes of $\mathcal{A}$ are orthogonal and, from Eq. (6), one may deduce that the energetic growth of a perturbation is linked to the existence of an

unstable global mode. In the case of a *non-normal* matrix—when the Jacobian does not commute with its adjoint—then this equivalence is not true anymore: Instantaneous energetic growth may exist although all global modes are asymptotically stable. This behavior will be called a *short-term instability*, or a *nonmodal instability*, or even an *algebraic instability* (since the perturbation energy then increases algebraically in time).

1.3 Oscillators and Noise-Amplifiers. According to Huerre and Rossi [13], occurrences of unsteadiness in open-flows can be classified into two main categories. The flow can behave as an *oscillator* and impose its own dynamics (intrinsic dynamics): Self-sustained oscillations are observed, which are characterized by a well-defined frequency, insensitive to low-level noise. Or the flow can behave as a *noise-amplifier*, which filters and amplifies in the downstream direction existing upstream noise: The spectrum of a measured signal, at some given downstream location, reflects, to some extent, the broadband noise present in the upstream flow (extrinsic dynamics). For example, the flow around a cylinder for Reynolds numbers in the range $47<\mathrm{Re}<180$ is typical of the oscillator-type, while a homogeneous jet or a boundary-layer flow is representative of noise-amplifiers.

These two types of dynamics have been extensively examined in the 1980s and 1990s for parallel and weakly-non-parallel base-flows. In the 1980s most of the studies were focused on finding exponential instabilities, i.e., linear perturbations that grow exponentially in time or space. The concepts of absolute and convective instabilities were introduced to describe the oscillator's and amplifier's dynamics, respectively [13]. Yet, the subcritical behavior of some flows, such as the Poiseuille or Couette flows, could not be described by an exponential instability. In the late 1980s/early 1990s, it was then recognized that the non-normality of the linearized Navier–Stokes operator could lead to strong transient energy growth, although all eigenmodes were asymptotically stable. In channel flows, due to the three-dimensional lift-up effect, streamwise oriented vortices grow into streamwise streaks [14–18] while the Orr mechanism [17,19] is responsible for transient growth of two-dimensional upstream tilted perturbations. These important findings made it possible to consider new transition scenarios to turbulence (although the importance of nonlinearity is determinant with this respect, see Sec. 7.2). The reader is referred to the book by Schmid and Henningson [12] for a comprehensive review on this subject. Optimization techniques based on direct-adjoint computations were then intensively used to find optimal initial perturbations in boundary-layer flows (Luchini and Bottaro [20] studied the optimal perturbation leading to Görtler vortices, Andersson et al. [21] and Luchini [22] the transients related to the lift-up effect in a spatially developing boundary-layer, Corbett and Bottaro [23] the energetic growth associated with oblique waves in boundary-layers subject to streamwise pressure gradient, Corbett and Bottaro [24] the instabilities in swept boundary-layers, and Guégan et al. [25,26] the optimal perturbations in swept Hiemenz flow).

In a global stability approach, which does not assume the parallelism of the base-flow, the oscillator and noise-amplifier dynamics may be related to different stability properties of the Jacobian matrix $\mathcal{A}$, as will be shown in Secs. 1.3.1 and 1.3.2.

1.3.1 Oscillators, Global Modes, and Prediction of Frequencies in a Global Approach. An oscillator-type dynamics may be observed when the base-flow is asymptotically unstable, since an unstable global mode $\sigma>0$ will then emerge at large times without any external forcing. As observed in the open-flow configurations studied within this review article, these global modes are generally physical global modes in the sense that they are only moderately sensitive to perturbations of the matrix $\mathcal{A}$. Furthermore, they also carry physical meaning since ω and $\hat{\mathbf{u}}$, respectively, characterize the frequency and spatial structure of the unsteadiness, at least in the vicinity of the bifurcation threshold. The amplification rate σ of the global mode allows identifying the critical parameters (Reynolds number, AoA for which $\sigma=0$) for the onset of the unsteadiness. The identification of these dynamical structures constitutes the key point to characterize an oscillator-type dynamics. As an example, the global mode in the case of the cylinder flow at $\mathrm{Re}=47$ is depicted in Fig. 2 by the real part of the cross-stream velocity of the eigenvector. Vortices of alternating sign are observed in the wake of the cylinder and are advected downstream. Note that the imaginary part of the eigenvector is approximately 1/4 spatial period out of phase, which enables a continuous downstream advection of the structures.

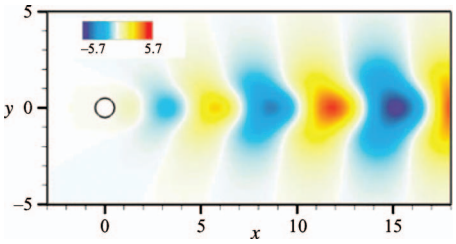

Fig. 2 Flow around a cylinder for Re=47. Marginal global mode characterized by the frequency $\omega=0.74$. The structure is visualized by isocontours of the real part of the cross-stream velocity ($\Re(\hat{v})$). Adapted from Ref. [38].

Computing global modes requires the solution of very large-scale eigenvalue problems (Eq. (5)). Indeed, given that the global eigenvector $\hat{\mathbf{u}}$ depends on the streamwise as well as cross-stream coordinate directions, the number of degrees of freedom (the dimension of the matrix $\mathcal{A}$) that are necessary for spatially converged results rapidly approaches the order of millions (number of mesh cells multiplied by the number of unknowns). Suitable algorithms to solve these equations are thus mandatory, as are powerful computing capabilities. The first eigenvalue computations within a global framework were carried out by Zebib [27] and Jackson [28] who described the bifurcation structure of the flow around a cylinder at $\mathrm{Re}=47$ (see also Ref. [29]). Natarajan and Acrivos [30] followed by studying axisymmetric flows around a disk and a sphere; Lin and Malik [31] investigated the stability of a swept Hiemenz flow. An important change in algorithmic techniques took place in the 1990s with the advent of the Arnoldi method: Edwards et al. [32], Barkley and Henderson [33], and Lehoucq and Sorensen [34] introduced and applied iterative algorithms based on Krylov subspaces to obtain parts of the global spectrum. The hydrodynamic stability community [35] has incorporated these new tools into the stability analyses of increasingly complex configurations, among them: Barkley et al. [36] for the case of a backward-facing step, Gallaire et al. [37] for the flow over a smooth bump, Sipp and Lebedev [38] for the flow over an open cavity, Åkervik et al. [39] for the case of recirculating flow in a shallow cavity, and Bagheri et al. [40] for a jet in cross-flow. Global stability analyses based on the compressible Navier–Stokes equations have also emerged very recently: Robinet [41] studied the case of a shock-boundary layer interaction, Brès and Colonius [42] treated the dynamics of an open cavity, and Mack et al. [43] investigated the instabilities of leading-edge flow around a Rankine body in the supersonic regime.

The prediction of the frequency of self-sustained oscillations has recently received much attention [44]. In the framework of weakly-non-parallel flows, linear [45] and fully nonlinear criteria [46] have successively been worked out to predict this frequency. In the case of wake flows, it was observed [47–51] that the linear saddle-point criterion [45] applied to the mean flow, rather than the base-flow, yields particularly good results. This is shown, for the cylinder flow, in Fig. 3, where the Strouhal number of the unsteadiness is given versus the Reynolds number. The thick solid line refers to the experimental data of Williamson [52], while the thin solid line (symbols) designates the global linear stability results associated with the base-flow (mean flow). As mentioned

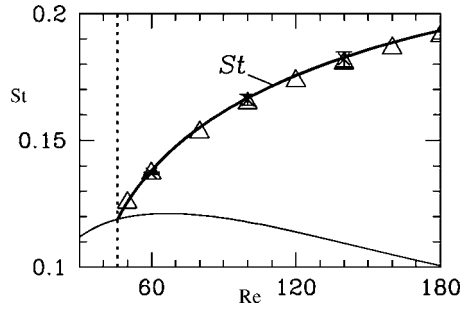

Fig. 3 Flow around a cylinder. Strouhal number versus Reynolds number. The thick solid line refers to experimental results [52], the thin solid line to a global linear stability analysis on the base-flow, and the symbols to a global linear stability analysis on the mean flow. Adapted from Ref. [49].

earlier, in the vicinity of the bifurcation threshold, the base-flow effectively yields the experimental frequency; but for supercritical Reynolds numbers, one observes that the mean flow, rather than the base-flow, has to be considered. One of the objectives in this review article is to explain these observations and show how a global stability analysis may predict the frequencies of the flow beyond the linear critical threshold, where nonlinearities are at play.

1.3.2 Noise-Amplifiers and Superposition of Eigenvectors in a Global Approach. A noise-amplifier-type dynamics may be observed when the base-flow is asymptotically stable, in which case an external forcing is required to sustain unsteadiness. In this case all global modes of $\mathcal{A}$ are damped ($\sigma<0$). As recognized by Trefethen et al. [53] and Farrell and Ioannou [17], the non-normality of the matrix $\mathcal{A}$ is of pivotal importance. Indeed, non-normal systems can exhibit strong responses for certain excitation frequencies, even though no eigenvalue of the system is close to the excitation frequency. This phenomenon is called *pseudoresonance*. Non-normality also induces that the eigenvectors of $\mathcal{A}$ are nonorthogonal and that a superposition of such structures may lead to *transient growth* although all eigenvectors of $\mathcal{A}$ are damped. This line of thought has been pursued first in the case of parallel channel flows [16–18].

Likewise, transient growth has first been viewed as a superposition of global modes in global stability approaches. For example, in the case of a spatially developing Blasius boundary-layer, Ehrenstein and Gallaire [54], Alizard and Robinet [55], and Akervik et al. [56] computed a set of stable global modes from which they deduced optimal perturbations. The case of a separating boundary-layer displaying a recirculation bubble has recently been analyzed, with the global mode approach, by Alizard et al. [57]. In open-flows, we will, in fact, show that studying noise-amplifier type dynamics is prawn to difficulties when transients are viewed as a superposition of global modes. The problem lies in the fact that stable global modes are generally unphysical (in the above defined sense, i.e., robustness to external matrix perturbations, such as discretization errors): For example, in the cylinder flow, none of the global modes are physical for the subcritical Reynolds number $\mathrm{Re}=20$. The shortcomings of the stable global modes to characterize a noise-amplifier-type dynamics in open-flows will be further discussed in Sec. 6. Instead, it will be shown that the singular values and vectors of the global resolvent $\mathcal{R}=(i\omega I-\mathcal{A})^{-1}$ will prove useful to characterize such a dynamics.

1.3.3 How Local Instabilities in Weakly-Non-Parallel Flows Are Captured by Global Stability Analyses. Absolute instabilities, such as exponential Kelvin–Helmholtz instabilities in plane counterflow mixing layers [58], generally lead to unstable eigenvectors in a global stability approach. Hence, oscillators are related to absolutely unstable flows in a local approach and to globally unstable flows in a global approach. If one wishes to compare a global mode stemming from a global stability approach to a global mode stemming from a weakly-non-parallel approach, then the linear saddle-point criterion by Monkewitz et al. [45] should be considered in the weakly-non-parallel approach. In the case of the cylinder flow, this comparison has been carefully achieved by Giannetti and Luchini [59], who showed that, despite the strong nonparallelism of the flow, weakly-non-parallel results compare reasonably well with those of a global stability approach (see thin solid line of Fig. 3 of the present article). On the other hand, the strongly-non-linear criterion by Pier and Huerre [46] (associated results are shown with filled squares in Fig.6 of Pier [48]) directly targets the frequency of the bifurcated flow on the limit-cycle (experimental results are recalled by a thick solid line in Fig. 3 of the present article). The results of the strongly-non-linear local theory should therefore rather be compared with those of the weakly-non-linear global analysis discussed in Sec. 3.4 (see, in particular, Eq. (15)).[2]

In the case of noise-amplifiers, streamwise growth of perturbations is expected, because of downstream advection by the base-flow. If the instability is locally convective, as is the case in exponential Tollmien–Schlichting instabilities in boundary-layers or exponential Kelvin–Helmholtz instabilities in plane coflow mixing layers [58], then the streamwise growth is exponential. But a weaker streamwise algebraic growth may also exist in the case of nonmodal instability (lift-up or Orr mechanisms). In both cases (streamwise exponential and streamwise algebraic growth), an exponentially stable (in time) but algebraically unstable (in time) flow is obtained in a global stability analysis. This link has been established in the case of a model equation mimicking open-flows [61] and for spatially developing boundary-layers [54,55].

1.4 Control of Oscillators. In the present review article, flow control specifically aims at suppressing unsteadinesses of oscillators by stabilizing the unstable global modes. The stabilization of noise-amplifier flows will briefly be discussed in Sec. 6. Other objectives such as flow separation control are not addressed here. For a more comprehensive review on flow control, the reader is referred to Gad- el-Hak et al. [62] and Collis et al. [63]. Generally speaking, the control strategies may be classified into closed-loop and open-loop control techniques, depending on whether the actuation is a function or not of flow measurements. Both strategies are considered here and have been adapted to the context of global stability analysis.

1.4.1 Open-Loop Control of Oscillators. A general presentation of open-loop control of wake flows is given in the article of Choi et al. [64]. Various physical mechanisms may be involved in open-loop control of oscillators, for instance, tuning of the system to a given frequency by upstream harmonic forcing (Pier [65]) or stabilizing the perturbation by acting on the base or mean flow (Hwang and Choi [66]). Also various types of actuations may be considered: passive actuations, as introducing a small object into the flow (Strykowski and Sreenivasan [67]), active actuations, as steady base blowing and suction [68–71], or periodic actuations [65,72]. The present review article will focus on a specific open-loop control problem that was introduced by Strykowski and Sreenivasan [67]. In the case of the cylinder flow, these authors suggested to suppress the vortex-shedding process at supercritical Reynolds numbers ($\mathrm{Re}\approx 50-100$) by introducing a small control cylinder in the flow. Figure 4 reproduces their experimental results: For each Reynolds number, this figure indicates a region in space inside which the placement of the small control cylinder

[2]Yet, for a given base-flow, poor results are expected from such a comparison, since the weakly-non-linear analysis presented in Sec. 3.4 blows up in the case of weakly-non-parallel flows [44,60], while the validity domain of the nonlinear local criterion by Pier and Huerre [46] is precisely restricted to weakly-non-parallel flows. Still, both approaches are complementary and concern different base-flows (weakly-non-parallel base-flows for the local approach and strongly-non-parallel ones for the global approach).

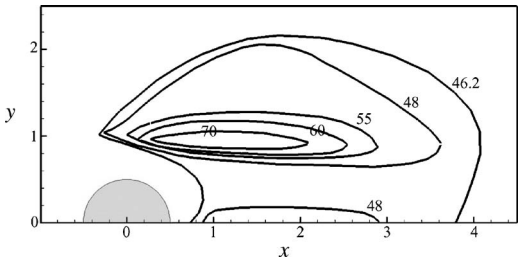

Fig. 4 Flow around a cylinder. Flow stabilization regions obtained experimentally for various Reynolds numbers. Adapted from Ref. [67].

suppresses the von Kármán vortex street. For Reynolds numbers close to the bifurcation threshold Re=48, there are two coexisting stabilizing regions: The first one is located on the symmetry axis close to $(x_0=2, y_0=0)$, and the second one is located on either side of the symmetry axis near $(x_0, y_0)=(1.2, \pm 1)$. As the Reynolds number increases, the first stabilizing region disappears, while the second becomes increasingly smaller near $(x_0, y_0)=(1.2, \pm 1)$. The same optimal positions were found by Kim and Chang [73] and Mittal and Raghuvanshi [74] from direct numerical simulations, and by Morzynski et al. [75] from global stability analyses. All these approaches successfully determined the optimal placement of a control cylinder to suppress the vortex shedding, but required that various locations of the control cylinder be tested and either experimental measurements, direct numerical simulations, or global stability analyses be carried out in each case. This review will address a new formalism based on global stability and sensitivity analyses, which allows predicting beforehand the regions of the flow where a control cylinder will be effective. This approach may also be viewed as an optimization problem (Gunzburger [76]) with a specific cost functional being the eigenvalue of the unstable global mode, the constraints the Navier–Stokes equations, and the control variable a force exerted on the base-flow, which mimics the presence of a control cylinder. This formalism may also deal with active control, such as steady base blowing and suction [77,78].

1.4.2 Closed-Loop Control of Oscillators and Reduced-Order-Models. Automatic control engineers have developed rigorous methods for closed-loop linear system control. Two common approaches based on $\mathcal{H}_2$- and $\mathcal{H}_\infty$-control are presented in Refs. [79,80]. These techniques were introduced to fluid mechanical application by Joshi et al. [81], Bewley and Liu [82], Cortelezzi and Speyer [83], and Högberg et al. [84] for the closed-loop control of channel flow transition. Hœpffner et al. [85] and Chevalier et al. [86] showed that a stochastic modeling of the measurement noise, of the initial condition, and of the external perturbations could appreciably improve the performance of an estimator. The control of a spatially developing boundary-layer was undertaken by Högberg and Henningson [87] using full-state information control and by Chevalier et al. [88] using an estimator. Drag reduction in turbulent flows was achieved by Cortelezzi et al. [89] and Lee et al. [90] (see Ref. [91] for a review). A summary of these results can be found in Refs. [92,93].

When applying flow control techniques in a global setting, a major difficulty arises. The very significant number of degrees of freedom of the system prevents the direct implementation of the $\mathcal{H}_2$- and $\mathcal{H}_\infty$-control strategies. For example, the Riccati equations, a central equation for determining the control and Kalman gain, cannot be solved for a number of degrees of freedom greater than about 2000. The solution does not only become prohibitive owing to restrictions in memory resources, the precision of the calculations using standard algorithms is compromised as well. For example, Lauga and Bewley [94] showed, using a one-dimensional model equation of open-flow, that the Riccati equations could not be solved with sufficient accuracy using 8-byte real arithmetic. As a response to these problems, Antoulas [95] showed how reduced-order-models of the flow-field, with a small number of degrees of freedom, may be built to capture—not all but—the most relevant features of the flow dynamics for the design of a control law. A physics-based way to do this is to look for a projection basis that complies with these requirements and then to project the governing equations on it.

The choice of the projection basis is crucial for good performance. Åkervik et al. [39] implemented a compensator for the first time in a global stability approach: Considering a reduced-order-model based on unstable global modes and few stable global modes, they implemented a $\mathcal{H}_2$-control strategy to stabilize an unstable shallow cavity flow. Global modes thus seem to constitute a first candidate for model reduction [96]. Antoulas [95] has noted, however, that the least damped eigenvectors do not generally constitute an appropriate basis for model reduction. A proper reduced-order-model is one which best approximates the input-output transfer function of the full (unreduced) system. Moore [97] showed how a basis for such an approximation may be found. After defining the controllability and observability Gramians (which yield a measure of controllability and observability of the system), he showed that the eigenvectors of the product of these two Gramians constitute a quasi-optimal basis in terms of the criterion defined above. This basis consists of balanced modes that are equally controllable and observable. Laub et al. [98] found an optimal and accurate algorithm for the calculation of this basis. However, this algorithm does not allow for large-scale systems. It was Willcox et al. [99] and Rowley [100] who would overcome this difficulty: they showed that the Gramians can be approximated using two series of snapshots resulting from two different numerical simulations and that the algorithm of Laub et al. [98] can be generalized to take into account these approximate Gramians. Due to the use of snapshots, this technique is also referred to as "balanced proper orthogonal decomposition" to highlight the connection of Rowley's algorithm [100] with proper orthogonal decomposition (POD) (see Refs. [101–103]). Moreover, Rowley [100] noted that the eigenvectors of the controllability Gramian (instead of the product of the Gramians) yield a POD-type basis. It should be noted that all these algorithms are based on the singular value decomposition of a matrix. The technique of Rowley [100] has been applied to several stable flows: Ilak and Rowley [104] studied a channel flow, and Bagheri et al. [105] investigated a one-dimensional model equation mimicking an open-flow and a boundary-layer flow [106]. Ahuja and Rowley [107] looked at a first unstable case corresponding to flow about a flat plate at an AoA of 35 deg.

Several bases for model reduction are available. Balanced modes constitute the best basis to reproduce the input-output dynamics of the full-system. However, more traditional bases, such as the modal basis or the POD basis, are also possible. As far as the stability of reduced-order-models is concerned, one notes that within a linearized framework, a stable matrix $\mathcal{A}$ yields a stable reduced-order-model if the latter is based on global modes, balanced modes, or POD-modes, independent of the dimension of the reduced-order-model. This remarkable property does not exist for the nonlinear case. Additional features, such as eddy viscosity, may then be used to stabilize the reduced-order-models [108]. Along this line, Samimy et al. [109] recently succeeded in experimentally controlling the unsteadiness of an open cavity. The reduced-order-model was given by a Galerkin projection of the 2D compressible Navier–Stokes equations on the leading POD-modes, obtained from velocity snapshots thanks to particle-image-velocimetry measurements. An estimate of the perturbation was given by stochastic estimation, which correlates surface pressure data with the perturbation structure, described in the POD basis. Linear-quadratic-regulators were then used to design the control gains.

All the previously mentioned reduced-order-models were

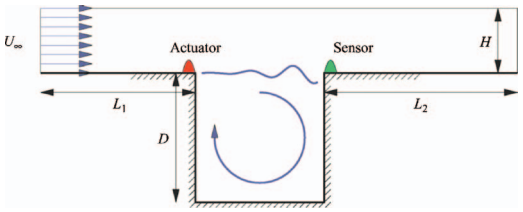

Fig. 5 Flow over an open cavity. Configuration and location of the actuator and sensor. Adapted from Ref. [141].

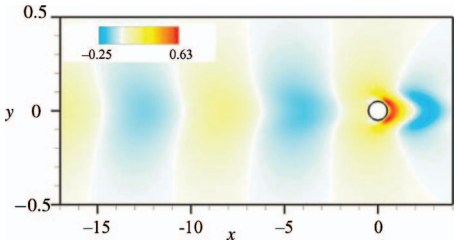

Fig. 6 Flow around a cylinder for Re=47. Marginal adjoint global mode. The structure is visualized by isocontours of the real part of the cross-stream velocity ($\Re(\hat{v})$). Adapted from Ref. [38].

physics-based: They were obtained from projection of the governing equations onto a given basis. Yet, one may also proceed with system identification techniques to build reduced-order-models. For example, the eigenvalue-realization-algorithm (Juang and Pappa [110]) identifies directly from the input-output data a linear state-space model. For data arising from a linear large-scale model (for example, data stemming from a simulation or an experiment with small-amplitude perturbations superposed on a base-flow), Ma et al. [111] showed that this algorithm has strong links with balanced-POD: The identified reduced-order state-space model actually governs the dynamics of the leading balanced modes. If one is able to store the state snapshots along with the input-output data (the Markov parameters), then the direct balanced modes may even be reconstructed. Note, however, that, in general, the amplitude of the perturbations is not small and the large-scale model is fully nonlinear, so that identifying a linear reduced-order-model from an underlying nonlinear dynamics may be ill-posed and prawn to difficulties. Finally, in order to determine accurately the Markov parameters, especially in a noisy environment, one may try, before applying the eigenvalue-realization-algorithm, to identify the input-output behavior, from the actuator to the measurement, with an empirical model containing a number of model parameters (for example, autoregressive linear and nonlinear models). Then, the unknown model parameters are estimated through error minimization techniques using the input-output data from the experiment (Huang and Kim [112]).

Our objective, within this review article, is to show how efficient reduced-order-models may be built from a global stability approach, in order to stabilize unstable global modes in open-flows, within a modern control framework. The models are obtained through projection of the linearized Navier–Stokes equations on various bases (modal, POD, and balanced-POD). As shown in Fig. 5, we choose an open cavity with a measurement downstream of the cavity and an action near its upstream corner.

1.5 Outline of Article. First (Sec. 2), the central notion of adjoint global mode will be defined. In Sec. 3, the bifurcations in various oscillator flows (cylinder and open cavity) are examined. In particular, the role of nonlinearities in the prediction of the dominant frequency of the unsteadiness, the generation of mean flows, and the stability properties of the latter will be studied. The sensitivity of the eigenvalues and the open-loop control approach to suppress unsteadiness are presented next (Sec. 4). Then, recent developments in the field of closed-loop control and model reduction (Sec. 5) are described. The next section (Sec. 6) is devoted to the case of noise-amplifiers and their open-loop control. Finally, issues related to three-dimensional configurations, nonlinearity, and high-Reynolds number flows (Sec. 7) are discussed.

2 Adjoint Global Modes and Non-Normality

Within the framework of local stability theory, the concept of adjoint equations and operators appeared when amplitude equations were constructed from weakly-non-linear theory. The adjoint mode is then required to enforce the compatibility conditions of nonhomogeneous problems [113,114]. Optimization techniques based on adjoints [76] were first introduced in fluid mechanics by Hill [115] and Luchini and Bottaro [20] for receptivity studies and by Bewley [92] and Corbett and Bottaro [116] for optimal control of instabilities. Note also that Bottaro et al. [117] introduced the concept of sensitivity of an eigenvalue with respect to base-flow modifications.

In a global framework, adjoint methods were first used in the context of shape optimization. By considering an objective functional depending on a large number of degrees of freedom, the adjoint system appears naturally when the gradient of the functional with respect to a change in the geometry is sought [118–120]. Hill [121] and Giannetti and Luchini [59] were the first to use adjoint techniques to study the sensitivity of global modes.

In the following, the adjoint global modes and the modal basis will first be defined (Sec. 2.1). Then, we show that the nonorthogonality of the modal basis may be quantified by looking at the angles of associated direct and adjoint global modes (Sec. 2.2). Then, we show why the adjoint global modes are different from the direct global modes in the case of linearized Navier–Stokes equations (Sec. 2.3). In particular, we will see that, in the case of open-flows, a specific convective mechanism induces very strong non-normalities.

2.1 Adjoint Global Modes and Modal Basis. Let λ be an eigenvalue associated with the direct global mode $\hat{\mathbf{u}}$. The structure $\hat{\mathbf{u}}$ is therefore an eigenvector of the matrix $\mathcal{A}$ and satisfies Eq. (5). We know that the spectrum of $\mathcal{A}^*$ is equal to the conjugate of the spectrum of $\mathcal{A}$, and thus there exists $\tilde{\mathbf{u}}$ such that

$$\mathcal{A}^*\tilde{\mathbf{u}} = \lambda^*\tilde{\mathbf{u}} \tag{8}$$

with the normalization condition $\langle\tilde{\mathbf{u}},\hat{\mathbf{u}}\rangle=1$. The quantity $\tilde{\mathbf{u}}$ is called the *adjoint global mode* associated with the direct global mode $\hat{\mathbf{u}}$. In the case of a cylinder flow at Reynolds Re=47, the adjoint global mode is presented in Fig. 6, with the isocontours showing the real part of the cross-stream component of the velocity. We notice that this structure is located in the region $x<5$ and, in particular, upstream of the cylinder.

The modal basis is made up of the complete set of direct global modes $(\hat{\mathbf{u}}_j, j\geq 1)$. In the case of a non-normal matrix, the global modes are nonorthogonal. Hence, it is not straightforward anymore to expand a given vector $\mathbf{u}'$ in this basis. For example, the component of $\mathbf{u}'$ on the jth global mode $\hat{\mathbf{u}}_j$ is not simply $\langle\hat{\mathbf{u}}_j,\mathbf{u}'\rangle/\langle\hat{\mathbf{u}}_j,\hat{\mathbf{u}}_j\rangle$ as would have been the case for a normal matrix. To circumvent this difficulty, one introduces a dual basis, which is made of the complete set of adjoint global modes $(\tilde{\mathbf{u}}_j, j\geq 1)$. The vectors $\hat{\mathbf{u}}_j$ and $\tilde{\mathbf{u}}_j$ are related to the eigenvalues λ_j by

$$\mathcal{A}\hat{\mathbf{u}}_j = \lambda_j\hat{\mathbf{u}}_j \tag{9}$$

$$\mathcal{A}^*\tilde{\mathbf{u}}_j = \lambda_j^*\tilde{\mathbf{u}}_j \tag{10}$$

where the adjoint global modes are normalized following $\langle\tilde{\mathbf{u}}_j,\hat{\mathbf{u}}_j\rangle=1$. The direct and adjoint bases taken together form a bi-orthogonal basis: $\langle\tilde{\mathbf{u}}_j,\hat{\mathbf{u}}_k\rangle=0$ if $j\neq k$ and $\langle\tilde{\mathbf{u}}_j,\hat{\mathbf{u}}_k\rangle=1$ if $j=k$. Any

field $\mathbf{u}'$ can therefore be expressed in a unique way in the modal basis as $\mathbf{u}'=\Sigma_{j\geq 1}\langle\tilde{\mathbf{u}}_j,\mathbf{u}'\rangle\hat{\mathbf{u}}_j$. Note that, if the Jacobian matrix is normal, then the basis is orthogonal and the direct and adjoint global modes are identical. If it is non-normal, then the modal basis is nonorthogonal and the direct and adjoint global modes are different.

2.2 Nonorthogonality and Adjoint Global Modes. As mentioned in Secs. 1.2 and 1.3.2, the level of nonorthogonality of the modal basis is central in the analysis of short-term instabilities. It may be assessed by comparing the direct and the adjoint global modes: In Sec. 2.1, it was found that the jth adjoint global mode was orthogonal to all direct global modes except the jth ($\langle\tilde{\mathbf{u}}_j,\hat{\mathbf{u}}_k\rangle=0$ if $j\neq k$). Therefore, the angle between the adjoint global mode $\tilde{\mathbf{u}}_j$ and the direct global mode $\hat{\mathbf{u}}_j$ exactly characterizes the nonorthogonality of $\hat{\mathbf{u}}_j$ with the remaining global modes of the basis. For a specific global mode $\hat{\mathbf{u}}$, this angle is directly related to the following coefficient:

$$\gamma=\sqrt{\langle\tilde{\mathbf{u}},\tilde{\mathbf{u}}\rangle}\times\sqrt{\langle\hat{\mathbf{u}},\hat{\mathbf{u}}\rangle} \tag{11}$$

Given that $\langle\tilde{\mathbf{u}},\hat{\mathbf{u}}\rangle=1$, it can easily be shown that this coefficient satisfies $\gamma\geq 1$. The larger γ, the more nonorthogonal the global mode $\hat{\mathbf{u}}$ is with respect to the remaining global modes of the basis. For the case of a flow around a cylinder at Re=47, we find that $\gamma=77.7$

2.3 Component-Type and Convective-Type Non-Normalities. Analyzing the linearized Navier–Stokes equations, it was shown [122] that two sources of non-normality exist in open-flows. To see this, Eqs. (5) and (8) governing the direct and adjoint global modes were written in the form

$$\lambda\hat{\mathbf{u}}+\underbrace{\nabla\hat{\mathbf{u}}\cdot\mathbf{u}^B}_{(1)}+\underbrace{\nabla\mathbf{u}^B\cdot\hat{\mathbf{u}}}_{(2)}=-\nabla\hat{p}+\frac{1}{\mathrm{Re}}\Delta\hat{\mathbf{u}},\quad \nabla\cdot\hat{\mathbf{u}}=0$$

$$\lambda^*\tilde{\mathbf{u}}\underbrace{-\nabla\tilde{\mathbf{u}}\cdot\mathbf{u}^B}_{(1)}+\underbrace{(\nabla\mathbf{u}^B)^*\cdot\tilde{\mathbf{u}}}_{(2)}=+\nabla\tilde{p}+\frac{1}{\mathrm{Re}}\Delta\tilde{\mathbf{u}},\quad \nabla\cdot\tilde{\mathbf{u}}=0$$

The notation $\nabla\hat{\mathbf{u}}$ refers to the tensor $\partial_j\hat{u}_i$ and $\cdot$ to the contraction operator. Two main differences, favoring orthogonality of the direct and adjoint global modes, exist in these equations.

1. We observe that terms (1), which represent the advection of the perturbation by the base-flow, have opposite signs in these two equations: The direct global mode is advected downstream while the adjoint global mode is advected upstream. This sign inversion causes a separation of the spatial support of the associated direct and adjoint global modes (upstream support for the adjoint mode and downstream support for the direct mode). This tends to make the direct and adjoint global modes be orthogonal and constitutes the so-called *convective-type non-normality* [44,61]. For the case of the flow around a cylinder, this phenomenon is illustrated in Figs. 2 and 6, where we observe that the direct global mode is located downstream of the cylinder and the adjoint global mode mainly upstream of it.
2. The appearance in the adjoint equations of a transconjugate operator * in terms (2) causes the associated direct and adjoint global modes to have amplitudes in different velocity components. This constitutes the so-called *component-type non-normality*. For example, in a shear-layer flow defined by the streamwise base velocity profile $u^B(y)$, the off-diagonal term $\partial_y u^B$ in the velocity gradient tensor induces streamwise velocity perturbations from cross-stream velocity perturbations in the direct global mode; in contrast, in the associated adjoint global mode, it generates cross-stream velocity perturbations from streamwise velocity perturbations. The traditional lift-up phenomenon is hence recovered, where the optimal perturbation consists of a streamwise vortex and the optimal response of a streamwise streak [14–16,18]. For the case of the marginal eigenmodes of the disk and the sphere [123], it was shown that the amplitudes of the ($m=1$) helicoidal direct eigenvectors were entirely concentrated in the streamwise component, while the corresponding adjoint modes were dominated by the cross-stream components. The same tendency was observed [122] for the three-dimensional nonoscillating marginal global mode that destabilizes a recirculation bubble in a Cartesian setting [36,37,124]. On the other hand, nonorthogonality due to component-type non-normality was never observed for two-dimensional instabilities occurring in cylinder and open-cavity flows, where the streamwise and cross-stream components of the perturbations were equally found present in the direct and adjoint global modes.

The amount of nonorthogonality due to component-type non-normality within total nonorthogonality γ is given by [123]

$$\delta=\frac{\langle\|\tilde{\mathbf{u}}\|,\|\hat{\mathbf{u}}\|\rangle}{\gamma} \tag{12}$$

where $\|\mathbf{u}\|=(\mathbf{u}\cdot\mathbf{u})^{1/2}$ stands for the norm induced by the standard Hermitian inner product $\mathbf{u}\cdot\mathbf{u}$, at some given location of the flow.[3] By using the Cauchy–Schwartz inequality, it can be shown that the coefficient δ satisfies $0\leq\delta\leq 1$. This coefficient allows us to determine whether the nonorthogonality of a global mode stems from component-type or convective-type non-normality: If δ is close to 0, the nonorthogonality stems from the convective mechanism, and if this coefficient is close to 1, the nonorthogonality is mostly due to the component-type non- normality. For the case of the flow around a cylinder at Re=47, we find that $\delta=0.016$. Similarly, for the case of the marginal global modes of the disk and the sphere [123], nonorthogonality due to the component-type non-normality was also found to be small compared to the nonorthogonality due the convective-type.

3 Oscillator Flows, Global Modes, and Prevision of Frequencies

The dynamics of oscillators is described using dynamical systems and bifurcation theory. These approaches were initially developed for and applied to simple closed-flows [125]. Chomaz [44] introduced them to open-flows, using a model equation representative of open-flows.

3.1 The Hopf Bifurcation in Cylinder Flow. The first amplitude equation derived from the two-dimensional Navier–Stokes equations for open-flows was worked out for the case of cylinder flow [38]. A Stuart–Landau equation describing a Hopf bifurcation is thus obtained that governs the amplitude of a global structure. If the latter is evaluated at a particular point of the flow then one recovers the results of Provansal et al. [126] and Dušek et al. [127], who postulated its existence and calibrated its coefficients so that its dynamical behavior reproduces experimental or numerical data at a given location in the flow. It is known that this Hopf bifurcation appears at Re=47: The flow is steady and symmetrical for a subcritical control parameter $\mathrm{Re}<47$, and unsteady and asymmetrical for $\mathrm{Re}>47$. This phenomenon is described schematically in Fig. 7(*a*) where the x-axis represents the control parameter (the Reynolds number Re). On the left of the figure, the small picture shows the characteristic isocontours of vorticity of the flow-field, observed for a subcritical Reynolds number (blue cross): The flow is symmetrical and steady. The picture on the top

[3]Note that $\|\cdot\|$ acts on a vector and not on a vector field. On the other hand, dependent on the specific context, $\langle\cdot,\cdot\rangle$ represents a scalar product acting on scalar fields or vector fields so that $\langle\|\mathbf{u}\|,\|\mathbf{u}\|\rangle=\langle\mathbf{u},\mathbf{u}\rangle$ yields the energy of the flow-field $\mathbf{u}$.

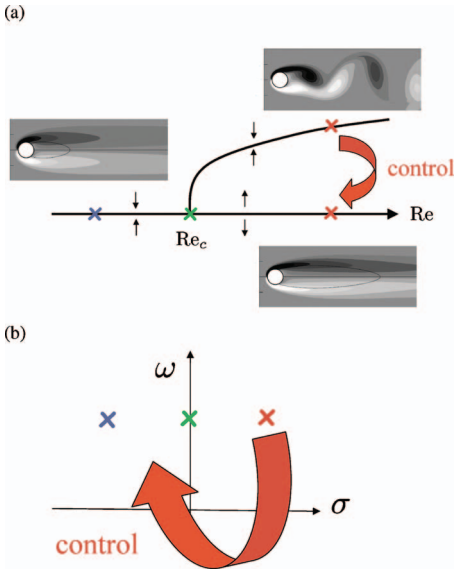

Fig. 7 Flow around a cylinder. (*a*) Bifurcation diagram. (*b*) The least damped eigenvalues in the (σ,ω)-plane for subcritical, critical, and supercritical Reynolds numbers.

relates to a supercritical Reynolds number (red cross) and presents an instantaneous field representative of the unsteady dynamics. The bifurcation diagram of Fig. 7(*a*) is constructed in the following way. First, a family of base-flows $\mathbf{u}^B(\mathrm{Re})$ is determined, which is parametrized by the Reynolds number Re. These fields are solutions of the steady Navier–Stokes equations, as defined by Eq. (2). For $\mathrm{Re}<\mathrm{Re}_c$, these flow-fields can be obtained by a direct numerical simulation: All initial conditions converge toward a single field, which is steady and symmetrical. Such fields also exist for $\mathrm{Re}>\mathrm{Re}_c$, even if these fields are not observed, since they are unstable. For example, the lower right picture of Fig. 7(*a*) shows the steady unstable base-flow related to the red cross on the *x*-axis. Continuation techniques, such as the Newton method, are used to obtain these fields. Next, for each Reynolds number, the stability of the associated base-flow is studied by solving eigenvalue problem (5). The eigenvalues corresponding to the subcritical case (blue cross) and supercritical case (lower red cross) are displayed schematically in the (σ,ω)-plane in Fig. 7(*b*): The base-flows are observed to be stable in the subcritical case and unstable in the supercritical case. Thus, the base-flow related to the red cross on the *x*-axis is unstable and the flow converges toward a nonlinear Hopf limit-cycle (red cross on the bifurcated branch). On the latter, the flow is unsteady, periodic in time, and asymmetrical.

To conclude, we should point out that this review does not consider bifurcations where two branches of steady solutions cross for some critical value of the control parameter. This happens when a real nonzero vector $\hat{\mathbf{u}}$ appears in the null-space of the Jacobian matrix: $\mathcal{A}\hat{\mathbf{u}}=\mathbf{0}$. In this case, the marginal global mode is nonoscillating ($\omega=0$) and has the same symmetries and homogeneity directions as the base-flow. The flow around a cylinder does not belong to this bifurcation category since it breaks the temporal invariance of the base-flow ($\omega\neq 0$) as well as its spatial symmetry.

3.2 Bifurcation Theory, Control, and Influence of Nonlinearity. The control strategies studied in this review article consist of stabilizing the unstable eigenvalues, as shown in Fig. 7(*b*). The open-loop control, which is steady, aims at modifying the base-flow to make it stable; this control is steady. Given that this control approach suppresses instabilities, the effects of nonlinearity within this control strategy are minimal: With instabilities eliminated, there no longer exists any mechanism to generate perturbations of large amplitudes. The closed-loop control, on the other hand, acts directly on the perturbations to stabilize the system. This control is unsteady and corresponds to an opposition control, where one attempts to generate structures that annihilate the naturally developing unstable perturbations. It thus stabilizes the steady unstable branch, which exists for $\mathrm{Re}>\mathrm{Re}_c$. Since the underlying mathematical formalism is only valid for flow states in the vicinity of the base-flow around which the Navier–Stokes equations have been linearized, this linear control action does not manage a priori to drive the flow from a limit-cycle toward the steady unstable branch. Rather, this approach can only ensure the stabilization of the system on this branch if the initial flow state has already been in its neighborhood. In principle, open-loop control is more costly than closed-loop control, with the former acting on the base-flow and the latter on the perturbations.

3.3 Problems Related to the Mean Flow. The mean flow corresponds to the temporal average of an unsteady flow. Its characteristics are often studied in numerical simulations and in experiments since it can be rather easily obtained. However, several questions arise. Is the mean flow different from the base-flow? If so, why and by how much? What does it mean to perform a stability analysis on a mean flow? New light will be shed on these points. The link between nonlinearities and the induced mean flow was first described by Zielinska et al. [128] for the case of wake flows. These authors showed that the nonlinearities were rather strong, resulting in a mean flow that substantially deviated from the base-flow. These nonlinearities are responsible for the decrease in the recirculation length observed at supercritical Reynolds numbers. Barkley [49] then studied the stability properties of mean flows. To this end, direct numerical simulations for Reynolds numbers between 47 and 180 were carried out. The corresponding mean flows were calculated by time-averaging the snapshots from the simulations, and global stability analyses of these mean flows were performed. The author observed, unexpectedly, that the amplification rates related to the mean flows were quasizero and that the frequencies were in agreement with the ones observed in the direct simulations. Although these results seem natural at first sight, they are nevertheless surprising since the mean flow is a statistical construct with no immediate inherent meaning, which makes the associated linear dynamics around it doubtful. In the same spirit, Piot et al. [129] observed good agreement between the frequencies extracted from large-eddy simulations and those predicted by stability analyses of the mean flow for the case of jets. As mentioned in the Introduction, for wake flows, Hammond and Redekopp [47] and Pier [48] showed that linear stability analyses of the mean flow can identify the true frequency of the flow. For the case of flow around a cylinder, we will provide a proof that corroborates the observations of Barkley [49]. In general, however, it will be shown that certain conditions have to be satisfied such that the linear dynamics based on the mean flow captures relevant properties of the flow, in particular, the marginal stability of the mean flow and the agreement between the associated frequencies with the nonlinear dynamics.

3.4 Hopf Bifurcation and Limit-Cycle. Global stability analysis is practical to describe the linear dynamics of oscillator flows. For Reynolds numbers above a critical value, however, it predicts the existence of exponentially growing perturbations in time, thereby invalidating, for large but finite time, the small-amplitude assumption underlying the linear stability theory. In other words, in the presence of instabilities, there exists a time beyond which the nonlinear terms can no longer be neglected. The nonlinear dynamics is studied in this section, based on a weakly-non-linear analysis. An asymptotic development of the solution in the vicinity of the bifurcation threshold is sought, where the small parameter $\varepsilon=\mathrm{Re}_c^{-1}-\mathrm{Re}^{-1}$ designates the departure of the Reynolds number from the critical Reynolds number. More precisely, the global flow-field $\mathbf{u}(x,y,t)$ is taken in the form [38]

$$\mathbf{u}(x,y,t) = \mathbf{u}_0(x,y) + \sqrt{\varepsilon}[Ae^{i\omega_0 t}\hat{\mathbf{u}}_1^A(x,y) + \text{c.c.}] + \varepsilon[\hat{\mathbf{u}}_2^1(x,y) + |A|^2\hat{\mathbf{u}}_2^{|A|^2}(x,y) + (A^2e^{2i\omega_0 t}\hat{\mathbf{u}}_2^{A^2}(x,y) + \text{c.c.})] + \ldots \tag{13}$$

where c.c. denotes the complex conjugate. The dominant term in this expansion corresponds to the base-flow $\mathbf{u}^B=\mathbf{u}_0(x,y)$ obtained for $\mathrm{Re}=\mathrm{Re}_c$ and is represented in Fig. 1. The solution at order $\sqrt{\varepsilon}$ consists of the marginal global mode $Ae^{i\omega_0 t}\hat{\mathbf{u}}_1^A$+c.c., which satisfies the eigenvalue problem $\mathcal{A}\hat{\mathbf{u}}_1^A=i\omega_0\hat{\mathbf{u}}_1^A$ for $\mathrm{Re}=\mathrm{Re}_c$ (Eq. (5)). The time evolution of this structure is described by the frequency $\omega_0=0.74$ and by its complex amplitude A, which is assumed to evolve on a slow characteristic time-scale $A(\varepsilon t)$. The marginal global mode is depicted in Fig. 2. The solution at order ε consists of three terms: the correction of the base-flow $\hat{\mathbf{u}}_2^1$ due to a departure from criticality,[4] the zeroth-order or mean-flow harmonic $|A|^2\hat{\mathbf{u}}_2^{|A|^2}$ resulting from the nonlinear interaction of the marginal global mode with its complex conjugate, and the second-order harmonic $A^2e^{2i\omega_0 t}\hat{\mathbf{u}}_2^{A^2}$ related to the interaction of the marginal global mode with itself. At order $\varepsilon\sqrt{\varepsilon}$, nonhomogeneous, linearly degenerate equations appear. Compatibility conditions have thus to be enforced, which lead to a Stuart–Landau equation

$$\frac{dA}{dt} = \varepsilon\kappa A - \varepsilon(\mu+\nu)A|A|^2 \tag{14}$$

which describes the slow time evolution of the complex amplitude A. The complex coefficients κ, μ, and ν are obtained [38] from scalar products involving the adjoint global mode $\tilde{\mathbf{u}}_1^A$, which is depicted in Fig. 6, and forcing terms depending on the various fields that have been introduced in Eq. (13). The first term on the right-hand side of Stuart–Landau equation (14) represents the linear instability dynamics while the second term describes the nonlinear mechanisms. The linear instability phenomenon is completely determined by the coefficient κ. It was shown [38] that $\kappa_r>0$, which indicates that the flow is unstable for supercritical Reynolds numbers ($\varepsilon>0$). As for the nonlinear mechanisms, they are characterized by the coefficients μ and ν, which are, respectively, related to the zeroth-order harmonic $\hat{\mathbf{u}}_2^{|A|^2}$ and second-order harmonic $\hat{\mathbf{u}}_2^{A^2}$. It turned out [38] that $\mu_r+\nu_r>0$, which implies that the system converges toward a limit-cycle: The nonlinear term has a stabilizing effect on the dynamics.[56] On this limit-cycle, the frequency of the flow in the vicinity of the bifurcation ($\varepsilon\ll 1$) is

$$\omega^{\mathrm{LC}} = \omega_0 + \varepsilon\kappa_i - \varepsilon\kappa_r\frac{\mu_i+\nu_i}{\mu_r+\nu_r} \tag{15}$$

where the first term on the right-hand side is the frequency of the marginal global mode and the second term is the linear correction of the frequency due to departure from criticality. The sum of these two terms corresponds to the linear prediction of the frequency $\omega^B=\omega_0+\varepsilon\kappa_i$. The third term in Eq. (15) is the nonlinear correction due to contributions of the zeroth-order and second-order harmonics. The numerical evaluation of these terms gives $\omega^{\mathrm{LC}}=0.74+3.3\varepsilon+31\varepsilon$. It clearly indicates that the nonlinear correction is much larger than the linear correction. The frequency of the limit-cycle ω^{LC} is thus significantly different from the linear prediction ω^B, which explains why a global stability of the base-flow may yield a very poor prediction of the frequency observed in direct numerical simulations for supercritical Reynolds numbers $0<\varepsilon\ll 1$. Finally, a comparison of the coefficients from the nonlinear correction term shows that $|\mu_r\gg\nu_r|$ and $|\mu_i\gg\nu_i|$. The zeroth-order harmonic is therefore mainly responsible for the change in the frequency of the limit-cycle.

Note that, in the case of an axisymmetric disk placed perpendicular to the incoming flow, a similar development has been led [132] in order to determine the global amplitude equations associated with the codimension 2 bifurcation. It was shown that the amplitude equations reproduce precisely the complex bifurcation scenario observed in direct numerical simulations by Fabre et al. [133].

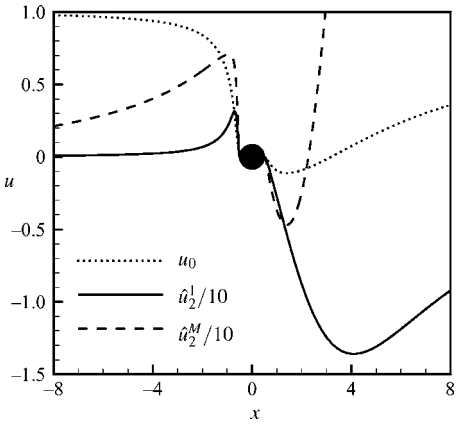

Fig. 8 Flow around a cylinder for Re=47. Streamwise velocity on the symmetry axis for the base-flow u_0 (dotted line), for the correction of the base-flow $\hat{u}_2^1$ (continuous line) and for the correction of the mean flow $\hat{u}_2^M$ (dashed line). Adapted from Ref. [38].

3.5 Mean Flow and Stability of Mean Flow. As mentioned previously, a global stability analysis of the mean flow yields surprisingly a good approximation of the frequency obtained from direct numerical simulations [49]. In this section the concept of mean flows and global stability of mean flows are addressed in light of the weakly-non-linear analysis presented above. While the base-flow is given by $\mathbf{u}^B=\mathbf{u}_0+\varepsilon\hat{\mathbf{u}}_2^1$, the *mean flow* $\mathbf{u}^M$ related to the limit-cycle is obtained by calculating an average over time[7] of expansion (13): $\mathbf{u}^M=\mathbf{u}_0+\varepsilon\hat{\mathbf{u}}_2^M$. Here $\hat{\mathbf{u}}_2^M$ is equal to the sum of the base-flow correction $\hat{\mathbf{u}}_2^1$ and the mean-flow harmonic $|A|^2\hat{\mathbf{u}}_2^{|A|^2}$. In Fig. 8, the streamwise velocity component for the base-flow u_0, for the correction of the base-flow $\hat{u}_2^1$, and for the correction of the mean flow $\hat{u}_2^M$, evaluated on the axis of symmetry, is displayed. We observe that the recirculation zone of the base-flow at the bifurcation threshold extends up to $x=3.2$ diameters. The correction of the base-flow $\hat{u}_2^1$ tends to increase this length ($\hat{u}_2^1<0$ in the wake) whereas the correction of the mean flow shortens it ($\hat{u}_2^M>0$ for $x>2.25$). This confirms the observations of Zielinska et al. [128] concerning the mean flow.

The stability of the mean flow has then been addressed in detail

[4] In fact, $\hat{\mathbf{u}}_2^1=d\mathbf{u}^B/d\varepsilon$ since the base-flow $\mathbf{u}^B(\varepsilon)$ depends on the Reynolds number ε.

[5] Chomaz [44] argued that the more the flow is parallel, the smaller $|\mu_r+\nu_r|$. This stems from the fact that, the more the flow is parallel, the further apart are the spatial supports of the direct and adjoint global modes. Hence, the mean flow and second-order harmonics have less and less impact on the dynamics since their support is more and more outside the wavemaker region (see Sec. 4.2.2 for definition). In this case, one has to resort to a strongly-non-linear approach, as presented by Pier and Huerre [46].

[6] The cylinder bifurcation corresponds to a supercritical instability; i.e., the flow is unstable solely for supercritical parameters $\varepsilon>0$. If $\mu_r+\nu_r<0$, then the bifurcation would be subcritical and an instability of an open-flow may arise for subcritical parameters $\varepsilon<0$ but only for finite-amplitude perturbations [130,131].

[7] If $\langle\,\rangle_T$ denotes the process of averaging over time, we thus obtain $\mathbf{u}^M=\langle\mathbf{u}(t)\rangle_T$. Letting $\mathbf{u}=\mathbf{u}^M+\mathbf{u}'$ with $\langle\mathbf{u}'\rangle_T=\mathbf{0}$ and averaging Eq. (1), the following equation governing the mean flow is obtained: $\mathbf{R}(\mathbf{u}^M)=-\langle\mathbf{R}(\mathbf{u}')\rangle_T$. It is noted that the mean flow $\mathbf{u}^M$ is not a base-flow, i.e., a solution of Eq. (2). For our case, we get $\mathbf{u}'=\sqrt{\varepsilon}[Ae^{i\omega_0 t}\hat{\mathbf{u}}_1^A(x,y)+\text{c.c.}]$ at the dominant order.

[38]. In particular, it is shown that the amplification rate σ^M and frequency ω^M of the global mode associated with the mean flow are given by

$$\sigma^M = \varepsilon\kappa_r \frac{\nu_r}{\mu_r + \nu_r}, \quad \omega^M = \omega_0 + \varepsilon\kappa_i - \varepsilon\kappa_r \frac{\mu_i}{\mu_r + \nu_r} \tag{16}$$

We observe that the frequency ω^M is not strictly equal to the frequency of the flow on the limit-cycle ω^{LC}, which was given in Eq. (15). Also, the growth rate σ^M is not strictly zero. Comparing these equations, we can see that the global stability of the mean flow gives a good prediction of the frequency of the limit-cycle, if

$$|\nu_i/\mu_i| \ll 1 \tag{17}$$

and that the mean flow is marginally stable, if

$$|\nu_r/\mu_r| \ll 1 \tag{18}$$

Since μ and ν, respectively, result from interactions of the marginal global mode with the zeroth-order and second-order harmonics, the above criteria can be physically interpreted as the predominance of the zeroth-order harmonic in the saturation process. For the case of the flow around a cylinder, $|\nu_r/\mu_r| \approx |\nu_i/\mu_i| \approx 0.03$ is obtained, which explains that $\sigma^M \approx 0$ and $\omega^M \approx \omega^{\mathrm{LC}}$. This gives a theoretical justification of the results of Barkley [49]. It can be further shown that the two conditions stated above are not satisfied for the case of an open-cavity flow. Consequently, the associated mean flow is not stable, and the frequency of its global mode is not equal to the frequency of the observed unsteadiness.

4 Sensitivity of Eigenvalues and Open-Loop Control

First, we will show how the use of the modal basis defined in Sec. 2.1 may yield an elementary form of sensitivity and open-loop control approach (Sec. 4.1). We will then see how an adjoint global mode can be used to acquire information about the sensitivity of an eigenvalue (Sec. 4.2) or to predict the influence of a small control cylinder on the dynamics of a flow (Sec. 4.3).

4.1 Toward Sensitivity and Open-Loop Control. Let us determine a forcing $\hat{\mathbf{f}}$ that maximizes the response $\hat{\mathbf{u}}$ at a given frequency. The equation that links $\hat{\mathbf{f}}$ to $\hat{\mathbf{u}}$ is given by

$$(i\omega I - \mathcal{A})\hat{\mathbf{u}} = \hat{\mathbf{f}} \tag{19}$$

In the modal basis, the solution of this equation can be written as

$$\hat{\mathbf{u}} = \sum_{j\geq 1} \frac{\langle \tilde{\mathbf{u}}_j, \hat{\mathbf{f}} \rangle}{i\omega - \lambda_j} \hat{\mathbf{u}}_j \tag{20}$$

The response of the jth component of $\hat{\mathbf{u}}$ is thus strongest when the jth eigenvalue λ_j is closest to the excitation frequency $i\omega$ and the structure of the global forcing $\hat{\mathbf{f}}$ closest to the jth adjoint global mode $\tilde{\mathbf{u}}_j$, so as to maximize $\langle \tilde{\mathbf{u}}_j, \hat{\mathbf{f}} \rangle / (i\omega - \lambda_j)$. Hence, to excite the jth global mode $\hat{\mathbf{u}}_j$ (with eigenvalue λ_j) as much as possible, the forcing must be applied at the frequency $\omega = \Im(\lambda_j)$ with a spatial structure of the forcing equal to the one of the adjoint global mode $\tilde{\mathbf{u}}_j$.[8] This control strategy has been explored for various flows. The sensitivity of the three-dimensional nonoscillating marginal global mode for a recirculation bubble in a Cartesian configuration has been considered in Ref. [122]. A similar analysis was carried out for axisymmetric configurations based on the marginal global modes of a sphere and a disk [123].

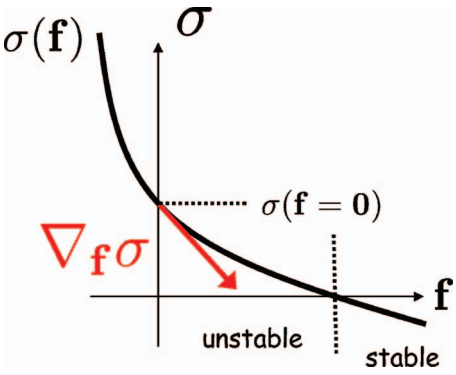

Fig. 9 Open-loop control by action on the base-flow by an external forcing. Diagram displaying the law $\sigma(\mathbf{f})$.

The modal basis introduced previously may also be useful to select the initial condition to maximize energy amplification at large times. To this end, the system is formulated in the time domain

$$\frac{d\mathbf{u}'}{dt} = \mathcal{A}\mathbf{u}', \quad \mathbf{u}'(t=0) = \mathbf{u}^I \tag{21}$$

and the solution can be written as

$$\mathbf{u}' = \sum_{j\geq 1} \langle \tilde{\mathbf{u}}_j, \mathbf{u}^I \rangle e^{\lambda_j t} \hat{\mathbf{u}}_j \tag{22}$$

At large times, this solution is dominated by $\hat{\mathbf{u}}_1$, since this mode is the least damped (or most unstable) mode. The amplitude of this mode is proportional to $\langle \tilde{\mathbf{u}}_1, \mathbf{u}^I \rangle$. Consequently, the initial perturbation that maximizes energy for large times corresponds to the most unstable adjoint global mode $\tilde{\mathbf{u}}_1$. This strategy was pursued for the optimization of the Crow instability in vortex dipoles [134]. It was also used by Marquet et al. [122] and Meliga et al. [123] in their analysis of a recirculation bubble in a Cartesian setting and of the wake of a disk and a sphere.

4.2 Sensitivity of the Eigenvalues. A formalism for open-loop control has been introduced [135] that enables the accurate prediction of the stabilization regions determined experimentally by Strykowski and Sreenivasan [67] and presented in Fig. 4. Following the precursory work of Hill [121], the idea is to consider the eigenvalue λ as a function of the base-flow $\mathbf{u}^B$ and the base-flow $\mathbf{u}^B$, in turn, as a function of an external forcing $\mathbf{f}$. This forcing is intended to model the presence of a small control cylinder. This functional relation is formalized as

$$\mathbf{f} \xrightarrow{\mathbf{R}(\mathbf{u}^B)+\mathbf{f}=\mathbf{0}} \mathbf{u}^B \xrightarrow{\mathcal{A}(\mathbf{u}^B)\hat{\mathbf{u}}=\lambda\hat{\mathbf{u}}} \lambda \tag{23}$$

The control problem is illustrated in Fig. 9. The horizontal axis represents the forcing $\mathbf{f}$ while the vertical axis displays the amplification rate $\sigma = \Re(\lambda)$. The continuous curve represents the function $\sigma(\mathbf{f})$. For $\mathbf{f}=\mathbf{0}$, the amplification rate is positive; that is, the uncontrolled system is unstable. To stabilize the system, we try to find a particular forcing $\mathbf{f}$ such that $\sigma(\mathbf{f}) \leq 0$. This problem is difficult to solve owing to the many degrees of freedom of $\mathbf{f}$. We focus on the gradient of the function $\sigma(\mathbf{f})$ evaluated at $\mathbf{f}=\mathbf{0}$, that is, for the case of an uncontrolled system. This will provide us with invaluable information regarding the most sensitive regions for control based on the underlying physics. We note that the nonlinear optimization problem that uses gradient calculations for descent algorithms will not be addressed in this review. Given the expression $\lambda(\mathbf{f}) = \lambda(\mathbf{u}^B(\mathbf{f}))$, the evaluation of the gradient of the function $\lambda(\mathbf{f})$ requires prior knowledge of the gradient of the func-

[8] It should be noted that this approach is only rigorously justified in the case of a marginal global mode forced in the vicinity of its natural frequency. In fact, it is the entire sum in Eq. (20) that should be considered as the functional objective and not just the response in a particular component. The relevant concept here should be the singular value decomposition of the resolvent that seeks the maximum response associated with a given forcing energy. This will be further discussed in the section dealing with noise-amplifiers in Sec. 6.

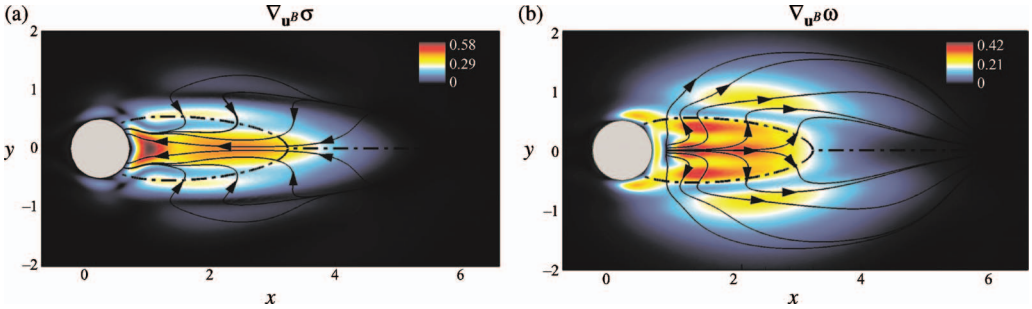

Fig. 10 Flow around a cylinder at Re=47 and sensitivities associated with a modification of the base-flow. (*a*) Sensitivity of the amplification rate. (*b*) Sensitivity of the frequency. Adapted from Ref. [135].

tion $\lambda(\mathbf{u}^B)$. This requirement is the subject of Sec. 4.2.1; the complete evaluation of the gradient of $\lambda(\mathbf{f})$ is the focus of Sec. 4.2.4. The gradient of $\lambda(\mathbf{u}^B)$ can be interpreted as the sensitivity of the eigenvalue with respect to a modification of the base-flow. A local version of this theory has been derived by Bottaro et al. [117]; in what follows, this formalism is extended to the global framework. In Sec. 4.2.2, we address the "wavemaker" notion, which is meant to identify the regions in space that are at the very origin of the instability. In Sec. 4.2.3, the expression of the gradient of $\lambda(\mathbf{u}^B)$ will reveal that the stabilization or destabilization of a flow can be linked either to a strengthening of the downstream advection of the perturbations or to a weakening of their production.

4.2.1 Sensitivity of the Eigenvalues to a Modification of the Base-Flow. Let λ be an eigenvalue associated with a direct global mode $\hat{\mathbf{u}}$ via eigenvalue problem (5). Recalling that λ is a function of $\mathbf{u}^B$, the following expression can be obtained by differentiation:

$$\delta\lambda = \langle \nabla_{\mathbf{u}^B}\lambda, \delta\mathbf{u}^B \rangle \tag{24}$$

The quantity $\nabla_{\mathbf{u}^B}\lambda$, for which an explicit expression will be given in this subsection, represents the *sensitivity of an eigenvalue to a modification of the base-flow*. It is a complex vector field defined over the entire flow domain; its real part (imaginary) defines the sensitivity of the amplification rate $\nabla_{\mathbf{u}^B}\sigma=\Re(\nabla_{\mathbf{u}^B}\lambda)$ (the sensitivity of the frequency $\nabla_{\mathbf{u}^B}\omega=-\Im(\nabla_{\mathbf{u}^B}\lambda)$) to a modification of the base-flow. The variation $\delta\lambda$ in Eq. (24) is defined using the scalar product $\langle\cdot,\cdot\rangle$. As will be shown, the gradient $\nabla_{\mathbf{u}^B}\lambda$ depends on the choice of the scalar product through the computation of adjoint quantities, but the variation $\delta\lambda$ in Eq. (24) is intrinsic. Generally speaking, it can be shown that for any variation $\delta\mathcal{A}$ of the Jacobian $\mathcal{A}$ the variation $\delta\lambda$ of the eigenvalue satisfies

$$\delta\lambda = \langle \tilde{\mathbf{u}}, \delta\mathcal{A}\hat{\mathbf{u}} \rangle \tag{25}$$

where $\tilde{\mathbf{u}}$ is the adjoint eigenvector given by $\mathcal{A}^*\tilde{\mathbf{u}}=\lambda^*\tilde{\mathbf{u}}$ (see Eq. (8)). The adjoint global mode is normalized such that $\langle\tilde{\mathbf{u}},\hat{\mathbf{u}}\rangle=1$. A specific variation of the matrix $\delta\mathcal{A}$ will now be specified, which represents a modification of the base-flow. Let us recall that the Jacobian $\mathcal{A}$ is a function of the base-flow $\mathbf{u}^B$. After differentiation, the matrix $\mathcal{B}(\mathbf{u}^B,\hat{\mathbf{u}})$ is obtained as follows:

$$\delta\mathcal{A}\hat{\mathbf{u}} = \underbrace{\frac{\partial}{\partial\mathbf{u}^B}[\mathcal{A}(\mathbf{u}^B)\hat{\mathbf{u}}]}_{\mathcal{B}(\mathbf{u}^B,\hat{\mathbf{u}})}\delta\mathbf{u}^B \tag{26}$$

After substituting this expression into Eq. (25), we obtain $\delta\lambda=\langle\mathcal{B}(\mathbf{u}^B,\hat{\mathbf{u}})^*\tilde{\mathbf{u}},\delta\mathbf{u}^B\rangle$ where $\mathcal{B}(\mathbf{u}^B,\hat{\mathbf{u}})^*$ is the adjoint matrix associated with $\mathcal{B}(\mathbf{u}^B,\hat{\mathbf{u}})$ based on the scalar product $\langle\cdot,\cdot\rangle$. After identifying this expression with Eq. (24), a final expression for the sensitivity of the eigenvalue to a modification of the base-flow is obtained as follows:

$$\nabla_{\mathbf{u}^B}\lambda = \mathcal{B}(\mathbf{u}^B,\hat{\mathbf{u}})^*\tilde{\mathbf{u}} \tag{27}$$

For the incompressible Navier–Stokes equations, it was shown [135] that an explicit expression of gradient (27) may be obtained in the form

$$\nabla_{\mathbf{u}^B}\lambda = -[\nabla\hat{\mathbf{u}}]^*\cdot\tilde{\mathbf{u}} + \nabla\tilde{\mathbf{u}}\cdot\hat{\mathbf{u}}^* \tag{28}$$

This gradient[9] is the sum of two terms, each of which involving the direct global mode $\hat{\mathbf{u}}$ and the adjoint global mode $\tilde{\mathbf{u}}$. For the flow around a cylinder at Re=47, the sensitivity of the amplification rate $\nabla_{\mathbf{u}^B}\sigma=\Re(\nabla_{\mathbf{u}^B}\lambda)$ and the sensitivity of the frequency $\nabla_{\mathbf{u}^B}\omega=-\Im(\nabla_{\mathbf{u}^B}\lambda)$ are displayed in Figs. 10(*a*) and 10(*b*). The streamlines of these fields are represented by continuous lines, their direction is indicated by small arrows, and the modulus of the fields is displayed by colors. The amplitudes of both fields tend to zero far from the cylinder, which is in agreement with the fact that the direct and adjoint modes vanish upstream and downstream of the cylinder, respectively. The most sensitive region for the amplification rate is located just downstream of the cylinder on the symmetry axis near $(x=1,y=0)$. As expected, a reduction in the back-flow velocity within this zone, $\delta\mathbf{u}^B=+\mathbf{e}_x$ (the recirculation bubble becomes smaller), stabilizes the system since the vectors $\nabla_{\mathbf{u}^B}\sigma$ and $\delta\mathbf{u}^B$ are parallel but directed in opposite directions in this region. As for frequency changes (see Fig. 10(*b*)), an increase in the frequency is observed. These results are in agreement with those presented in Sec. 3: The action of the nonlinearities reduces the size of the recirculation zone (since $u_2^{|A|^2}>0$), the frequency associated with the mean flow increases, but its amplification rate decreases. More precisely, we see that the eigenvalue defined in Eq. (16) and associated with the mean flow $\lambda^M=\sigma^M+i\omega^M$ can be linked to the eigenvalue associated with the base-flow $\lambda^B=\omega_0+\varepsilon\kappa$, as follows:

$$\lambda^M = \lambda^B + \varepsilon\frac{\kappa_r}{\mu_r+\nu_r}\langle\nabla_{\mathbf{u}^B}\lambda,\hat{\mathbf{u}}_2^{|A|^2}\rangle \tag{29}$$

The importance of both the sensitivity field $\nabla_{\mathbf{u}^B}\lambda$ and the zeroth-order harmonic $\hat{\mathbf{u}}_2^{|A|^2}$ for determining the stability properties of the mean flow arises clearly from this expression.

4.2.2 The Wavemaker Concept. The wavemaker concept may be introduced in the case of weakly-non-parallel flows by considering the linear saddle-point criterion [45,137]. Indeed, the associated theory identifies a specific spatial position (in the complex x-plane, where x is the streamwise coordinate), which acts as a wavemaker, providing a precise frequency selection criterion and revealing some important insights pertaining to the forcing of

[9]Meliga [136] analyzed this gradient in the case of compressible Navier–Stokes equations. He showed for an axisymmetric bluff body how the sensitivity fields may be used to study the effect of compressibility on the instability.

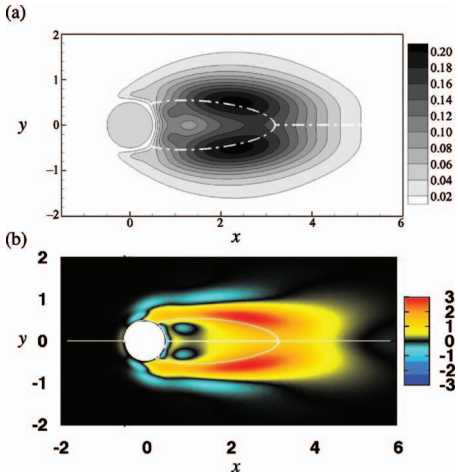

Fig. 11 Flow around a cylinder. (*a*) Wavemaker region for Re =50 according to Giannetti and Luchini [59]. (*b*) Wavemaker region for Re=47 identified by the field *W* in the vicinity of the bifurcation threshold.

these modes. Chomaz [44] and Giannetti and Luchini [59] then tried to define a wavemaker region in the case of a strongly-non-parallel flow. It relies on the concept of local feedback acting at the perturbation level. This feedback is modeled by a volume forcing in the momentum equations and is taken proportional to the perturbation, i.e., $\phi(x,y)\hat{\mathbf{u}}$. The feedback function $\phi(x,y)$ allows us to localize this feedback in regions of interest within the flow domain. The modified eigenvalue problem becomes

$$(\mathcal{A} + \phi(x,y)I)\hat{\mathbf{u}} = \lambda\hat{\mathbf{u}} \tag{30}$$

The derivation that follows is a reformulation of the ideas of Chomaz [44] and Giannetti and Luchini [59] using a gradient-based formalism. The eigenvalue λ depends on the feedback function $\phi(x,y)$. In particular, if $\phi=0$, Eq. (30) yields the original eigenvalue problem (5). We may show that $\delta\lambda=\langle\nabla_\phi\lambda,\delta\phi\rangle$ with

$$\nabla_\phi\lambda(x,y) = \tilde{\mathbf{u}}(x,y)\cdot\hat{\mathbf{u}}(x,y) \tag{31}$$

In this expression, $\tilde{\mathbf{u}}$ is the adjoint global mode associated with $\hat{\mathbf{u}}$, which satisfies $(\mathcal{A}^*+\phi(x,y)^*I)\tilde{\mathbf{u}}=\lambda^*\tilde{\mathbf{u}}$ and is normalized such that $\langle\tilde{\mathbf{u}},\hat{\mathbf{u}}\rangle=1$. The expression of the gradient given in Eq. (27) is structurally analogous to the simpler one given here. If the change in feedback function $\delta\phi$ is equal to a Dirac function located at (x_0,y_0), then $\delta\lambda(x_0,y_0)=\tilde{\mathbf{u}}(x_0,y_0)\cdot\hat{\mathbf{u}}(x_0,y_0)$, and the following relation given by Chomaz [44] and Giannetti and Luchini [59]:

$$|\delta\lambda(x_0,y_0)| \le \|\tilde{\mathbf{u}}(x_0,y_0)\| \times \|\hat{\mathbf{u}}(x_0,y_0)\| \tag{32}$$

is recovered from Cauchy–Schwartz. The right-hand-side of this expression is used to identify the wavemaker region. For the flow around a cylinder at Re=50 this latter expression is presented in Fig. 11(*a*). Giannetti and Luchini [59] noted that the locations of the maxima in this figure are consistent with those given by the linear saddle-point criterion, justifying their approach. To underline the effectiveness of their concept, Chomaz [44] and Giannetti and Luchini [59] also argued that the wavemaker region resembled the stabilization regions identified experimentally by Strykowski and Sreenivasan [67], which are recalled in Fig. 4. A quick comparison of Figs. 11(*a*) and 4 shows that the wavemaker concept indeed roughly reproduces the experimentally obtained stabilizing regions. Note that Luchini et al. [138] extended the wavemaker concept to finite-amplitude oscillations, by using a Floquet stability analysis.

We propose here an alternative definition of the wavemaker region. For a given Reynolds number $\varepsilon=\mathrm{Re}_c^{-1}-\mathrm{Re}^{-1}$ (which is not necessarily small), we first note that the amplification rate of the leading global mode for the Reynolds number ε is given by $\sigma(\varepsilon)-\sigma(0)=\int_0^\varepsilon(d\sigma/d\varepsilon)d\varepsilon'$, where $\sigma(0)=0$ since at the bifurcation threshold the amplification rate is zero. The eigenvalue $\lambda=\sigma+i\omega$ is a function of the base-flow $\mathbf{u}^B$ and of the Reynolds number ε (since ε explicitly appears in eigenproblem (5) in the diffusion part $(\mathrm{Re}_c^{-1}-\varepsilon)\Delta\hat{\mathbf{u}}$). Also, the base-flow is a function of the Reynolds number: $\mathbf{u}^B(\varepsilon)$. Hence, the eigenvalue is solely a function of the Reynolds number: $\lambda(\mathbf{u}^B(\varepsilon),\varepsilon)$. After differentiation, we obtain $d\lambda/d\varepsilon=(\partial\lambda/\partial\mathbf{u}^B)(d\mathbf{u}^B/d\varepsilon)+\partial\lambda/\partial\varepsilon$. The two parts of this expression reflect two distinct mechanisms. The first is related[10] to the modification of the base-flow: $(\partial\lambda/\partial\mathbf{u}^B)(d\mathbf{u}^B/d\varepsilon)=\langle\nabla_{\mathbf{u}^B}\lambda,\mathcal{A}^{-1}(\Delta\mathbf{u}^B)\rangle$, while the second refers[11] to an increase in the Reynolds number in the governing equations: $\partial\lambda/\partial\varepsilon=-\langle\tilde{\mathbf{u}},\Delta\hat{\mathbf{u}}\rangle$. Hence, considering the real part of $d\lambda/d\varepsilon$, the amplification rate for the Reynolds number ε may be given in closed form as an integral in space of a scalar field $W(\varepsilon)$ as follows:

$$\sigma(\varepsilon) = \int\int W(\varepsilon)dxdy \tag{33}$$

$$W(\varepsilon) = \int_0^\varepsilon \{\nabla_{\mathbf{u}^B}\sigma\cdot[\mathcal{A}^{-1}(\Delta\mathbf{u}^B)] - \Re(\tilde{\mathbf{u}}\cdot\Delta\hat{\mathbf{u}})\}d\varepsilon' \tag{34}$$

where $\cdot$ refers to the Hermitian scalar product of two vectors. The scalar field $W(\varepsilon)$ defines the wavemaker of the instability at the Reynolds number ε. To compute $W(\varepsilon)$, we may approximate the continuous integral in ε by a discrete sum involving the knowledge of $\nabla_{\mathbf{u}^B}\sigma$, $\mathcal{A}$, $\mathbf{u}^B$, $\tilde{\mathbf{u}}$, and $\hat{\mathbf{u}}$ for some discrete values of ε' within the interval $0\le\varepsilon'\le\varepsilon$. Here, for conciseness, we only represent and discuss the wavemaker W in the vicinity of the bifurcation threshold $|\varepsilon|\ll1$. Hence, $W=(dW/d\varepsilon)d\varepsilon$ and it is more convenient to discuss $(dW/d\varepsilon)$ rather than W. The quantity $dW/d\varepsilon$ is depicted in Fig. 11(*b*) for the flow around a cylinder. Since the integral over space of this quantity yields the amplification rate σ/ε, the regions of the flow where this quantity is zero do not play a role in the instability. The wavemaker will therefore be defined as the regions where this quantity is nonzero. We remark that regions characterized by positive values contribute favorably to the instability whereas regions of negative values inhibit the instability. We also emphasize that the present definition of the wavemaker also reflects the existence of a feedback mechanism as proposed by Giannetti and Luchini [59]. But rather than assuming a local feedback, i.e., a local force depending on the velocity, the present definition is based on a global feedback. Moreover, this forcing does not only depend on the perturbation $\hat{\mathbf{u}}$, as assumed by Giannetti and Luchini [59], but also on the base-flow $\mathbf{u}^B$. Despite such differences in the two analyses, a comparison of Figs. 11(*a*) and 11(*b*) shows that similar wavemaker regions are identified here. Hence, this definition of the wavemaker is also consistent with the initial definition of the wavemaker in the weakly-non-parallel case.

4.2.3 Advection/Production Decomposition. The two terms that make up the expression of gradient (28) have a different origin and physical meaning. Let us recall that the global mode $\hat{\mathbf{u}}$ is governed by the equation

[10]The base-flow correction $d\mathbf{u}^B/d\varepsilon$ is defined by $\mathbf{R}(\mathbf{u}^B+d\mathbf{u}^B,\varepsilon+d\varepsilon)=\mathbf{0}$. Linearizing this equation and noting that $\partial\mathbf{R}/\partial\varepsilon=-\Delta\mathbf{u}^B$, we obtain $\mathcal{A}d\mathbf{u}^B-\Delta\mathbf{u}^Bd\varepsilon=\mathbf{0}$, which yields $d\mathbf{u}^B/d\varepsilon=\mathcal{A}^{-1}(\Delta\mathbf{u}^B)$. Note that Δ refers here to the matrix related to the Laplace operator.

[11]The variation of the eigenvalue $d\lambda$ with respect to an increase in the Reynolds number $d\varepsilon$—with the base-flow $\mathbf{u}^B$ frozen—may be obtained from Eq. (25), using the following perturbation matrix: $\delta\mathcal{A}=-\Delta$, i.e., the negative of the matrix standing for the Laplace operator.

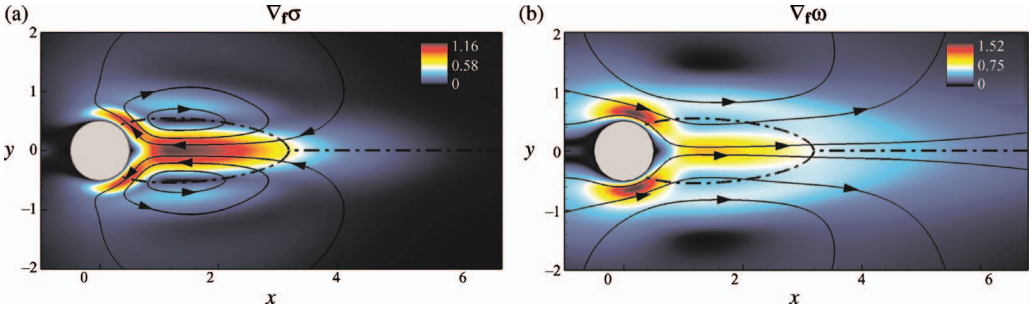

Fig. 12 Flow around a cylinder at Re=47 and sensitivities associated with a steady forcing of the base-flow. (*a*) Sensitivity of the amplification rate. (*b*) Sensitivity of the frequency. Adapted from Ref. [135].

$$\lambda\hat{\mathbf{u}} + \nabla\hat{\mathbf{u}}\cdot\mathbf{u}^{\mathbf{B}} + \nabla\mathbf{u}^{\mathbf{B}}\cdot\hat{\mathbf{u}} = -\nabla\hat{p} + \frac{1}{\mathrm{Re}}\Delta\hat{\mathbf{u}}, \quad \nabla\cdot\hat{\mathbf{u}} = 0 \tag{35}$$

As explained in Sec. 2.3, the base-flow $\mathbf{u}^B$ appears twice in this equation: $\nabla\hat{\mathbf{u}}\cdot\mathbf{u}^{\mathbf{B}}$ describes the advection of perturbations whereas $\nabla\mathbf{u}^{\mathbf{B}}\cdot\hat{\mathbf{u}}$ stands for the production of perturbations. It can be shown that these two terms produce, respectively, the two terms in gradient expression (28). The resulting sensitivity measure then breaks down as follows:

$$\nabla_{\mathbf{u}^B}\lambda = \nabla_{\mathbf{u}^B}\lambda\big|^{(A)} + \nabla_{\mathbf{u}^B}\lambda\big|^{(P)} \tag{36}$$

with $\nabla_{\mathbf{u}^B}\lambda\big|^{(A)} = -[\nabla\hat{\mathbf{u}}]^*\cdot\tilde{\mathbf{u}}$ and $\nabla_{\mathbf{u}^B}\lambda\big|^{(P)} = \nabla\tilde{\mathbf{u}}\cdot\hat{\mathbf{u}}^*$. One may then deduce [135] that the destabilization of a global mode by a base-flow modification $\delta\mathbf{u}^B$ is

1. either due to a weaker advection of the perturbations by the base-flow $(\nabla_{\mathbf{u}^B}\sigma\big|^{(A)}\cdot\delta\mathbf{u}^B > 0)$
2. or due to a stronger production of perturbations $(\nabla_{\mathbf{u}^B}\sigma\big|^{(P)}\cdot\delta\mathbf{u}^B > 0)$

These ideas are reminiscent of certain concepts of the local theory by Huerre and Monkewitz [139]; we know that absolute instability is promoted either because the downstream advection becomes weaker or because the production mechanism becomes more significant. Let us also note that these two effects cannot be isolated within the classical convective/absolute framework [13]. However, this decomposition appears rather naturally from a sensitivity approach of the eigenvalue with respect to base-flow modifications.

For the flow around a cylinder at Re=47, the sensitivity field associated with advection is directed upstream [135] throughout the flow domain; as expected, an increase in the velocity of the base-flow tends to stabilize the global mode, by strengthening of the downstream perturbation advection. It was also shown that the sensitivity field related to advection is much smaller than the sensitivity field associated with the production of perturbations. We thus conclude that any stabilization or destabilization of flow will be due mainly to the modification of the mechanism responsible for perturbation production rather than downstream perturbation advection.

4.2.4 Sensitivity of the Eigenvalues to a Steady Forcing of the Base-Flow. We now return to our initial objective: a measure of eigenvalue sensitivity to a forcing $\mathbf{f}$ of the base-flow. This is defined by the following expression:

$$\delta\lambda = \langle\nabla_{\mathbf{f}}\lambda, \delta\mathbf{f}\rangle \tag{37}$$

where the term $\nabla_{\mathbf{f}}\lambda$ corresponds to this sensitivity. It represents a complex vector field whose real part is related to the sensitivity of the amplification rate to a steady forcing of the base-flow $\nabla_{\mathbf{f}}\sigma = \Re(\nabla_{\mathbf{f}}\lambda)$ while its imaginary part measures the sensitivity of the frequency $\nabla_{\mathbf{f}}\omega = -\Im(\nabla_{\mathbf{f}}\lambda)$. To give an explicit expression of this sensitivity field, let us recall that the base-flow $\mathbf{u}^B$ depends on the steady forcing $\mathbf{f}$ via the equation governing the base-flow, $\mathbf{R}(\mathbf{u}^B) + \mathbf{f} = \mathbf{0}$. By differentiating this equation, we obtain the expression $\mathcal{A}\delta\mathbf{u}^B + \delta\mathbf{f} = \mathbf{0}$. Substituting the expression for $\delta\mathbf{u}^B$ into Eq. (24), the following result is obtained:

$$\nabla_{\mathbf{f}}\lambda = -\mathcal{A}^{*-1}\nabla_{\mathbf{u}^B}\lambda \tag{38}$$

where $\mathcal{A}^*$ is again the adjoint matrix corresponding to $\mathcal{A}$. As discussed previously, to calculate the sensitivity to a steady forcing of the base-flow, the sensitivity to a modification of the base-flow should be evaluated first. Application of the matrix $-\mathcal{A}^{*-1}$ enables us to go from a sensitivity to a modification of the base-flow to a sensitivity to a steady forcing of the base-flow. For flow around a cylinder at Re=47, both fields $\nabla_{\mathbf{f}}\sigma$ and $\nabla_{\mathbf{f}}\omega$ are displayed in Figs. 12(*a*) and 12(*b*). These are appreciably different from those presented in Figs. 10(*a*) and 10(*b*), which only show sensitivities to a modification of the base-flow. Despite this observation, general trends are identical. Thus, a force placed inside the recirculation bubble and acting in the downstream direction stabilizes the flow-field and increases the frequency.

4.3 Open-Loop Control With a Small Control Cylinder. In this section we use the sensitivities of the amplification rate and the frequency associated with a steady forcing of the base-flow, which were presented in Figs. 12(*a*) and 12(*b*), to predict the stabilization zones for the flow around a cylinder described by Strykowski and Sreenivasan [67] and displayed in Fig. 4. For this reason, it is necessary to find a forcing field $\mathbf{f}$ that adequately describes the presence of a small control cylinder located at (x_0, y_0). This modeling is, in fact, a rather complex problem. It was addressed by Hill [121], then formalized by Marquet et al. [140] by means of an asymptotic expansion based on two small parameters, one accounting for the amplitude of the marginal global mode, and the other describing the size of the small control cylinder. The small control cylinder acts both on the level of the base-flow and the level of the perturbations by imposing a zero velocity on these two flow-fields at the location of the control cylinder. It turns out that its impact on the perturbation level remains rather weak (at least for the case of the bifurcation of the flow around a cylinder at Re=47). We therefore restrict our discussion to the forcing's influence on the base-flow. To model the presence of the small control cylinder on the base-flow, we note that the base-flow $\mathbf{u}^B$ exerts a force $\mathbf{F}$ on the small control cylinder. Invoking the action/reaction principle, the small control cylinder then exerts the force $-\mathbf{F}$ on the base-flow $\mathbf{u}^B$. We hence obtain a force field $\mathbf{f}$, which is zero everywhere except at the location of the small control cylinder where it is represented by a Dirac function of intensity $-\mathbf{F}$. It thus remains to model the force $\mathbf{F}$ exerted on the small cylinder by the base-flow. In this review article, only the simplest modeling is considered: We focus on the direction of the force and leave aside its strength. We assume that

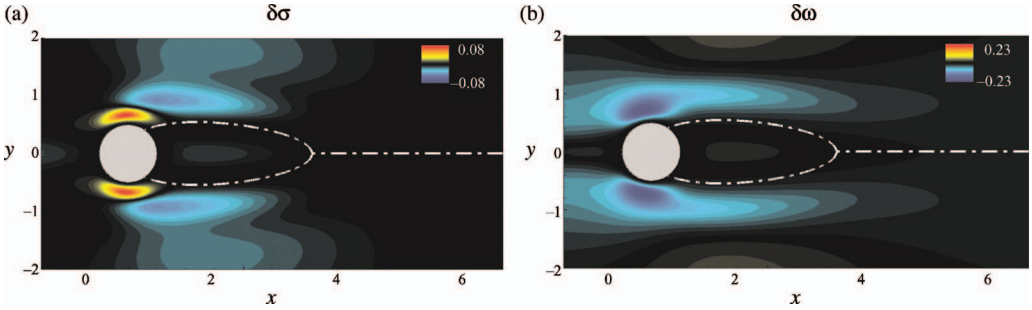

Fig. 13 Flow around a cylinder at Re=47. (*a*) Variation of the amplification rate with respect to the placement of a control cylinder of infinitesimal size located at the current point. (*b*) Associated variation of the frequency. Adapted from Ref. [135].

the force exerted on the small cylinder, located at (x_0, y_0), is parallel but opposite to the velocity vector of the base-flow at (x_0, y_0). We have

$$\delta\mathbf{f}(x,y) = -\mathbf{u}^B(x_0,y_0)\,\delta(x-x_0,y-y_0) \tag{39}$$

Hence, the small control cylinder is only subjected to a drag force[12] that is assumed steady.[13] From Eq. (37), the variation of the eigenvalue $\delta\lambda(x_0,y_0)$ based on the presence of a small control cylinder at (x_0,y_0) is thus given by

$$\delta\lambda(x_0,y_0) = -\nabla_{\mathbf{f}}\lambda(x_0,y_0)\cdot\mathbf{u}^B(x_0,y_0) \tag{40}$$

This field corresponds to the negative scalar product at each point between the sensitivity field $\nabla_{\mathbf{f}}\lambda$ and the base-flow $\mathbf{u}^B$. It takes into account the level of sensitivity, the amplitude of the base-flow velocity, as well as the respective directions of the sensitivity and the base-flow. The real and imaginary parts of this complex field are depicted in Figs. 13(*a*) and 13(*b*). These two fields represent, respectively, the variations of growth rate and frequency as a small control cylinder is placed into the flow at a given point. If the figure on the left is compared with the isocontour for Re=48 in Fig. 4, we observe very strong analogies: The two stabilization zones determined by Strykowski and Sreenivasan [67] are well recovered, their spatial extent and location seem well predicted, and the destabilizing zone near the small control cylinder, where the boundary-layer detaches, is also identified. In Fig. 13(*b*), we notice that the introduction of a small control cylinder into the flow always yields a reduced frequency of the unsteadiness. This result is in agreement with the observations of Strykowski and Sreenivasan [67].

The decomposition in terms of advection/production, introduced in Sec. 4.2.3, is used next to provide an interpretation of the stabilization/destabilization phenomenon. We consider a small control cylinder located at the place of maximum stabilization, i.e., at $(x_0,y_0)=(1.2,1)$. The modification of the base-flow associated with the introduction of this cylinder at (x_0,y_0) is given by $\delta\mathbf{u}^B=-\mathcal{A}^{-1}\delta\mathbf{f}$, with the force $\delta\mathbf{f}$ defined by Eq. (39). Thus, the variation of the eigenvalue can be evaluated using either the sensitivity field associated with a steady forcing of the base-flow: $\delta\lambda=\langle\nabla_{\mathbf{f}}\lambda,\delta\mathbf{f}\rangle$, or the sensitivity field associated with a modification of the base-flow: $\delta\lambda=\langle\nabla_{\mathbf{u}^B}\lambda,\delta\mathbf{u}^B\rangle$. Resorting to the decomposition introduced in Sec. 4.2.3, it is found that stabilization is due to a weaker production mechanism; the advection properties, on the other hand, are slightly destabilizing.

A model for the forcing amplitude $\mathbf{F}$ was not required here since the computation of the stabilizing zones at the bifurcation threshold is independent of such a model. However, a model becomes essential if we want to determine the stabilization regions at supercritical Reynolds numbers. This work was completed in Ref. [135], and the final result is reproduced in Fig. 14. We note that this figure matched rather well the experimental results of Strykowski and Sreenivasan [67] shown in Fig. 4.

5 Model Reduction and Closed-Loop Control

Contrary to open-loop control, which modifies the base-flow in order to stabilize the unstable eigenvalues, closed-loop control acts directly on the perturbations. It is by nature unsteady and consists of an opposition control strategy where structures are generated by the actuator that annihilates the unstable perturbations that would otherwise develop naturally. A measurement of the flow is necessary to estimate the phase and the amplitude of the disturbance after which one constructs a control law linking the measurement to the action. This control law must be simple and designed for application in real-time in an experiment. To this end, it should be based on only a moderate number of degrees of freedom, at the most on the order of a few tens. The control law is obtained within the linear quadratic Gaussian (LQG) control framework, which requires the implementation of an estimator. The estimator and the controller are both based on a model of the flow that must be low-dimensional and reproduce certain flow properties, as will be specified below. Model reduction techniques based on Petrov–Galerkin projections and the choice of a basis (such as POD, balanced, or global modes) are required to build this model. In this section, we will design and implement a closed-loop control strategy for an unstable open-cavity flow. The configuration of this flow is first described (Sec. 5.1). For the chosen parameters, the flow is unstable, and a reduced-order-model of the unstable subspace is constructed based on the unstable global modes. Next, we concentrate on the stable subspace. First, we show why the stable subspace has to be modeled appro-

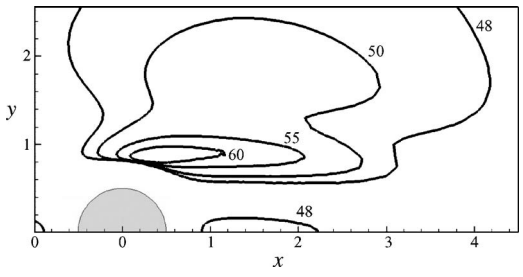

Fig. 14 Flow around a cylinder. Stabilization zones for the unsteadinesses as obtained by the sensitivity approach for different Reynolds numbers. The results should be compared with the experimental results displayed in Fig. 4. Adapted from Ref. [135].

[12]This is incorrect if the small control cylinder is located in a shear flow. In this case, a lift force must also be taken into account.

[13]For this, a control cylinder of a sufficiently small diameter is chosen such that the Reynolds number based on the local velocity of the base-flow and the diameter of the small control cylinder is lower than $\mathrm{Re}_c=47$.

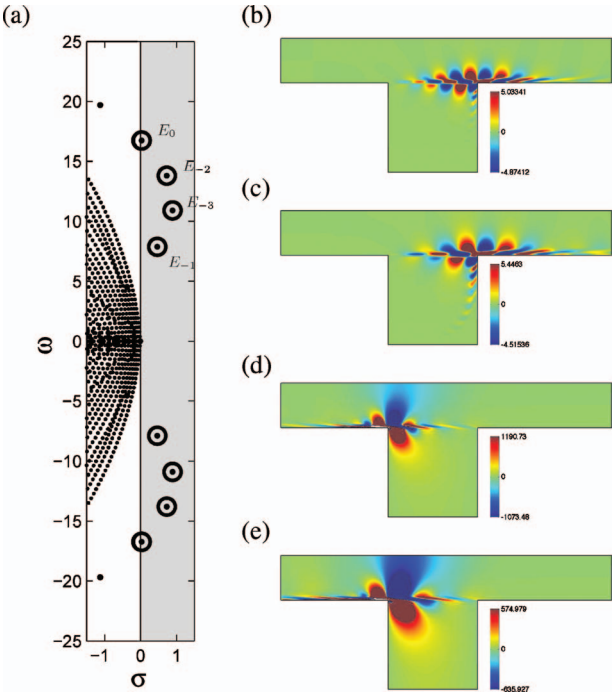

Fig. 15 Flow over an open cavity for Re=7500. (*a*) Spectrum of the matrix $\mathcal{A}$, (*b*) real part of the streamwise velocity of the most unstable global mode, (*c*) same for the unstable global mode with the lowest frequency, (*d*) likewise for the most unstable adjoint global mode, and (*e*) likewise for the unstable adjoint global mode with the lowest frequency. Adapted from Ref. [141].

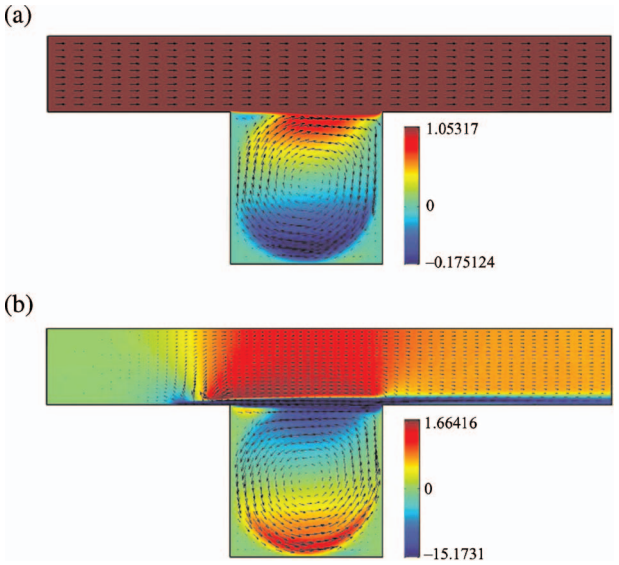

Fig. 16 Flow over an open cavity for Re=7500 visualized by streamwise velocity contours and velocity vectors. (*a*) Base-flow. (*b*) Control matrix $\mathcal{C}$. Adapted from Ref. [141].

priately (Sec. 5.2) after which we proceed to determine a model for this stable subspace (Sec. 5.3). Finally (Sec. 5.4), a closed-loop control scheme based on the LQG control framework is implemented where various reduced-order-models (global modes, balanced modes, and POD-modes) will be considered and tested as their effectiveness in stabilizing the flow.

5.1 Configuration and Reduced-Order-Model for the Unstable Subspace. The configuration has been presented in Fig. 5. The actuator is located upstream of the cavity and consists of blowing/suction at the wall described by the law $\rho(t)$. The sensor, taking the measurement $m(t)$, is situated downstream from the cavity and reads the wall shear-stress integrated over a small segment.

This flow exhibits a first Hopf bifurcation at a Reynolds number equal to $\mathrm{Re}_c=4140$ [38]. For the supercritical Reynolds number of Re=7500, the spectrum of the flow, which is displayed in Fig. 15(*a*), shows four unstable (physical) global modes (eight if the complex conjugates are counted). The spatial structures of the two unstable global modes with the lowest frequency are presented in Figs. 15(*b*) and 15(*c*). These structures, visualized by the streamwise velocity component, correspond to Kelvin–Helmholtz instabilities located atop the shear-layer. The dynamics of the perturbation $\mathbf{u}'$ is governed by a large-scale state-space model, which is obtained by a spatial discretization of the Navier–Stokes equations linearized about the base-flow for Re=7500. Taking into account the perturbation dynamics, the control, and the measurement, we have

$$\frac{d\mathbf{u}'}{dt} = \mathcal{A}\mathbf{u}' + \mathcal{C}c \tag{41}$$

$$m = \mathcal{M}\mathbf{u}' \tag{42}$$

where $\mathcal{M}$ represents the measurement matrix related to the wall shear-stress measurement mentioned above, and $\mathcal{C}$ denotes the control matrix. This is a single-input-single-output (SISO) problem. Hence, $\mathcal{C}$ and $\mathcal{M}$, respectively, designate matrices of dimension $(n,1)$ and $(1,n)$, where n is the number of degrees of freedom in the state vector $\mathbf{u}'$. The base-flow is shown in Fig. 16(*a*), visualized by contours of the streamwise velocity and velocity vectors. The control matrix $\mathcal{C}$ is obtained by a lifting procedure since the control consists in blowing/suction at the wall. This matrix satisfies $\mathcal{AC}=\mathbf{0}$ together with a unit blowing $(\rho(t)=1)$ boundary condition imposed on the control segment. The resulting flow-field is shown in Fig. 16(*b*). The control function $c(t)$ in Eq. (41) is equal to the negative derivative of the blowing/suction function $\rho(t)$.

A reduced-order-model of these equations is obtained by a Petrov–Galerkin projection onto a bi-orthogonal basis $(\mathcal{W},\mathcal{V})$, which satisfies $\langle\mathcal{W}_i,\mathcal{V}_j\rangle=0$ if $i\neq j$ and $\langle\mathcal{W}_i,\mathcal{V}_j\rangle=1$ if $i=j$. We denote by $\mathcal{W}_i$ and $\mathcal{V}_j$, respectively, the ith and jth vector of the dual and primal bases $\mathcal{W}$ and $\mathcal{V}$. By introducing the reduced variables $\mathbf{u}_i^r=\langle\mathcal{W}_i,\mathbf{u}'\rangle$ (or equivalently $\mathbf{u}'=\Sigma_i\mathcal{V}_i\mathbf{u}_i^r$), the following is obtained:

$$\frac{d\mathbf{u}^r}{dt} = \mathcal{A}^r\mathbf{u}^r + \mathcal{C}^r c \tag{43}$$

$$m = \mathcal{M}^r\mathbf{u}^r \tag{44}$$

where the reduced matrices are defined by $\mathcal{A}^r_{i,j}=\langle\mathcal{W}_i,\mathcal{A}\mathcal{V}_j\rangle$, $\mathcal{C}^r_{i,1}=\langle\mathcal{W}_i,\mathcal{C}\rangle$, and $\mathcal{M}^r_{1,j}=\mathcal{M}\mathcal{V}_j$.

At this point, the following important questions must be raised: Which basis should be chosen and what should be the dimension of this basis? The modal basis, presented in Sec. 2.1 and formed by direct global modes $\hat{\mathbf{u}}_j$, at first looked like a natural choice to us within a linearized framework. This basis comprises both physical global modes representing the dynamics atop the shear-layer and inside the cavity and unphysical global modes (advection-diffusion of perturbations in the freestream). These modes are grouped into the rectangular matrices $\mathcal{V}$ and $\mathcal{W}$, respectively, arranged by decreasing amplification rate. The matrix $\mathcal{A}^r$ is then diagonal, and the values along the diagonal consist of the

dominant eigenvalues of $\mathcal{A}$. The four (physical) unstable global modes (direct and adjoint) represent the core of the reduced-order-model. The unstable subspace of the matrix $\mathcal{A}$ is thus modeled by capturing its dynamic features. This model describes exactly, and with the least number of degrees of freedom, a rich and complex dynamics. The locations of the actuator and sensor were decided such that the controllability coefficients $\mathcal{C}^r_{i,1}$ and the measurement coefficients $\mathcal{M}^r_{1,j}$ are large for the unstable global modes. This is the reason for taking the measurement downstream of the cavity where the unstable direct global modes have significant amplitudes; the actuator is located upstream of the cavity where the control matrix $\mathcal{C}$ and the adjoints of the unstable modes are both large. We recall that Figs. 15(*b*) and 15(*c*) display the two unstable global modes with the lowest frequency. In Figs. 15(*d*) and 15(*e*) the associated adjoint global modes are visualized in the same manner. The coefficient $\mathcal{M}^r_{1,j}$ corresponds to the measurement of the *j*th direct global mode, and the coefficient $\mathcal{C}^r_{i,1}$ corresponds to the scalar product of the *i*th adjoint global mode and the steady unit-control flow-field presented in Fig. 16(*b*).

5.2 Why Is the Modeling of the Stable Subspace Necessary? We will now explain why a reduced-order-model based only on unstable global modes may not be able to yield a stable compensated system. The answer to this question can be formulated as follows. A general action at the upstream edge of the cavity certainly acts on the unstable global modes but may also excite the stable global modes. Due to their stability, the excitation of the stable modes may not be problematic by itself. The problem, however, lies in the fact that these stable modes will corrupt the measurement. In other words, the measurement obtained at the downstream edge of the cavity certainly includes the useful measurement, that is, the measurement associated with the unstable global modes, but also the measurement associated with the stable global modes excited by the actuator. Even though the global modes may be damped, they may nevertheless significantly contribute to the input-output dynamics of the system. If the estimator is based on a reduced-order-model that only incorporates features from the unstable subspace, it will not manage to extract the unstable dynamics from the corrupted measurement. The estimated unstable state will be inaccurate and, as a consequence, the control law based on the estimated unstable flow-field will be ineffective and even lead to instabilities in the compensated system.

To overcome this difficulty, the idea is to incorporate the stable subspace into the reduced-order-model. For this reason, the reduced-order-model should be built not only on the unstable modes but should also contain a certain number of stable modes. But what criterion should be adopted to select them? A naive approach would consist in retaining only the *p* least stable global modes, following the argument that the neglected modes are too damped to contribute significantly to the system's dynamics. Although this strategy has been successfully pursued by Åkervik et al. [39], in general it appears to be erroneous. Indeed, as suggested in the preceding paragraph, it is necessary to select the stable global modes that contribute most to the system's input-output dynamics. To identify these modes, it was suggested [141] to use the following quantity:

$$\Gamma_j = \frac{|\mathcal{C}^r_{j,1}||\mathcal{M}^r_{1,j}|}{|\Re(\mathcal{A}^r_{j,j})|} \tag{45}$$

which is defined for each global mode *j*. Noting that $|\Re(\mathcal{A}^r_{j,j})|$ denotes the damping rate of the *j*th eigenvector, this criterion selects modes, which are highly controllable ($|\mathcal{C}^r_{j,1}|$ large), highly observable ($|\mathcal{M}^r_{1,j}|$ large), and least damped ($|\Re(\mathcal{A}^r_{j,j})|$ small). It may be shown that this criterion represents a good measure of the importance of the *j*th global mode regarding system's input-output dynamics. In Fig. 17, the value of the criterion Γ_j is presented, for each stable global mode, by the color of the eigenvalue. The warmer the color, the more significantly an eigenvalue contributes to the input-output dynamics. The results show that

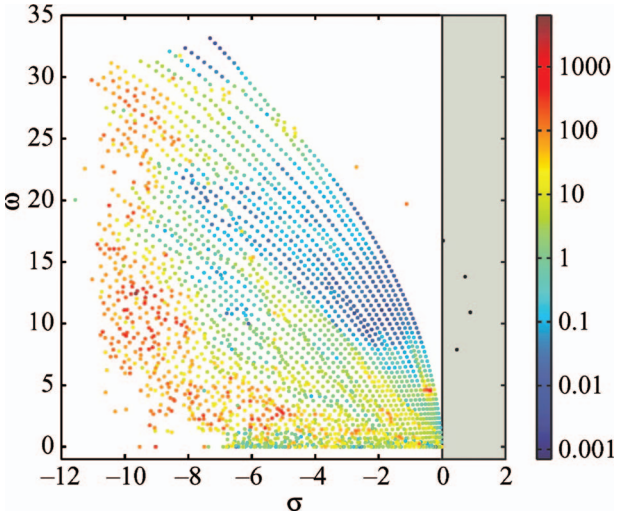

Fig. 17 Flow over an open cavity for Re=7500. Spectrum of the flow with the eigenvalues colored according to the criterion Γ_j. Adapted from Ref. [141].

1. the modes that contribute most to the input-output dynamics are very damped
2. the higher the damping rate, the larger the number of modes, which contribute to the input-output dynamics

For this specific configuration, this observation certainly disqualifies the original idea of a reduced-order-model solely built on global modes. The shortcomings of stable global modes will be further analyzed in Sec. 6.1, where it will be shown that most of the stable global modes in an open-flow configuration display a very bad behavior and that the modal basis constitutes, generally speaking, an ineffective and ill-posed projection basis in open-flows.

This argument has shown the need to model the stable subspace. The selection criterion defined by Γ_j highlighted the importance of the input-output dynamics for this modeling and introduced the concepts of controllability and observability. As for a proper choice of basis for model reduction, we have found that the modeling of the unstable subspace with global modes seems justified and efficient, but that the same is not true for modeling the stable subspace. The (unphysical) stable global modes represent an ineffective and ill-posed basis to reproduce the system's input-output dynamics.

5.3 How Should the Stable Subspace Be Modeled? The properties of a basis suitable for the representation of the stable subspace of $\mathcal{A}$ will now be defined. Since the dynamics of the unstable and stable subspaces are decoupled, it is possible to study the dynamics restricted to the stable subspace of $\mathcal{A}$; i.e.,

$$\frac{d\mathbf{u}'}{dt} = \mathcal{A}\mathbf{u}' + \mathcal{P}_s\mathcal{C}c \tag{46}$$

$$m = \mathcal{M}\mathbf{u}' \tag{47}$$

where $\mathcal{P}_s$ is the projection matrix onto the stable subspace. The initial condition for this simulation is chosen in the stable subspace. The input-output dynamics in this subspace is characterized by the impulse response: $H(t) = \mathcal{M}e^{\mathcal{A}t}\mathcal{P}_s\mathcal{C}$. In an equivalent way, it can be defined by the transfer function, which is the Fourier trans-

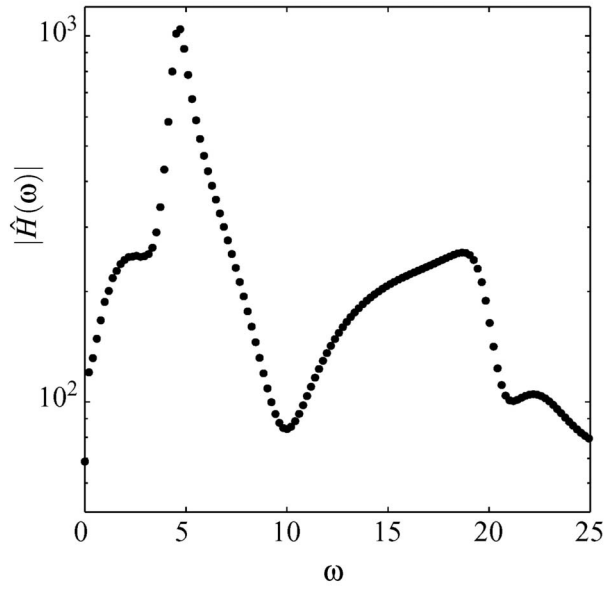

Fig. 18 Flow over an open cavity for Re=7500. Transfer function $|\hat{H}(\omega)|$ representative of the input-output dynamics of the stable subspace. Adapted from Ref. [141].

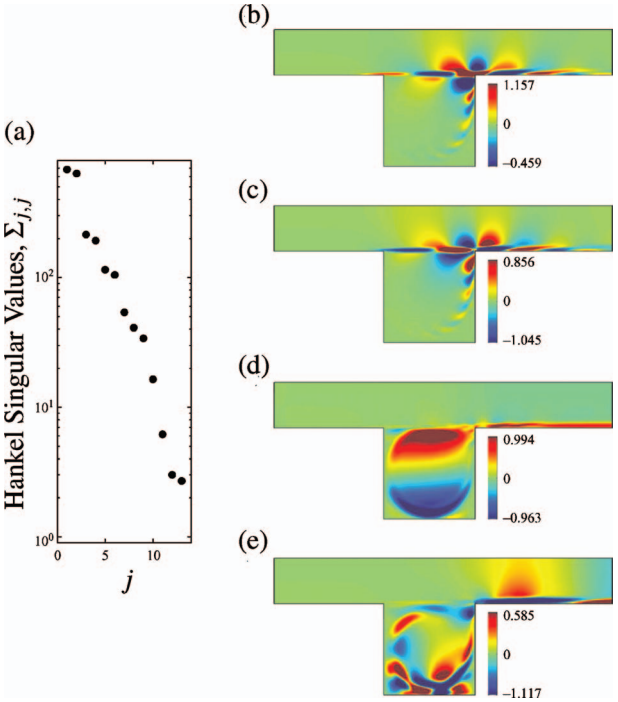

Fig. 19 Flow over an open cavity for Re=7500. (*a*) Singular values of the Hankel matrix. ((*b*)–(*e*)) Streamwise velocity of the 1st, 2nd, 9th, and 13th balanced modes. Adapted from Ref. [141].

form of $H(t)$; we get $\hat{H}(\omega)=\int_{-\infty}^{\infty}H(t)e^{-i\omega t}dt$.[14] The modulus of $\hat{H}(\omega)$ is shown in Fig. 18 for our case study. We observe that a strong response is observed at a frequency $\omega=4.6$. An effective reduced-order basis of the stable subspace is characterized by an accurate representation of the input-output dynamics of the full-system, i.e., by an associated reduced transfer function $\hat{H}^r(\omega)$, which accurately reproduces that of the original system $\hat{H}(\omega)$. The quantification of the difference between the two transfer functions is preferably done using the norm $\|\hat{H}\|_\infty=\sup_\omega|\hat{H}(\omega)|$, since theoretical results are readily available for this norm.

The theory of balanced truncation introduced by Moore [97] yields an algorithm to build a quasi-optimal basis measured in the $\|\cdot\|_\infty$ norm. First, we recall that the input-output dynamics in the stable subspace is characterized by the matrices $(\mathcal{A},\mathcal{P}_s\mathcal{C},\mathcal{M})$. The controllability and observability Gramians are defined as

$$\mathcal{G}_c=\int_0^\infty e^{\mathcal{A}t}\mathcal{P}_s\mathcal{C}\mathcal{C}^*\mathcal{P}_s^*e^{\mathcal{A}^*t}dt \tag{48}$$

$$\mathcal{G}_o=\int_0^\infty e^{\mathcal{A}^*t}\mathcal{P}_s^*\mathcal{M}^*\mathcal{M}\mathcal{P}_s e^{\mathcal{A}t}dt \tag{49}$$

The integrals are convergent because of our restriction to the stable subspaces of $\mathcal{A}$ and $\mathcal{A}^*$. These two matrices define the concept of controllability and observability of a structure $\mathbf{u}'$ of the stable subspace. Thus, $\mathbf{u}'^*\mathcal{G}_c^{-1}\mathbf{u}'$ corresponds to the minimum energy $\int_0^\infty c^2(t)dt$ that has to be expended to drive a system from state $\mathbf{u}'$ to 0 whereas $\mathbf{u}'^*\mathcal{G}_o\mathbf{u}'$ is equal to the maximum measurement $\int_0^\infty m^2(t)dt$ induced by the system if it has been initialized by $\mathbf{u}'$. It is then possible to show that a reduced-order bi-orthogonal basis $(\mathcal{W}_s,\mathcal{V}_s)$ of the stable subspace of $\mathcal{A}$ can be obtained by solving the following eigenvalue problems:

$$\mathcal{G}_c\mathcal{G}_o\mathcal{V}_s=\mathcal{V}_s\Sigma^2 \tag{50}$$

$$\mathcal{G}_o\mathcal{G}_c\mathcal{W}_s=\mathcal{W}_s\Sigma^2 \tag{51}$$

where $\mathcal{W}_s$ has been normalized so that $\langle\mathcal{W}_{si},\mathcal{V}_{si}\rangle=1$. The basis $\mathcal{V}_s$ comprises the balanced modes, which are equally controllable and observable. It is straightforward to verify that $\langle\mathcal{W}_{si},\mathcal{V}_{sj}\rangle=0$ if $i\neq j$. The theory shows that the values on the diagonal of Σ are also the singular values of the Hankel matrix associated with linear systems (46) and (47). The transfer function $\hat{H}^r$ related to the reduced-order-model incorporating the first p balanced modes satisfies [95]

$$\|\hat{H}^r-\hat{H}\|_\infty\leq 2\sum_{j\geq p+1}\Sigma_{j,j} \tag{52}$$

This basis is often close to the optimum, since, for any basis of order p, the following relation holds:

$$\|\hat{H}^r-\hat{H}\|_\infty>\Sigma_{p+1,p+1} \tag{53}$$

Laub et al. [98] introduced an efficient algorithm to solve eigenvalue problems (50) and (51) for systems of low-dimensions. Willcox and Peraire [99] and Rowley [100] introduced a POD-type technique to treat large-scale problems. For this, two series of snapshots, obtained, respectively, from a temporal simulation of the direct problem $d\mathbf{u}'/dt=\mathcal{A}\mathbf{u}'$ with $\mathbf{u}'(t=0)=\mathcal{P}_s\mathcal{C}$ and a temporal simulation of the adjoint problem $d\mathbf{u}'/dt=\mathcal{A}^*\mathbf{u}'$ with $\mathbf{u}'(t=0)=\mathcal{P}_s^*\mathcal{M}^*$, are used to approximate the controllability and observability Gramians. The original eigenvalue problems (50) and (51) are then reformulated into a singular value problem whose dimension is equal to the number of snapshots. These calculations are not detailed here; we only describe some of the results. The largest singular values Σ obtained for our case are presented in Fig. 19(*a*). The decay behavior of this curve directly determines the dimension of our reduced basis. For a given error threshold, the upper limit of the error bound given in Eq. (52) straightforwardly yields the dimension of the reduced model. In Figs. 19(*b*)–19(*e*), the balanced modes associated with the 1st, 2nd, 9th,

[14]It may be shown that this function is also equal to $\hat{H}(\omega)=\mathcal{M}(i\omega\mathcal{I}-\mathcal{A})^{-1}\mathcal{P}_s\mathcal{C}$.

and 13th singular values in Σ are displayed using the streamwise velocity. Let us recall that all these modes belong to the stable subspace of $\mathcal{A}$. In particular, the first two modes are bi-orthogonal to the unstable global modes presented in Figs. 15(*b*) and 15(*c*). This means that the scalar products of the unstable adjoint global modes (see Figs. 15(*d*) and 15(*e*)) and the balanced structures are zero. Once the bases $\mathcal{V}_s$ and $\mathcal{W}_s$ have been determined, the reduced matrices $\mathcal{A}^r$, $\mathcal{C}^r$, and $\mathcal{M}^r$ can be calculated and the associated transfer function $\hat{H}^r$ can be determined. The relative error $\|\hat{H}^r - \hat{H}\|_\infty / \|\hat{H}\|_\infty$ is shown in Fig. 20(*a*) as a function of the number p of balanced modes considered. In this figure, the upper and lower bounds for the error defined in Eqs. (52) and (53) have also been included. As required, the error related to the reduced-order-model of order p falls within these two bounds. We also observe that taking ten balanced modes ($p \approx 10$) yields a nearly perfect approximation of the input-output dynamics of the stable part of the system. For comparison, we have also given, in Fig. 20(*b*), the results pertaining to the modal basis discussed in Sec. 5.2. We observe a decrease in the error for the first thousand global modes, after which the curve becomes erratic and grows again for $p > 3000$. Hence, independent of the number of included global modes, the reduced-order-model based on these structures does not approximate the transfer function of the original system. This result corroborates the conclusions drawn in Sec. 5.2.

Rowley [100] pointed out that the eigenvectors of $\mathcal{G}_c$ could be interpreted as POD-modes [102] of the simulation $d\mathbf{u}'/dt = \mathcal{A}\mathbf{u}'$ initialized by the control matrix $\mathbf{u}'(t=0) = \mathcal{P}_s\mathcal{C}$. These modes maximize controllability but do not take into account any requirements regarding observability. Nevertheless, the quality of such reduced-order-models has been assessed by estimating, as in the case of balanced modes and global modes, the error between the reduced transfer function and the transfer function of the full-system. The results are given in Fig. 20(*c*). The behavior of these bases is very good, with a steady decrease in the approximation error as the dimension p of the reduced-order-model increases. For $p=100$, very small error levels, equivalent to those obtained with 13 balanced modes, are reached. Note, however, that significantly more POD-modes than balanced modes are required to achieve similar accuracy.

5.4 Closed-Loop Control: Analysis of the Compensated System. The objective of this section is to analyze the compensated systems. For this, we couple a direct numerical simulation of the large-scale dynamical problem to an estimator and a controller, both of which are based on the reduced-order-models built previously. We know (see Secs. 5.1–5.3) that the reduced-order-models based on eight unstable global modes and a series of balanced or POD-modes reproduce the unstable dynamics as well as the input-output dynamics of the stable subspace, if sufficient balanced modes or POD-modes are taken into account. The number of modes that will stabilize the compensated system cannot be determined a priori. For example, a threshold below which the compensated system would certainly be stable cannot be given for the approximation error of the transfer function $\|\hat{H}^r - \hat{H}\|_\infty / \|\hat{H}\|_\infty$. The final steps in the design of the estimator and controller can now be taken. For this, control gains for the controller and Kalman gains for the estimator are calculated using the LQG-framework [79]. Following previous statements, a reduced-order-model based on all unstable global modes was chosen and augmented by a series of p balanced or POD-modes for the stable subspace. The computation of the gains, based on solving the respective Riccati equations, is performed within the small-gain limit [79]. This means that the control cost is assumed infinite and that the measurement errors are infinitely larger than the model errors (which seems reasonable for our case since the models are obtained by an accurate Petrov–Galerkin projection). In this limit, it is neither necessary to specify the state-dependent part of the cost functional (the energy of the perturbations, for example) nor to model the structure of the external noise sources associated with the model. Moreover, the gains are the smallest possible and are nonzero only for the unstable structures of the reduced-order-model. Thus, the controller specifies the smallest values for the

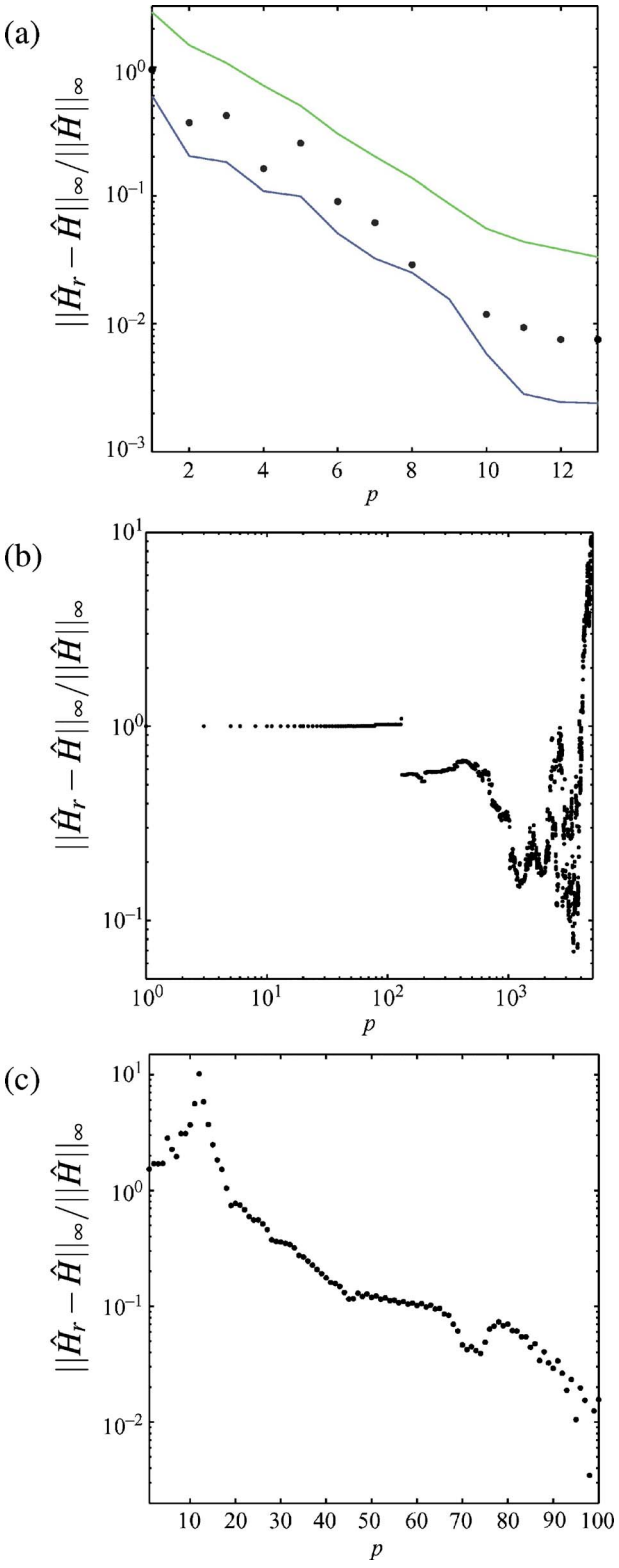

Fig. 20 Flow over an open cavity for Re=7500. Approximation error of reduced-order-models versus their dimension. (*a*) balanced modes, (*b*) global modes, and (*c*) POD-modes. In (*a*), the continuous curves represent the upper and lower bounds of the error (52) and (53). Adapted from Ref. [141].

control law $c(t)$ (due to the infinite control cost), and the estimator is driven the least by the measurement error since we are more confident in the validity of the model than in the measurements (in other words, the measurement error is infinitely larger than the model error). In this case, according to Burl [79], the eigenvalues of the compensated system are equal to the stable eigenvalues of the reduced-order-model, but the unstable eigenvalues of the uncompensated system are reflected about the imaginary axis $\sigma=0$ when a small-gain-limit compensator is added.

A numerical simulation code solving Eq. (41) has then been combined with the controller and estimator that have just been defined. The estimator takes as input the measurements $m(t)$ of the direct simulation. The reduced-order-model of the flow is integrated in time and driven in real-time by the measurement $m(t)$ of the simulation via the Kalman gain. It then provides the controller with an estimate of the real state of the flow, which is subsequently used by the controller to generate a control law $c(t)$ via the control gain. Depending on the selected reduced-order-model (based on balanced modes or POD-modes for the stable subspace) and its dimension $8+p$, the stabilization of the simulations by the compensator is more or less effective. The results for the compensated simulations are presented in Fig. 21. Figure 21(a) shows simulations with a reduced-order-model based on balanced modes, and Fig. 21(b) displays the results for a reduced-order-model using POD-modes. The x-axis denotes time while the y-axis shows the energy of the perturbation $\mathbf{u}'$. In Fig. 21(a), the curve labeled $p=0$ represents a reduced-order-model including only the eight unstable global modes. As previously mentioned, we see that this simulation diverges, which again confirms that the modeling of the stable subspace is mandatory. As the number of balanced modes incorporated into the reduced-order-model increases, the system eventually stabilizes. For $p=7$, the energy of the perturbations remains bounded; for $p>7$, the energy decreases. The dark line in the figure represents the best possible control, toward which the curves for the reduced-order-models converge as p increases. This best control is obtained when the reduced-order-model exactly reproduces the transfer function of the original system. Similar results are observed in Fig. 21(b) with POD-modes. We note, however, that the number of POD-modes to stabilize the system is significantly higher than the number of balanced modes to reach the same goal: Twenty-eight POD-modes are necessary to render the compensated system stable, whereas only seven balanced modes are needed to accomplish the same.

In the last paragraph, the control law, which has been synthetized by the linear LQG approach, has been evaluated using a linearized direct numerical simulation (DNS) code, solving Eq. (41). This should be strictly equivalent to solving nonlinear Navier–Stokes equation (1) with a small-amplitude initial perturbation (so that the perturbation amplitude remains small and in the linear regime during the whole simulation). If the initial perturbation amplitude is not small, then the nonlinear term acting on the perturbation is not negligible anymore and there is no guarantee that the linear LQG compensator will work. Preliminary nonlinear simulations effectively show that the results from the linearized simulations are recovered in the case of small-amplitude initial perturbations but that the performance of the compensator deteriorates when the amplitude of the initial perturbation increases.

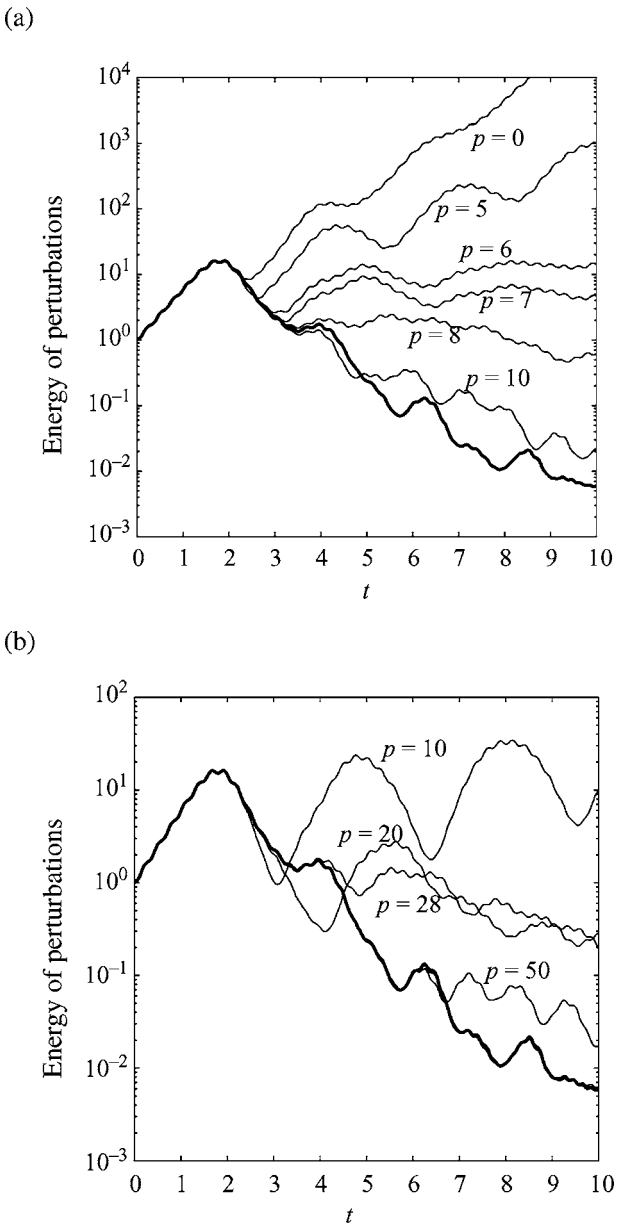

Fig. 21 Flow over an open cavity for Re=7500. Linearized direct numerical simulations with a controller and an estimator obtained by the LQG approach. (*a*) Reduced-order-model consisting of eight unstable global modes and *p* balanced modes. (*b*) Likewise, but *p* POD-modes. Adapted from Ref. [141].

6 The Case of Noise-Amplifiers

Sections 3–5 were all concerned with the occurrence of unsteadiness linked to an oscillator dynamics; for this scenario, the Jacobian matrix $\mathcal{A}$ had at least one unstable eigenvalue. As mentioned in Sec. 1.3, flows like boundary-layers or jets display unsteadiness even though the Jacobian matrix $\mathcal{A}$ is asymptotically stable. External perturbations as for instance turbulence, acoustics, or roughness elements may continuously sustain the unsteadiness of the flow-field. The Jacobian matrix $\mathcal{A}$ then acts as a linear filter on the external disturbance environment, thus creating a frequency selection mechanism, which leads to a broadband low-frequency spectrum for the perturbation field. The question arises on how to characterize the dynamics of a noise-amplifier within a global stability approach.

As seen in Sec. 2.3, the non-normality of the Navier–Stokes equations results in nonorthogonal global modes in open-flows. In Sec. 1.3.2, the noise-amplifier dynamics in a global stability analysis has first been characterized through transient growth properties viewed in terms of a superposition of nonorthogonal global modes. We will now show the shortcomings of such an approach for open-flows (Sec. 6.1). Then (Sec. 6.2), we mention how transient growth may properly be computed by a direct-adjoint approach. Finally (Sec. 6.3), we show that selection frequency mechanisms are better viewed in the frequency domain by computing optimal forcing distributions and their associated responses. An example with a Blasius boundary-layer will be given

to illustrate the approach. Open-loop control of noise-amplifiers will also be discussed in the light of sensitivity analyses with respect to base-flow modifications.

6.1 Transient Growth as a Superposition of Global Modes: Shortcomings of Stable Global Modes. We will first show, on the example of the open-cavity flow discussed in Sec. 5, that computing stable global modes is generally a bad idea in open-flows: Most of the stable global modes do not carry any physical meaning and are unphysical in the sense introduced in Sec. 1.2—they are extremely sensitive to external perturbations of the Jacobian matrix. The spectrum of the open-cavity flow was given in Fig. 17, where the coloring indicated the importance of a given global mode in the input-output dynamics. We saw that very damped modes did significantly contribute to this dynamics. A detailed analysis of the problem shows that nearly all stable global modes (except few physical ones that represent the dynamics inside the cavity) are located at the downstream boundary of the computational domain whereas their corresponding adjoints are located at the upstream boundary. These modes are unphysical in the sense introduced in Sec. 1.2 and represent the advection of the perturbations by the base-flow $\mathbf{u}^B$ in the freestream. We recall that, taken individually, these modes carry no dynamic significance, and only the superposition of a great many of them yields physically relevant features. They are a consequence of the strong convective driven nonorthogonality of the stable global modes [142], which is further evidenced by a large nonorthogonality coefficient γ (see Eq. (11)). This coefficient can reach values of $\gamma=10^{15}$ for the strongly damped eigenvalues. In addition, displacing the left boundary (the right boundary) of the computational domain further upstream (downstream) will increase this coefficient even further. At a certain point, the convective driven nonorthogonality has become so large that numerical methods fail to accurately compute these modes. We recall that the coefficient γ also corresponds to the condition number of the associated eigenvalue problem. It is known that when this number is large, the eigenvectors and eigenvalues become very sensitive to perturbations of the matrix. For example, in the present flow over an open cavity, it is impossible to calculate more discrete eigenvalues than those already presented in Fig. 17.

As recognized by Trefethen and Embree [142], the problem evidenced in the previous paragraph arises in all advection-diffusion problems when boundary conditions are introduced at artificial upstream and downstream boundaries. In the case of streamwise unbounded flows, the spectrum of the linearized Navier–Stokes operator should, in fact, hold a continuous spectrum. For example, in the case of the constant coefficient equation $\partial_t u=\partial_x u+\partial_{xx}u/\mathrm{Re}$, if one looks for eigenfunctions of the form $u=\hat{u}\exp(\lambda t+ikx)$, then the dispersion relation reads $\lambda=ik-k^2/\mathrm{Re}$; i.e., there exists a continuous set of eigenvalues/eigenvectors since k is real. Note also that this problem is normal in the sense that the eigenfunctions are all orthogonal. If the boundary conditions $u(0)=u(1)=0$ are added to the definition of the problem (because a mesh always starts and ends at some given artificial input-output boundaries), then the eigenvalues become discrete; i.e., only an infinite discrete countable set of eigenvalues exists [142]. These eigenvalues lie along the negative real-axis in the (σ,ω)-plane. Furthermore, in the case of high-Reynolds numbers, these eigenvalues are extremely sensitive to external perturbations of the operator and are unphysical in the sense introduced in Sec. 1.2. These perturbations are introduced when the equations are spatially discretized with a numerical scheme, which explains the lack of robustness of the eigenvalues with respect to discretization changes. Also, Trefethen and Embree [142] showed that the resolvent norm was extremely high in a parabola shaped area lying along the negative real-axis in the (σ,ω)-plane: This means that this whole area is nearly an eigenvalue when extremely small perturbations to the governing operator are added. This same feature could be observed in the case of the open-cavity flow with two-dimensional Navier–Stokes equations: The eigenvalues were most difficult to compute near the negative real-axis (see Fig. 17).

In conclusion, we can state that most of the stable global modes, when considered individually, are at best physically irrelevant and at worst impossible to compute. Therefore, the modal basis constitutes, generally speaking, an ineffective and ill-posed projection basis for the stable subspace in open-flows.

6.2 Noise-Amplifiers in the Temporal Domain. Even though none of the global modes of $\mathcal{A}$ may be physical, the initial-value problem described by Eq. (3) is well-defined and robust to external perturbations of the matrix $\mathcal{A}$, like discretization errors. For example, for sufficiently fine meshes and for a given initial condition, the perturbation solution has an intrinsic existence, which is weakly sensitive to external perturbations. Therefore, instead of computing transient growth from a superposition of a small number of global modes, one should directly look for transient growth stemming from the large-scale matrix $\mathcal{A}$ and study energetic growth solely from robust initial-value problem (3). Note that the transient growth problem in open-flows is structurally robust since the transient growths and the optimal perturbations on a time horizon T are solution of an eigenproblem involving the Hermitian matrix $e^{\mathcal{A}T}e^{\mathcal{A}^*T}$. Hence, the condition number of this eigenproblem is equal to 1, showing the weak sensitivity of the energetic gains and optimal perturbations to external perturbations of the matrix $\mathcal{A}$. This eigenproblem may also be viewed as a large-scale optimization problem [11,20,76] that may be solved thanks to direct-adjoint techniques. Here, for a given optimization time T, one iteratively solves the direct problem $d\mathbf{u}'/dt=\mathcal{A}\mathbf{u}'$ forwardly in time on $[0,T]$ and the adjoint problem $d\mathbf{u}'/dt=-\mathcal{A}^*\mathbf{u}'$ backwardly on $[T,0]$. The initial condition of the adjoint problem is the final state of the direct problem, while the initial condition of the direct problem is the final state of the adjoint problem. First studies on this strategy in a global stability approach were carried out by Marquet et al. [143,144] on a rounded backward-facing step and by Blackburn et al. [145,146] on a backward-facing step and stenotic flows. This type of analysis produces unprecedented stability information for the characterization of noise-amplifiers in complex flows.

6.3 Noise-Amplifiers in the Frequency Domain. An initial optimal perturbation problem, as presented in Sec. 6.2, well describes transients and the physics of energetic growth in noise-amplifiers. Nevertheless, the above-identified initial optimal perturbations may not straightforwardly be linked to the upstream perturbations that a flow may experience in simulations or experiments. In such situations, one usually knows—or may know—some characteristic features of the upstream noise, such as a frequency spectrum, a spatial structure, and a preferred location. Then, one aims at predicting the features of the downstream sustained unsteadiness, also in the form of a frequency spectrum, spatial structure, and location. For this, it is more natural to resort to the frequency domain and achieve the singular value decomposition of the global resolvent, as shown below [147,148].

For this, let us consider an asymptotically stable base-flow $\mathbf{u}^B$, solution of Eq. (2), and a perturbation $\mathbf{u}'$ superposed on $\mathbf{u}^B$ that is driven by some external forcing $\mathbf{f}'$. For a small-amplitude forcing $\mathbf{f}'$, the flow response $\mathbf{u}'$ is governed by the linearized Navier–Stokes equations, which after spatial discretization read

$$\frac{d\mathbf{u}'}{dt}=\mathcal{A}\mathbf{u}'+\mathbf{f}' \tag{54}$$

We then consider a forcing $\mathbf{f}'$ and a response $\mathbf{u}'$ characterized by a given real frequency ω: $\mathbf{f}'=e^{i\omega t}\hat{\mathbf{f}}(x,y)$ and $\mathbf{u}'=e^{i\omega t}\hat{\mathbf{u}}(x,y)$. The harmonic forcing $\hat{\mathbf{f}}$ then induces the following harmonic response $\hat{\mathbf{u}}$ in the flow:

$$\hat{\mathbf{u}} = \mathcal{R}(\omega)\hat{\mathbf{f}} \tag{55}$$

where $\mathcal{R}(\omega)=(i\omega I-\mathcal{A})^{-1}$ is referred to as the global resolvent. This matrix is defined for any real frequency ω since all eigenvalues of $\mathcal{A}$ are strictly damped. If the energy norm induced by the scalar product $\langle\cdot,\cdot\rangle$ is considered, the *optimal forcing* $\hat{\mathbf{f}}$ corresponds to the forcing, which maximizes the energetic gain

$$\mu^2 = \sup_{\hat{\mathbf{f}}} \frac{\langle\hat{\mathbf{u}},\hat{\mathbf{u}}\rangle}{\langle\hat{\mathbf{f}},\hat{\mathbf{f}}\rangle} \tag{56}$$

This optimal forcing can be calculated using the singular values of the global resolvent $\mathcal{R}(\omega)$ given by

$$\mathcal{R}^*\mathcal{R}\hat{\mathbf{f}} = \mu^2\hat{\mathbf{f}} \tag{57}$$

In the above, μ^2 is a real positive eigenvalue related to the *optimal forcing* $\hat{\mathbf{f}}$ of unit norm and $\mathcal{R}^*$ is the matrix adjoint to $\mathcal{R}$ and defined in such a way that $\langle\mathbf{u}_A,\mathcal{R}\mathbf{u}_B\rangle=\langle\mathcal{R}^*\mathbf{u}_A,\mathbf{u}_B\rangle$ for any vector $\mathbf{u}_A$, $\mathbf{u}_B$. The *optimal response* $\hat{\mathbf{u}}$ of unit norm is obtained by solving $\hat{\mathbf{u}}=\mu^{-1}\mathcal{R}(\omega)\hat{\mathbf{f}}$. Since eigenvalue problem (57) is Hermitian, the set of *optimal forcings* $(\hat{\mathbf{f}}_j, j\geq 1)$ defines an orthonormal basis, which is adequate to represent the forcing space $\hat{\mathbf{f}}=\Sigma_j\langle\hat{\mathbf{f}}_j,\hat{\mathbf{f}}\rangle\hat{\mathbf{f}}_j$. In the same way, it is possible to show that the set of *optimal responses* $(\hat{\mathbf{u}}_j, j\geq 1)$ also forms an orthonormal basis. This latter basis is meant to represent the response space $\hat{\mathbf{u}}=\Sigma_j\langle\hat{\mathbf{u}}_j,\hat{\mathbf{u}}\rangle\hat{\mathbf{u}}_j$. The singular values $(\mu_j, j\geq 1)$ satisfy $\mathcal{R}(\omega)\hat{\mathbf{f}}_j=\mu_j\hat{\mathbf{u}}_j$.

To summarize, if we are given the structure of the harmonic forcing $\hat{\mathbf{f}}$ at some frequency ω, we readily obtain the structure of the response in the form

$$\hat{\mathbf{u}} = \sum_{j\geq 1} \mu_j\langle\hat{\mathbf{f}}_j,\hat{\mathbf{f}}\rangle\hat{\mathbf{u}}_j \tag{58}$$

and the energy of the response is simply

$$\langle\hat{\mathbf{u}},\hat{\mathbf{u}}\rangle = \sum_{j\geq 1} \mu_j^2\langle\hat{\mathbf{f}}_j,\hat{\mathbf{f}}\rangle^2 \tag{59}$$

Hence, to maximize the response of the flow-field, the external forcing $\hat{\mathbf{f}}$ should drive the flow with a structure as close as possible to the optimal forcing $\hat{\mathbf{f}}_1$, in which case the response of the flow will closely resemble the optimal response $\hat{\mathbf{u}}_1$.

Finally, note that the condition number of eigenproblem (57) is equal to one due to the Hermitian nature of the underlying matrix; the eigenvalues μ_j^2, optimal forcings $\hat{\mathbf{f}}_j$, and responses $\hat{\mathbf{u}}_j$ are therefore numerically well-posed and only very weakly sensitive to external perturbations of the matrix $\mathcal{A}$. These quantities are therefore (structurally) physical, in the sense introduced in Sec. 1.2, contrary to the stable global modes.

To illustrate this new approach, let us take the example of a boundary-layer flow that develops over a flat plate located between $x=0$ and $x=1$. The computational domain extends from $x=-1$ to $x=1$, its height being equal to $y=1$. The Reynolds number based on the upstream velocity and the plate length is taken as Re=200,000. After having determined the base-flow, we verify that the Jacobian matrix has only stable eigenvalues even though the velocity profiles extracted for $0.4\leq x\leq 1$ are convectively unstable since the Reynolds number based on the displacement thickness ranges from 500 to 770 in this interval. Hence, the global Jacobian matrix $\mathcal{A}$ should show strong amplifications in some low-frequency range due to the development of Tollmien–Schlichting waves in the boundary-layer. In Fig. 22(*a*), we display the dominant singular value μ_1^2 as a function of the frequency ω. We observe that this curve displays a maximum for the low-frequency $\omega\nu/U_\infty^2=0.00018$. The present formalism based on the global resolvent thus explains the frequency selection in Blasius boundary-layers. The optimal forcing and associated optimal response at the frequency of maximum amplification are displayed in Figs. 22(*b*) and 22(*c*). The optimal forcing is located around $x\approx 0.3$ while the associated response displays Tollmien–Schlichting waves developing downstream. The present results show that if external perturbations (turbulence) are present near $x\approx 0.3$, Tollmien–Schlichting waves will be sustained on the flat plate.

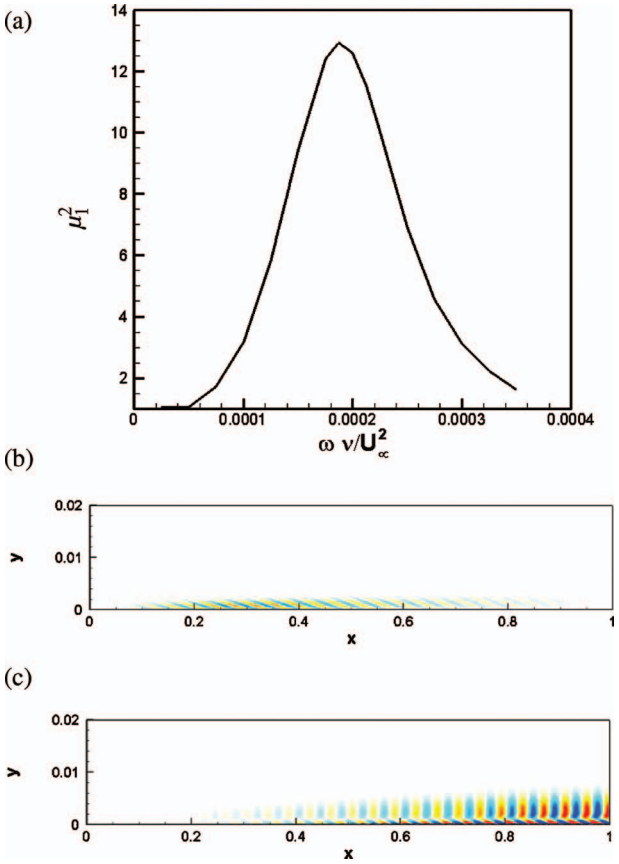

Fig. 22 Boundary-layer flow over a flat plate for Re=200,000. (*a*) Frequency response of the flow $\mu_1^2(\omega)$, (*b*) real part of streamwise momentum forcing for $\hat{\mathbf{f}}_1$ at $\omega\nu/U_\infty^2=0.00018$, and (*c*) associated optimal response $\hat{\mathbf{u}}_1$ (real part of streamwise velocity).

These results are complementary to the modal analyses by Ehrenstein and Gallaire [54], Akervik et al. [56], and Alizard and Robinet [55]. Moreover, if a transverse wavenumber β is considered, the lift-up and oblique wave phenomena highlighted within a local framework by Andersson et al. [21], Luchini [22], Corbett and Bottaro [23], and Levin and Henningson [149] should be recovered. This formalism is also well suited for receptivity studies, in the spirit of studies by Crouch [150] within a local framework.

Last, we will briefly demonstrate how the sensitivity concept and the open-loop control design may be extended to the case of noise-amplifier flows. For this, we consider a given optimal forcing $\hat{\mathbf{f}}$ and the associated optimal response $\hat{\mathbf{u}}$ such that $\mathcal{R}^*\mathcal{R}\hat{\mathbf{f}}=\mu^2\hat{\mathbf{f}}$ and $\hat{\mathbf{u}}=\mu^{-1}\mathcal{R}\hat{\mathbf{f}}$. These fields are normalized according to $\langle\hat{\mathbf{f}},\hat{\mathbf{f}}\rangle=1$ and $\langle\hat{\mathbf{u}},\hat{\mathbf{u}}\rangle=1$. The singular value μ^2 is a function of the base-flow $\mathbf{u}^B$, due to the dependence of the resolvent $\mathcal{R}$ on the latter. Differentiation of the above expression leads to

Table 1 Computational time and memory usage for a real matrix inverse in 2D and 3D configurations using a scalable direct LU solver

	Configuration	No. of elements	No. of DOFs ($\times 10^6$)	No. of processors	Memory (Gbyte)	Memory/processor (Gbyte)	Time (s)	Time/processor (s)
Cavity	2D	193,708	0.9	1	2.7	2.7	175	175
Flat plate	2D	491,416	2.2	1	6.7	6.7	431	431
Wing	3D	491,653	2.1	48	168	3.5	129,144	2700

$$\delta\mu^2 = \langle \nabla_{\mathbf{u}^B}\mu^2, \delta\mathbf{u}^B \rangle \tag{60}$$

where $\nabla_{\mathbf{u}^B}\mu^2$ is the sensitivity of the singular value with respect to a modification of the base-flow. A simple calculation shows that

$$\nabla_{\mathbf{u}^B}\mu^2 = \mu^3 \mathcal{B}(\mathbf{u}^B, \hat{\mathbf{u}})^* \hat{\mathbf{f}} + \text{c.c.} \tag{61}$$

where $\mathcal{B}(\mathbf{u}^B, \hat{\mathbf{u}})$ is the matrix defined in Eq. (26) and $\mathcal{B}(\mathbf{u}^B, \hat{\mathbf{u}})^*$ is its adjoint. This expression is the equivalent of Eq. (27), with the optimal forcing as the adjoint global mode and the optimal response as the direct global mode. Hence, all the procedures and tools for open-loop control of oscillator flows may readily be transcribed and applied to noise-amplifier flows. Such an approach may complement the studies by Pralits et al. [151] and Airiau et al. [152] on the stabilization of Tollmien–Schlichting waves with wall-suction.

7 Issues Related to Three-Dimensionality, Nonlinearity, and High-Reynolds Numbers

Three issues will be discussed in this final prospect section: Can we deal (Sec. 7.1) with three-dimensional configurations? How does nonlinearity (Sec.7.2) enter the problem? What new problems (Sec. 7.3) are encountered as the Reynolds number increases?

7.1 Toward Three-Dimensional Configurations. All the examples presented up to know concerned two-dimensional configurations for which only two directions in space were fully resolved (streamwise and one cross-stream direction). Conceptually speaking, all notions that have been introduced so far (base-flows, global modes, adjoint modes, gradients, Gramians, and balanced modes) straightforwardly extend to fully three-dimensional configurations. There is therefore no theoretical problem but there may be a computational one: Can these structures still be computed in a three-dimensional configuration in terms of memory requirements and CPU time? We will first estimate the cost of global stability analyses within the computational strategy that has been followed by the authors during these past years. We use Newton methods to compute base-flows, ARPACK[15] in shift-invert mode to extract given eigenvalues, and ARPACK in regular mode to compute the singular value decomposition of the resolvent. The bottleneck of all these algorithms is the solution of large-scale linear systems. Hence, the cost of the approach presented in this article is roughly the cost of solving a large-scale linear problem. Space discretization is achieved with finite elements. To achieve second-order accuracy in space, classical Taylor–Hood elements with P2 elements for the velocity components and P1 elements for the pressure are used. The free software FreeFem++ [16] then explicitly computes the sparse matrices and the right-hand-sides. Large-scale solutions of the associated linear problems are performed with a sparse scalable direct lower-upper (LU) solver[17] [153].

For example, in the case of the open-cavity flow at Re=7500 studied in Sec. 5, the mesh comprised 193,708 triangles (97,659 vertices), which led to 0.9×10^6 degrees of freedom for a velocity-pressure (u,v,p) unknown. The memory usage and computational time are given in Table 1: The computations may be achieved on a single processor, take 170 s, and require 2.7 Gbytes of memory. In the case of the two-dimensional Blasius boundary-layer at Re=200,000 (Sec. 6), the mesh comprised 491,416 triangles (247,735 vertices), which led to 2.2×10^6 degrees of freedom for the velocity-pressure unknown. From Table 1, it is seen that, comparing to the open-cavity flow case, both the computational time and the required memory have been multiplied by 2.5, which is precisely the ratio between the number of elements in the Blasius boundary-layer case and in the open-cavity flow case. Hence, the memory usage and computational time scale linearly with the number of elements in the mesh. All two-dimensional configurations studied within this review article may be handled out on a PC. For three-dimensional configurations, the cost rises substantially. In the case of a low-aspect ratio NACA0012 wing (AR=4), the mesh comprised 491,653 tetrahedra (83,290 vertices), leading to 2.2×10^6 degrees of freedom for an (u,v,w,p) unknown. An inversion was completed on a cluster using 48 processors: From Table 1, it is seen that the inversion lasts 2700 s (elapsed CPU time) and that 3.5 Gbytes of memory per processor were required. The cost therefore increases drastically from 2D to 3D configurations, although the same number of degrees of freedoms is involved in the last two presented computations. The reason for this blowup stems from the difference in sparsity of the two matrices: In two-dimensional settings, the matrices have approximately 29 nonzero elements per line (with Taylor–Hood elements), while for a three-dimensional mesh, this value raises to 98. On the whole, the computations are short in time but require a large amount of memory. Moving to domain decomposition methods should greatly improve scalability of the large-scale linear problems when using a high number of processors.

Matrix-free methods, in which the Jacobian matrix $\mathcal{A}$ is never formed explicitly, have also been developed over the past years. The original idea was worked out by Tuckerman and co-workers [32,154,155]. It has been taken over recently by Henningson and co-workers [148,156], with the aim of performing global stability analyses by using solely a linear or nonlinear DNS-solver. For example, following Ref. [157], the action of the Jacobian matrix on a given vector $\mathbf{u}'$ may be approximated through $\mathcal{A}\mathbf{u}' = (\mathbf{R}(\mathbf{u}^B + \alpha\mathbf{u}') - \mathbf{R}(\mathbf{u}^B))/\alpha$ for a sufficiently small α. Here, solely the evaluation of the nonlinear residual of the Navier–Stokes equations is required to perform $\mathcal{A}\mathbf{u}'$. Initial-value problem (3) may then be solved numerically with the method of exponential propagation [32], which only requires evaluations of $\mathcal{A}\mathbf{u}'$ or directly from the time integration of nonlinear governing equation (1) by using $\mathbf{u} = \mathbf{u}^B + \alpha\mathbf{u}'$ (see Ref. [157]). It is then possible, with Krylov subspace methods [32], to look for the least damped global modes by identifying the largest eigenvalues (in modulus) of the matrix $e^{\mathcal{A}T}$, where T is an arbitrary time of the order of the instability time-scale. Indeed, ARPACK in regular mode solely requires the action of $e^{\mathcal{A}T}$ on some given vector $\hat{\mathbf{u}}$, which may be obtained by time-marching Eq. (3) or Eq. (1) with the initial condition $\mathbf{u}'(t=0) = \hat{\mathbf{u}}$ from $t=0$ to $t=T$. As for the computation of the resolvent, one may just march in time the equations $d\hat{\mathbf{u}}/dt = -i\omega\hat{\mathbf{u}} + \mathcal{A}\hat{\mathbf{u}} + \hat{\mathbf{f}}$ until convergence—we note that $(-i\omega I + \mathcal{A})$ is an asymptotically stable matrix in the case of noise-amplifiers, which justifies the

[15] http://www.caam.rice.edu/software/ARPACK/
[16] www.freefem.org
[17] MUMPS. http://mumps.enseeiht.fr/

convergence of the equations. As for the identification of base-flows, a vast literature deals with implementing cheap Newton methods [32]. Also DNS-based approaches for the identification of base-flows have recently emerged with the selective frequency damping technique (Åkervik et al. [158]). On the whole, the matrix-free methods take much more CPU time but require a smaller amount of memory. A first three-dimensional global stability computation has been performed using such strategies by Bagheri et al. [40].

7.2 Nonlinearity. This review article concerns linearized equations, which govern the dynamics of a small-amplitude perturbation in the vicinity of a base-flow $\mathbf{u}^B$. The influence of nonlinearities is now briefly discussed in the case of oscillators and noise-amplifiers.

In the case of oscillator flows, the effects of nonlinearities have partly been addressed in Sec. 3.2 when the various control approaches have been presented in the light of bifurcation analyses, in Sec. 1.3.3 when the local instabilities were related to the global ones, and in Sec. 5.4 when testing the robustness of the LQG control law for initial perturbations of increasing amplitude. Within the linearized framework presented in this review article, the effects of nonlinearities may be accounted for only in the case of weakly supercritical flows ($0<\varepsilon\ll 1$): The nonlinearities are then weak and may be captured by a weakly-non-linear approach. For such an analysis to hold, the base-flow should not be too parallel. Indeed, in the case of weakly-non-parallel flows, the dynamics associated with exponential instabilities becomes strongly-non-linear immediately above the critical linear threshold [44,60]. A local description of the flow in terms of front dynamics is then more appropriate [44]. In the present review article, we have studied configurations that were, in fact, sufficiently nonparallel so that the dynamics near the critical threshold was captured by a weakly-non-linear approach. Although not covered in this review, secondary global linear instabilities, as discussed by Chomaz [44,159], may also be analyzed straightforwardly within the present global stability approach: One then studies the global stability of the bifurcated states, which appear above the primary linear instability threshold. In this case, continuation methods have first to be used to identify the bifurcated states. In the case of the cylinder flow where a Hopf bifurcation occurs, the bifurcated state is a periodic flow, which may be identified by time marching the two-dimensional Navier–Stokes equations. Then a Floquet stability analysis may be used to study the three-dimensional linear stability characteristics of this new state [33]. Note that subcritical instabilities may also exist in open-flows, for which the linear dynamics is stabilizing and the nonlinear dynamics destabilizing [130,131]: A finite-amplitude perturbation is then required to destabilize the flow and these instabilities are out of reach of a purely linear description. At least, for sufficiently nonparallel flows, a weakly-non-linear approach has to be used to tackle such problems (the coefficient $\mu_r+\nu_r$, as introduced in Sec. 3.4, will then be negative).

For noise-amplifier flows, the influence of nonlinearities is governed by the amplitude of the upstream forcing. If this amplitude is sufficiently small, then the linear approach presented in Sec. 6 is valid and one does not need to take into account nonlinearities. If not, then a first step would be to achieve a weakly-non-linear approach based on a small parameter being the amplitude of the upstream forcing. If one aims at predicting transition to turbulence, then a strongly-non-linear approach is required. The linear mechanisms just yield the potential for amplification but the nonlinearities determine the critical threshold (in terms of amplitude of the perturbation) for transition toward a fully turbulent flow. This amplitude threshold may be determined by exploring, with a direct numerical simulation approach, the so-called edge-states, discovered recently by Nagata [160], Waleffe [161], and Faisst and Eckhardt [162]. These edge-states are located on a hypersurface, which constitutes a laminar/turbulent boundary, separating initial conditions, which relaminarize uneventfully from those that become turbulent (Duguet et al. [163]). For the control of transitional flows, such as boundary-layers, it may be less expensive to consider these edge-states as objectives for closed-loop control. Indeed, these states may be easier to reach than the initial short-term unstable configurations. Finally, note also that secondary instabilities may be studied in noise-amplifier configurations, as, for example, Cossu et al. [164] with the perturbations developing on streaks in a plane channel flow.

7.3 High-Reynolds Number Flows. As the Reynolds number increases, the determination of base-flows to linearize about becomes an increasingly difficult task. Indeed, continuation methods are effective on moderately large Reynolds numbers only. But, for very high values of this control parameter, these flows may not even exist. Note that, in the case of noise-amplifiers such as jets or boundary-layers, finding base-flows seems more easy than for oscillator flows. In a numerical approach with high-order discretization schemes (so as to minimize discretization errors, which could be seen as upstream sustained noise), since the base-flow is asymptotically stable, one just solves nonlinear equation (1) in time until convergence [43]. For example, it is easy to compute the base-flow for a flat plate boundary-layer, even for Reynolds numbers up to 10^6, while this is impossible for the cylinder or open-cavity flow owing to the numerous successive bifurcations that may exist, as the Reynolds number increases.

For very high-Reynolds numbers, such as the buffeting of airfoils, a solution to the above issue may be to consider the unsteady Navier–Stokes equations augmented by a turbulence model. In the English literature on this subject, the acronym URANS is used for this set of equations (unsteady Reynolds-averaged Navier–Stokes equations). Usually, the assumption of a decoupling of scales is made to justify the adequacy of these models: Small spatial scales related to high frequencies are accounted for by the turbulence model, while large scales, characterized by low frequencies, are captured by temporal integration. This way it is possible to redefine the concept of an equilibrium point, which now means a steady flow-field of the URANS equations. By this extension, equilibrium points may exist even for flows at very large Reynolds numbers. The concept of linear dynamics thus makes reference to large spatial scales and low-frequency perturbations whose dynamics is governed by the URANS equations linearized around an equilibrium point defined above. Techniques derived from optimal control theory can then be applied to determine the best possible actions—within the validity of this model—to stabilize or destabilize the low-frequency modes. The first global stability analysis that included a (Spalart–Allmaras) turbulence model has been carried out by Crouch et al. [165] who studied the onset of transonic shock-buffeting on airfoils. The same technique has been considered by Cossu et al. [166] to identify streaks in turbulent boundary-layers. As far as model reduction is concerned, Luchtenburg et al. [72] considered URANS simulations with a $k-\omega$ turbulence model to build a physics-based reduced-order-model based on a Galerkin projection with POD-modes. The model is intended to capture the effect of high-frequency actuation on the mean flow and therefore on the natural instabilities that develop on it.

Acknowledgment

Laurent Jacquin, Peter Schmid, and Jean-Marc Chomaz are warmly acknowledged for support, ideas, discussions, and fruitful collaboration. Also, the authors are grateful to Peter Schmid for having carefully read through this article and given suggestions for improvement. They are also grateful to the FreeFem++ team (www.freefem.org) for the wonderful software they have developed.

Nomenclature

$\mathbf{u}$ = flow velocity
$\mathbf{u}^B$ = base-flow

$\mathbf{u}^M$ = mean flow
$\mathbf{R}(\mathbf{u})$ = residual of the Navier–Stokes equations
$\mathcal{A}$ = linearized Navier–Stokes matrix or Jacobian
$\mathcal{A}^*$ = adjoint matrix of $\mathcal{A}$
Re = Reynolds number
ε = Reynolds number in the form of departure from criticality $\varepsilon = \mathrm{Re}_c^{-1} - \mathrm{Re}^{-1}$
λ = eigenvalue of $\mathcal{A}$
σ = amplification rate
ω = frequency
$\langle \cdot, \cdot \rangle$ = scalar product of two scalar or vector fields
$\hat{\mathbf{u}}$ = direct global mode
$\tilde{\mathbf{u}}$ = adjoint global mode
γ = measure of nonorthogonality of a global mode $\hat{\mathbf{u}}$
δ = amount of nonorthogonality due to component-type non-normality within total nonorthogonality
$\nabla_{\mathbf{u}^B}\lambda$ = sensitivity of eigenvalue λ to a modification of the base-flow
$\nabla_{\mathbf{f}}\lambda$ = sensitivity of eigenvalue λ to a steady forcing of the base-flow
$\mathcal{C}$ = control matrix
$\mathcal{M}$ = measurement matrix
$\mathcal{P}_S$ = projection matrix onto the stable subspace of $\mathcal{A}$
$(\mathcal{W}, \mathcal{V})$ = bi-orthogonal basis
$\hat{H}(\omega)$ = input-output transfer function
$\mathcal{G}_c$ = controllability Gramian
$\mathcal{G}_o$ = observability Gramian
$\mathcal{R}(\omega)$ = resolvent matrix
μ^2 = squared singular value of the resolvent matrix
$\nabla_{\mathbf{u}^B}\mu^2$ = sensitivity of the squared singular value μ^2 to base-flow modifications
$W(\varepsilon)$ = scalar field representing the wavemaker region

References

[1] Reed, H. L., Saric, W. S., and Arnal, D., 1996, "Linear Stability Theory Applied to Boundary Layers," Annu. Rev. Fluid Mech., **28**(1), pp. 389–428.
[2] Chedevergne, F., Casalis, G., and Féraille, T., 2006, "Biglobal Linear Stability Analysis of the Flow Induced by Wall Injection," Phys. Fluids, **18**, p. 014103.
[3] Jacquin, L., Fabre, D., Sipp, D., and Coustols, E., 2005, "Unsteadiness, Instability and Turbulence in Trailing Vortices," C. R. Phys., **6**(4–5), pp. 399–414.
[4] Jacquin, L., Molton, P., Deck, S., Maury, B., and Soulevant, D., 2009, "Experimental Study of Shock Oscillation Over a Transonic Supercritical Profile," AIAA J., **47**(9), pp. 1985–1994.
[5] Deprés, D., Reijasse, P., and Dussauge, J., 2004, "Analysis of Unsteadiness in Afterbody Transonic Flows," AIAA J., **42**(12), pp. 2541–2550.
[6] Chauvet, N., Deck, S., and Jacquin, L., 2007, "Numerical Study of Mixing Enhancement in a Supersonic Round Jet," AIAA J., **45**(7), pp. 1675–1687.
[7] Rowley, C., Colonius, T., and Basu, A., 2002, "On Self-Sustained Oscillations in Two-Dimensional Compressible Flow Over Rectangular Cavities," J. Fluid Mech., **455**, pp. 315–346.
[8] Khorrami, M. R., Berkman, M. E., and Choudhari, M., 2000, "Unsteady Flow Computations of a Slat With a Blunt Trailing Edge," AIAA J., **38**(11), pp. 2050–2058.
[9] Mauffrey, Y., Rahier, G., and Prieur, J., 2009, "Numerical Investigation on Blade/Wake-Interaction Noise Generation," J. Aircr., **46**(5), pp. 1479–1486.
[10] Nash, E. C., Lowson, M. V., and McAlpine, A., 1999, "Boundary-Layer Instability Noise on Aerofoils," J. Fluid Mech., **382**, pp. 27–61.
[11] Schmid, P. J., 2007, "Nonmodal Stability Theory," Annu. Rev. Fluid Mech., **39**, pp. 129–162.
[12] Schmid, P. J., and Henningson, D. S., 2001, *Stability and Transition in Shear Flows*, Springer-Verlag, New York.
[13] Huerre, P., and Rossi, M., 1998, "Hydrodynamic Instabilities in Open Flows," *Hydrodynamics and Nonlinear Instabilities*, C. Godrèche and P. Manneville, eds., Cambridge University Press, Cambridge, pp. 81–294.
[14] Ellingsen, T., and Palm, E., 1975, "Stability of Linear Flow," Phys. Fluids, **18**(4), pp. 487–488.
[15] Landahl, M. T., 1980, "A Note on an Algebraic Instability of Inviscid Parallel Shear Flows," J. Fluid Mech., **98**, pp. 243–251.
[16] Butler, K. M., and Farrell, B. F., 1992, "3-Dimensional Optimal Perturbations in Viscous Shear-Flow," Phys. Fluids A, **4**(8), pp. 1637–1650.
[17] Farrell, B. F., and Ioannou, P. J., 1993, "Optimal Excitation of 3-Dimensional Perturbations in Viscous Constant Shear-Flow," Phys. Fluids A, **5**(6), pp. 1390–1400.
[18] Reddy, S. C., and Henningson, D. S., 1993, "Energy Growth in Viscous Channel Flows," J. Fluid Mech., **252**, pp. 209–238.
[19] Farrell, B. F., 1988, "Optimal Excitation of Perturbations in Viscous Shear Flow," Phys. Fluids, **31**(8), pp. 2093–2102.
[20] Luchini, P., and Bottaro, A., 1998, "Gortler Vortices: A Backward-in-Time Approach to the Receptivity Problem," J. Fluid Mech., **363**, pp. 1–23.
[21] Andersson, P., Berggren, M., and Henningson, D. S., 1999, "Optimal Disturbances and Bypass Transition in Boundary Layers," Phys. Fluids, **11**(1), pp. 134–150.
[22] Luchini, P., 2000, "Reynolds-Number-Independent Instability of the Boundary Layer Over a Flat Surface: Optimal Perturbations," J. Fluid Mech., **404**, pp. 289–309.
[23] Corbett, P., and Bottaro, A., 2000, "Optimal Perturbations for Boundary Layers Subject to Stream-Wise Pressure Gradient," Phys. Fluids, **12**(1), pp. 120–130.
[24] Corbett, P., and Bottaro, A., 2001, "Optimal Linear Growth in Swept Boundary Layers," J. Fluid Mech., **435**, pp. 1–23.
[25] Guégan, A., Huerre, P., and Schmid, P. J., 2007, "Optimal Disturbances in Swept Hiemenz Flow," J. Fluid Mech., **578**, pp. 223–232.
[26] Guégan, A., Schmid, P. J., and Huerre, P., 2008, "Spatial Optimal Disturbances in Swept Attachment-Line Boundary Layers," J. Fluid Mech., **603**, pp. 179–188.
[27] Zebib, A., 1987, "Stability of a Viscous Flow Past a Circular Cylinder," J. Eng. Math., **21**(2), pp. 155–165.
[28] Jackson, C. P., 1987, "A Finite-Element Study of the Onset of Vortex Shedding in Flow Past Variously-Shaped Bodies," J. Fluid Mech., **182**, pp. 23–45.
[29] Noack, B. R., and Eckelmann, H., 1994, "A Global Stability Analysis of the Steady and Periodic Cylinder Wake," J. Fluid Mech., **270**, pp. 297–330.
[30] Natarajan, R., and Acrivos, A., 1993, "The Instability of the Steady Flow Past Spheres and Disks," J. Fluid Mech., **254**, pp. 323–344.
[31] Lin, R. S., and Malik, M. R., 1996, "On the Stability of Attachment-Line Boundary Layers. Part 1. The Incompressible Swept Hiemenz Flow," J. Fluid Mech., **311**, pp. 239–255.
[32] Edwards, W. S., Tuckerman, L. S., Friesner, R. A., and Sorensen, D. C., 1994, "Krylov Methods for the Incompressible Navier-Stokes Equations," J. Comput. Phys., **110**, pp. 82–102.
[33] Barkley, D., and Henderson, R. D., 1996, "Three-Dimensional Floquet Analysis of the Wake of a Circular Cylinder," J. Fluid Mech., **322**, pp. 215–241.
[34] Lehoucq, R. B., and Sorensen, D. C., 1996, "Deflation Techniques for an Implicitly Restarted Arnoldi Iteration," SIAM J. Matrix Anal. Appl., **17**(4), pp. 789–821.
[35] Theofilis, V., 2003, "Advances in Global Linear Instability Analysis of Nonparallel and Three-Dimensional Flows," Prog. Aerosp. Sci., **39**(4), pp. 249–315.
[36] Barkley, D., Gomes, M. G. M., and Henderson, R. D., 2002, "Three-Dimensional Instability in Flow Over a Backward-Facing Step," J. Fluid Mech., **473**, pp. 167–190.
[37] Gallaire, F., Marquillie, M., and Ehrenstein, U., 2007, "Three-Dimensional Transverse Instabilities in Detached Boundary Layers," J. Fluid Mech., **571**, pp. 221–233.
[38] Sipp, D., and Lebedev, A., 2007, "Global Stability of Base and Mean Flows: A General Approach and Its Applications to Cylinder and Open Cavity Flows," J. Fluid Mech., **593**, pp. 333–358.
[39] Åkervik, E., Hoepffner, J., Ehrenstein, U., and Henningson, D. S., 2007, "Optimal Growth, Model Reduction and Control in a Separated Boundary-Layer Flow Using Global Eigenmodes," J. Fluid Mech., **579**, pp. 305–314.
[40] Bagheri, S., Schlatter, P., Schmid, P. J., and Henningson, D. S., 2009, "Global Stability of a Jet in Cross-Flow," J. Fluid Mech., **624**, pp. 33–44.
[41] Robinet, J.-C., 2007, "Bifurcations in Shock-Wave/Laminar-Boundary-Layer Interaction: Global Instability Approach," J. Fluid Mech., **579**, pp. 85–112.
[42] Brès, G. A., and Colonius, T., 2008, "Three-Dimensional Instabilities in Compressible Flow Over Open Cavities," J. Fluid Mech., **599**, pp. 309–339.
[43] Mack, C. J., Schmid, P. J., and Sesterhenn, J. L., 2008, "Global Stability of Swept Flow Around a Parabolic Body: Connecting Attachment-Line and Crossflow Modes," J. Fluid Mech., **611**, pp. 205–214.
[44] Chomaz, J.-M., 2005, "Global Instabilities in Spatially Developing Flows: Non-Normality and Nonlinearity," Annu. Rev. Fluid Mech., **37**, pp. 357–392.
[45] Monkewitz, P. A., Huerre, P., and Chomaz, J.-M., 1993, "Global Linear-Stability Analysis of Weakly Nonparallel Shear Flows," J. Fluid Mech., **251**, pp. 1–20.
[46] Pier, B., and Huerre, P., 2001, "Nonlinear Self-Sustained Structures and Fronts in Spatially Developing Wake Flows," J. Fluid Mech., **435**, pp. 145–174.
[47] Hammond, D. A., and Redekopp, L. G., 1997, "Global Dynamics of Symmetric and Asymmetric Wakes," J. Fluid Mech., **331**, pp. 231–260.
[48] Pier, B., 2002, "On the Frequency Selection of Finite-Amplitude Vortex Shedding in the Cylinder Wake," J. Fluid Mech., **458**, pp. 407–417.
[49] Barkley, D., 2006, "Linear Analysis of the Cylinder Wake Mean Flow," Europhys. Lett., **75**(5), pp. 750–756.
[50] Khor, M., Sheridan, J., Thompson, M. C., and Hourigan, K., 2008, "Global Frequency Selection in the Observed Time-Mean Wakes of Circular Cylinders," J. Fluid Mech., **601**(1), pp. 425–441.
[51] Leontini, J. S., Thompson, M. C., and Hourigan, K., 2010, "A Numerical Study of Global Frequency Selection in the Time-Mean Wake of a Circular Cylinder," J. Fluid Mech., **645**(1), pp. 435–446.
[52] Williamson, C. H., 1988, "Defining a Universal and Continuous Strouhal-Reynolds Number Relationship for the Laminar Vortex Shedding of a Circular

Cylinder," Phys. Fluids, **31**(10), pp. 2742–2744.
[53] Trefethen, L. N., Trefethen, A. E., Reddy, S. C., and Driscoll, T. A., 1993, "Hydrodynamic Stability Without Eigenvalues," Science, **261**(5121), pp. 578–584.
[54] Ehrenstein, U., and Gallaire, F., 2005, "On Two-Dimensional Temporal Modes in Spatially Evolving Open Flows: The Flat-Plate Boundary Layer," J. Fluid Mech., **536**, pp. 209–218.
[55] Alizard, F., and Robinet, J.-C., 2007, "Spatially Convective Global Modes in a Boundary Layer," Phys. Fluids, **19**(11), p. 114105.
[56] Akervik, E., Ehrenstein, U., Gallaire, F., and Henningson, D. S., 2008, "Global Two-Dimensional Stability Measures of the Flat Plate Boundary-Layer Flow," Eur. J. Mech. B/Fluids, **27**(5), pp. 501–513.
[57] Alizard, F., Cherubini, S., and Robinet, J.-C., 2009, "Sensitivity and Optimal Forcing Response in Separated Boundary Layer Flows," Phys. Fluids, **21**(6), p. 064108.
[58] Huerre, P., and Monkewitz, P. A., 1985, "Absolute and Convective Instabilities in Free Shear Layers," J. Fluid Mech., **159**, pp. 151–168.
[59] Giannetti, F., and Luchini, P., 2007, "Structural Sensitivity of the First Instability of the Cylinder Wake," J. Fluid Mech., **581**, pp. 167–197.
[60] Le Dizès, S., Huerre, P., and Chomaz, J.-M., 1993, "Nonlinear Stability Analysis of Slowly-Varying Medias: Limitations of the Weakly Nonlinear Approach," *Proceedings of the IUTAM Symposium on Bluff-body Wakes, Dynamics and Instabilities*, Springer, Berlin, pp. 147–152.
[61] Cossu, C., and Chomaz, J.-M., 1997, "Global Measures of Local Convective Instabilities," Phys. Rev. Lett., **78**(23), pp. 4387–4390.
[62] Gad-el Hak, M., Pollard, A., and Bonnet, J.-P., 1998, *Flow Control: Fundamentals and Practices*, Springer-Verlag, Berlin.
[63] Collis, S. S., Joslin, R. D., Seifert, A., and Theofilis, V., 2004, "Issues in Active Flow Control: Theory, Control, Simulation, and Experiment," Prog. Aerosp. Sci., **40**(4–5), pp. 237–289.
[64] Choi, H., Jeon, W.-P., and Kim, J., 2008, "Control of Flow Over a Bluff Body," Annu. Rev. Fluid Mech., **40**, pp. 113–139.
[65] Pier, B., 2003, "Open-Loop Control of Absolutely Unstable Domains," Proc. R. Soc. London, Ser. A, **459**(2033), pp. 1105–1115.
[66] Hwang, Y., and Choi, H., 2006, "Control of Absolute Instability by Basic-Flow Modification in a Parallel Wake at Low Reynolds Number," J. Fluid Mech., **560**, pp. 465–475.
[67] Strykowski, P. J., and Sreenivasan, K. R., 1990, "On the Formation and Suppression of Vortex Shedding at Low Reynolds-Numbers," J. Fluid Mech., **218**, pp. 71–107.
[68] Delaunay, Y., and Kaiktsis, L., 2001, "Control of Circular Cylinder Wakes Using Base Mass Transpiration," Phys. Fluids, **13**(11), pp. 3285–3302.
[69] Arcas, D. R., and Redekopp, L. G., 2004, "Aspects of Wake Vortex Control Through Base Blowing/Suction," Phys. Fluids, **16**(2), pp. 452–456.
[70] Sevilla, A., and Martinez-Bazan, C., 2004, "Vortex Shedding in High Reynolds Number Axisymmetric Bluff-Body Wakes: Local Linear Instability and Global Bleed Control," Phys. Fluids, **16**(9), pp. 3460–3469.
[71] Sanmiguel-Rojas, E., Sevilla, A., Martinez-Bazan, C., and Chomaz, J.-M., 2009, "Global Mode Analysis of Axisymmetric Bluff-Body Wakes: Stabilization by Base Bleed," Phys. Fluids, **21**(11), p. 114102.
[72] Luchtenburg, D. M., Gunther, B., Noack, B. R., King, R., and Tadmor, G., 2009, "A Generalized Mean-Field Model of the Natural and High-Frequency Actuated Flow Around a High-Lift Configuration," J. Fluid Mech., **623**, pp. 283–316.
[73] Kim, H., and Chang, K., 1995, "Numerical Study on Vortex Shedding From a Circular Cylinder Influenced by a Nearby Control Wire," Comput. Fluid Dyn. J., **4**, pp. 151–164.
[74] Mittal, S., and Raghuvanshi, A., 2001, "Control of Vortex Shedding Behind Circular Cylinder for Flows at Low Reynolds Numbers," Int. J. Numer. Methods Fluids, **35**(4), pp. 421–447.
[75] Morzynski, M., Afanasiev, K., and Thiele, F., 1999, "Solution of the Eigenvalue Problems Resulting From Global Non-Parallel Flow Stability Analysis," Comput. Methods Appl. Mech. Eng., **169**(1–2), pp. 161–176.
[76] Gunzburger, M. D., 2003, *Perspectives in Flow Control and Optimization*, SIAM, United States.
[77] Meliga, P., Sipp, D., and Chomaz, J.-M., 2010, "Open-Loop Control of Compressible Afterbody Flows Using Adjoint Methods," Seventh IUTAM Symposium on Laminar-Turbulent Transition, P. Schlatter and D. S. Henningson, eds., Vol. 18, pp. 283–288.
[78] Marquet, O., and Sipp, D., 2010, "Active Steady Control of Vortex Shedding: An Adjoint-Based Sensitivity Approach," Seventh IUTAM Symposium on Laminar-Turbulent Transition, P. Schlatter and D. S. Henningson, eds., Vol. 18, pp. 259–264.
[79] Burl, J. B., 1999, *Linear Optimal Control. $\mathcal{H}_2$ and $\mathcal{H}_\infty$ Methods*, Addison-Wesley, Reading, MA.
[80] Zhou, K., Doyle, C., and Glover, E., 1996, *Robust and Optimal Control*, Prentice-Hall, Englewood Cliffs, NJ.
[81] Joshi, S. S., Speyer, J. L., and Kim, J., 1997, "A Systems Theory Approach to the Feedback Stabilization of Infinitesimal and Finite-Amplitude Disturbances in Plane Poiseuille Flow," J. Fluid Mech., **332**, pp. 157–184.
[82] Bewley, T. R., and Liu, S., 1998, "Optimal and Robust Control and Estimation of Linear Paths to Transition," J. Fluid Mech., **365**, pp. 305–349.
[83] Cortelezzi, L., and Speyer, J., 1998, "Robust Reduced-Order Controller of Laminar Boundary Layer Transitions," Phys. Rev. E, **58**(2), pp. 1906–1910.
[84] Högberg, M., Bewley, T. R., and Henningson, D. S., 2003, "Linear Feedback Control and Estimation of Transition in Plane Channel Flow," J. Fluid Mech., **481**, pp. 149–175.
[85] Hœpffner, J., Chevalier, M., Bewley, T. R., and Henningson, D. S., 2005, "State Estimation in Wall-Bounded Flow Systems. Part 1. Laminar Flows," J. Fluid Mech., **534**, pp. 263–294.
[86] Chevalier, M., Hopffner, J., Bewley, T. R., and Henningson, D. S., 2006, "State Estimation in Wall-Bounded Flow Systems. Part 2. Turbulent Flows," J. Fluid Mech., **552**, pp. 167–187.
[87] Högberg, M., and Henningson, D. S., 2002, "Linear Optimal Control Applied to Instabilities in Spatially Developing Boundary Layers," J. Fluid Mech., **470**, pp. 151–179.
[88] Chevalier, M., Hoepffner, J., Akervik, E., and Henningson, D. S., 2007, "Linear Feedback Control and Estimation Applied to Instabilities in Spatially Developing Boundary Layers," J. Fluid Mech., **588**, pp. 163–187.
[89] Cortelezzi, L., Lee, K. H., Kim, J., and Speyer, J. L., 1998, "Skin-Friction Drag Reduction via Robust Reduced-Order Linear Feedback Control," Int. J. Comput. Fluid Dyn., **11**(1), pp. 79–92.
[90] Lee, K. H., Cortelezzi, L., Kim, J., and Speyer, J., 2001, "Application of Reduced-Order Controller to Turbulent Flows for Drag Reduction," Phys. Fluids, **13**(5), pp. 1321–1330.
[91] Kim, J., 2003, "Control of Turbulent Boundary Layers," Phys. Fluids, **15**(5), pp. 1093–1105.
[92] Bewley, T. R., 2001, "Flow Control: New Challenges for a New Renaissance," Prog. Aerosp. Sci., **37**(1), pp. 21–58.
[93] Kim, J., and Bewley, T. R., 2007, "A Linear Systems Approach to Flow Control," Annu. Rev. Fluid Mech., **39**, pp. 383–417.
[94] Lauga, E., and Bewley, T. R., 2003, "The Decay of Stabilizability With Reynolds Number in a Linear Model of Spatially Developing Flows," Proc. R. Soc. London, Ser. A, **459**, pp. 2077–2095.
[95] Antoulas, A. C., 2005, *Approximation of Large-Scale Dynamical Systems*, SIAM, United States.
[96] Henningson, D. S., and Akervik, E., 2008, "The Use of Global Modes to Understand Transition and Perform Flow Control," Phys. Fluids, **20**(3), p. 031302.
[97] Moore, B., 1981, "Principal Component Analysis in Linear Systems: Controllability, Observability, and Model Reduction," IEEE Trans. Autom. Control, **26**, pp. 17–32.
[98] Laub, A. J., Heath, M. T., Page, C. C., and Ward, R. C., 1987, "Computation of System Balancing Transformations and Other Applications of Simultaneous Diagonalization Algorithms," IEEE Trans. Autom. Control, **32**(2), pp. 115–122.
[99] Willcox, K., and Peraire, J., 2002, "Balanced Model Reduction via Proper Orthogonal Decomposition," AIAA J., **40**, pp. 2323–2330.
[100] Rowley, C. W., 2005, "Model Reduction for Fluids Using Balanced Proper Orthogonal Decomposition," Int. J. Bifurcation Chaos Appl. Sci. Eng., **15**, pp. 997–1013.
[101] Lumley, J. L., 1970, *Stochastic Tools in Turbulence*, Academic, New York.
[102] Sirovich, L., 1987, "Turbulence and the Dynamics of Coherent Structures," Q. Appl. Math., **45**(3), pp. 561–590.
[103] Berkooz, G., Holmes, P., and Lumley, J. L., 1993, "The Proper Orthogonal Decomposition in the Analysis of Turbulent Flows," Annu. Rev. Fluid Mech., **25**, pp. 539–575.
[104] Ilak, M., and Rowley, C. W., 2008, "Modeling of Transitional Channel Flow Using Balanced Proper Orthogonal Decomposition," Phys. Fluids, **20**, p. 034103.
[105] Bagheri, S., Henningson, D. S., Hoepffner, J., and Schmid, P. J., 2009, "Input-Output Analysis and Control Design Applied to a Linear Model of Spatially Developing Flows," Appl. Mech. Rev., **62**(2), p. 020803.
[106] Bagheri, S., Brandt, L., and Henningson, D. S., 2009, "Input-Output Analysis, Model Reduction and Control of the Flat-Plate Boundary Layer," J. Fluid Mech., **620**, pp. 263–298.
[107] Ahuja, S., and Rowley, C. W., 2008, "Low-Dimensional Models for Feedback Stabilization of Unstable Steady States," AIAA Paper No. 2008-553.
[108] Aubry, N., Holmes, P., Lumley, J. L., and Stone, E., 1988, "The Dynamics of Coherent Structures in Wall Region of a Turbulent Boundary Layer," J. Fluid Mech., **192**, pp. 115–175.
[109] Samimy, M., Debiasi, M., Caraballo, E., Serrani, A., Yuan, X., Little, J., and Myatt, J., 2007, "Feedback Control of Subsonic Cavity Flows Using Reduced-Order Models," J. Fluid Mech., **579**, pp. 315–346.
[110] Juang, J. N., and Pappa, R. S., 1985, "An Eigensystem Realization Algorithm for Modal Parameter Identification and Model Reduction," J. Guid. Control Dyn., **8**(5), pp. 620–627.
[111] Ma, Z., Ahuja, S., and Rowley, C., 2010, "Reduced-Order Models for Control of Fluids Using the Eigensystem Realization Algorithm," Theor. Comput. Fluid Dyn., in press.10.1007/s00162-010-0184-8
[112] Huang, S.-C., and Kim, J., 2008, "Control and System Identification of a Separated Flow," Phys. Fluids, **20**, p. 101509.
[113] Watson, J., 1960, "On the Non-Linear Mechanics of Wave Disturbances in Stable and Unstable Parallel Flows. Part 2: The Development of a Solution for Plane Poiseuille Flow and for Plane Couette Flow," J. Fluid Mech., **9**(3), pp. 371–389.
[114] Stuart, J., 1971, "Nonlinear Stability Theory," Annu. Rev. Fluid Mech., **3**, pp. 347–370.
[115] Hill, D. C., 1995, "Adjoint Systems and Their Role in the Receptivity Problem for Boundary Layers," J. Fluid Mech., **292**, pp. 183–204.
[116] Corbett, P., and Bottaro, A., 2001, "Optimal Control of Nonmodal Disturbances in Boundary Layers," Theor. Comput. Fluid Dyn., **15**(2), pp. 65–81.
[117] Bottaro, A., Corbett, P., and Luchini, P., 2003, "The Effect of Base Flow Variation on Flow Stability," J. Fluid Mech., **476**, pp. 293–302.

[118] Pironneau, O., 1984, *Optimal Shape Design for Elliptic Systems*, Springer, New York.
[119] Jameson, A., Martinelli, L., and Pierce, N. A., 1998, "Fluid Dynamics Optimum Aerodynamic Design Using the Navier–Stokes Equations," Theor. Comput. Fluid Dyn., **10**, pp. 213–237.
[120] Mohammadi, B., and Pironneau, O., 2004, "Shape Optimization in Fluid Mechanics," Annu. Rev. Fluid Mech., **36**, pp. 255–279.
[121] Hill, D. C., 1992, "A Theoretical Approach for Analyzing the Restabilization of Wakes," AIAA Paper No. 1992-0067.
[122] Marquet, O., Lombardi, M., Chomaz, J.-M., Sipp, D., and Jacquin, L., 2009, "Direct and Adjoint Global Modes of a Recirculation Bubble: Lift-Up and Convective Non-Normalities," J. Fluid Mech., **622**, pp. 1–21.
[123] Meliga, P., Chomaz, J.-M., and Sipp, D., 2009, "Unsteadiness in the Wake of Disks and Spheres: Instability, Receptivity and Control Using Direct and Adjoint Global Stability Analyses," J. Fluids Struct., **25**, pp. 601–616.
[124] Theofilis, V., Hein, S., and Dallmann, U., 2000, "On the Origins of Unsteadiness and Three-Dimensionality in a Laminar Separation Bubble," Philos. Trans. R. Soc. London, Ser. A, **358**(1777), pp. 3229–3246.
[125] Manneville, P., 1991, *Structures Dissipatives, Chaos et Turbulence*, Aléa-Saclay, CEA, France.
[126] Provansal, M., Mathis, C., and Boyer, L., 1987, "Benard-von Karman Instability—Transient and Forced Regimes," J. Fluid Mech., **182**, pp. 1–22.
[127] Dušek, J., Le Gal, P., and Fraunié, P., 1994, "A Numerical and Theoretical Study of the First Hopf Bifurcation in a Cylinder Wake," J. Fluid Mech., **264**, pp. 59–80.
[128] Zielinska, B. J. A., Goujon-Durand, S., Dusek, J., and Wesfreid, J. E., 1997, "Strongly Nonlinear Effect in Unstable Wakes," Phys. Rev. Lett., **79**(20), pp. 3893–3896.
[129] Piot, E., Casalis, G., Muller, F., and Bailly, C., 2006, "Investigation of the PSE Approach for Subsonic and Supersonic Hot Jets. Detailed Comparisons With LES and Linearized Euler Equations Results," Int. J. Aeroacoust., **5**(4), pp. 361–393.
[130] Gondret, P., Ern, P., Meignin, L., and Rabaud, M., 1999, "Experimental Evidence of a Nonlinear Transition From Convective to Absolute Instability," Phys. Rev. Lett., **82**(7), pp. 1442–1445.
[131] Viaud, B., Serre, E., and Chomaz, J.-M., 2008, "The Elephant Mode Between Two Rotating Disks," J. Fluid Mech., **598**, pp. 451–464.
[132] Meliga, P., Chomaz, J.-M., and Sipp, D., 2009, "Global Mode Interaction and Pattern Selection in the Wake of a Disk: A Weakly Nonlinear Expansion," J. Fluid Mech., **633**, pp. 159–189.
[133] Fabre, D., Auguste, F., and Magnaudet, J., 2008, "Bifurcations and Symmetry Breaking in the Wake of Axisymmetric Bodies," Phys. Fluids, **20**(5), p. 051702.
[134] Brion, V., Sipp, D., and Jacquin, L., 2007, "Optimal Amplification of the Crow Instability," Phys. Fluids, **19**(11), p. 111703.
[135] Marquet, O., Sipp, D., and Jacquin, L., 2008, "Sensitivity Analysis and Passive Control of Cylinder Flow," J. Fluid Mech., **615**, pp. 221–252.
[136] Meliga, P., Sipp, D., and Chomaz, J.-M., 2010, "Open-Loop Control of Compressible Afterbody Flows Using Adjoint Methods," Phys. Fluids, in press.
[137] Chomaz, J., Huerre, P., and Redekopp, L., 1991, "A Frequency Selection Criterion in Spatially Developing Flows," Stud. Appl. Math., **84**(2), pp. 119–144.
[138] Luchini, P., Giannetti, F., and Pralits, J., 2009, "Structural Sensitivity of the Finite-Amplitude Vortex Shedding Behind a Circular Cylinder," IUTAM Symposium on Unsteady Separated Flows and Their Control, Corfu, Greece, Jun. 18–22, M. Braza and K. Hourigan, eds., Vol. 14, p. 151.
[139] Huerre, P., and Monkewitz, P. A., 1990, "Local and Global Instabilities in Spatially Developing Flows," Annu. Rev. Fluid Mech., **22**, pp. 473–537.
[140] Marquet, O., Sipp, D., Jacquin, L., and Chomaz, J.-M., 2008, "Multiple Time Scale Analysis and Sensitivity Analysis for the Passive Control of the Cylinder Flow," AIAA Paper No. 2008-4228.
[141] Barbagallo, A., Sipp, D., and Schmid, P. J., 2009, "Closed-Loop Control of an Open Cavity Flow Using Reduced-Order Models," J. Fluid Mech., **641**, pp. 1–50.
[142] Trefethen, L. N., and Embree, M., 2005, *Spectra and Pseudospectra: The Behavior of Nonnormal Matrices and Operators*, Princeton University Press, Princeton, NJ.
[143] Marquet, O., Sipp, D., and Jacquin, L., 2006, "Global Optimal Perturbations in a Separated Flow Over a Backward-Rounded-Step," AIAA Paper No. 2006-2879.
[144] Marquet, O., Sipp, D., Chomaz, J.-M., and Jacquin, L., 2008, "Amplifier and Resonator Dynamics of a Low-Reynolds-Number Recirculation Bubble in a Global Framework," J. Fluid Mech., **605**, pp. 429–443.
[145] Blackburn, H. M., Barkley, D., and Sherwin, S. J., 2008, "Convective Instability and Transient Growth in Flow Over a Backward-Facing Step," J. Fluid Mech., **603**, pp. 271–304.
[146] Blackburn, H. M., Sherwin, S. J., and Barkley, D., 2008, "Convective Instability and Transient Growth in Steady and Pulsatile Stenotic Flows," J. Fluid Mech., **607**, pp. 267–277.
[147] Marquet, O., 2007, "Stabilité globale et contrôle d'écoulements de recirculation," Ph.D. thesis, Université de Poitiers, Poitiers, France.
[148] Monokrousos, A., Åkervik, E., Brandt, L., and Henningson, D. S., 2010, "Global Three-Dimensional Optimal Disturbances in the Blasius Boundary-Layer Flow Using Time-Steppers," J. Fluid Mech., in press.
[149] Levin, O., and Henningson, D. S., 2003, "Exponential vs Algebraic Growth and Transition Prediction in Boundary Layer Flow," Flow, Turbul. Combust., **70**, pp. 182–210.
[150] Crouch, J. D., 1992, "Localized Receptivity of Boundary Layers," Phys. Fluids A, **4**(7), pp. 1408–1414.
[151] Pralits, J. O., Hanifi, A., and Henningson, D. S., 2002, "Adjoint-Based Optimization of Steady Suction for Disturbance Control in Incompressible Flows," J. Fluid Mech., **467**, pp. 129–161.
[152] Airiau, C., Bottaro, A., Walther, S., and Legendre, D., 2003, "A Methodology for Optimal Laminar Flow Control: Application to the Damping of Tollmien-Schlichting Waves in a Boundary Layer," Phys. Fluids, **15**(5), pp. 1131–1145.
[153] Amestoy, P. R., Duff, I. S., Koster, J., and L'Excellent, J.-Y., 2001, "A Fully Asynchronous Multifrontal Solver Using Distributed Dynamic Scheduling," SIAM J. Matrix Anal. Appl., **23**(1), pp. 15–41.
[154] Mamun, C. K., and Tuckerman, L. S., 1995, "Asymmetry and Hopf Bifurcation in Spherical Couette Flow," Phys. Fluids, **7**(1), pp. 80–91.
[155] Tuckerman, L., and Barkley, D., 2000, "Bifurcation Analysis for Timesteppers," *Numerical Methods for Bifurcation Problems and Large-Scale Dynamical Systems* (IMA Volumes in Mathematics and Its Applications Vol. 119), E. Doedel and L. S. Tuckerman, eds., Springer, New York, pp. 453–466.
[156] Bagheri, S., Akervik, E., Brandt, L., and Henningson, D. S., 2009, "Matrix-Free Methods for the Stability and Control of Boundary Layers," AIAA J., **47**(5), pp. 1057–1068.
[157] Mack, C. J., and Schmid, P. J., 2010, "A Preconditioned Krylov Technique for Global Hydrodynamic Stability Analysis of Large-Scale Compressible Flows," J. Comput. Phys., **229**(3), pp. 541–560.
[158] Åkervik, E., Brandt, L., Henningson, D. S., Hœpffner, J., Marxen, O., and Schlatter, P., 2006, "Steady Solutions of the Navier-Stokes Equations by Selective Frequency Damping," Phys. Fluids, **18**(6), p. 068102.
[159] Chomaz, J.-M., 2004, "Transition to Turbulence in Open Flows: What Linear and Fully Nonlinear Local and Global Theories Tell Us," Eur. J. Mech. B/Fluids, **23**, pp. 385–399.
[160] Nagata, M., 1990, "Three Dimensional Finite Amplitude Solutions in Plane Couette Flow: Bifurcation From Infinity," J. Fluid Mech., **217**, pp. 519–527.
[161] Waleffe, F., 1997, "On the Self-Sustaining Process in Shear Flows," Phys. Fluids, **9**, pp. 883–900.
[162] Faisst, H., and Eckhardt, B., 2003, "Travelling Waves in Pipe Flow," Phys. Rev. Lett., **91**, p. 224502.
[163] Duguet, Y., Willis, A. P., and Kerswell, R., 2008, "Transition in Pipe Flow: The Saddle Structure on the Boundary of Turbulence," J. Fluid Mech., **613**, pp. 255–274.
[164] Cossu, C., Chevalier, M., and Henningson, D. S., 2007, "Optimal Secondary Energy Growth in a Plane Channel Flow," Phys. Fluids, **19**(5), p. 058107.
[165] Crouch, J. D., Garbaruk, A., and Magidov, D., 2007, "Predicting the Onset of Flow Unsteadiness Based on Global Instability," J. Comput. Phys., **224**(2), pp. 924–940.
[166] Cossu, C., Pujals, G., and Depardon, S., 2009, "Optimal Transient Growth and Very Large-Scale Structures in Turbulent Boundary Layers," J. Fluid Mech., **619**, pp. 79–94.